Bendix Guidance Systems Division

THE
BENDIX
CORPORATION

GUIDANCE
SYSTEMS
DIVISION

TETERBORO,
NEW JERSEY 07608

MODULAR DESIGN ATTITUDE CONTROL SYSTEM

FINAL REPORT

MARCH 8, 1982

PREPARED FOR:

GEORGE C. MARSHALL
SPACE FLIGHT CENTER
HUNTSVILLE, ALABAMA

NASA CONTRACT NO.
NAS8-33979
EXHIBIT A
(AUGUST 15, 1980
-OCTOBER 15, 1981)

APPROVED BY:

J. LEVINTHAL
ENGINEERING MANAGER
SYSTEMS DESIGN

PREPARED BY:

F. D. CHICHESTER
TECHNICAL MANAGER

df

FORWARD

This final report is submitted in accordance with the "Scope of Work, Exhibit A" for Contract NAS8-33979. The study was directed from the Guidance Systems Division (GSD) of The Bendix Corporation. The engineering managers at this location were Dr. David Zomick and Mr. Joel Levinthal while Dr. Frederick Chichester* was the technical manager. The principal contributors from GSD were Dr. Chichester who wrote all sections of the report and Mr. Raymond Kaczynski who provided some technical assistance. Simulation of the spacecraft models and their control systems as well as a major portion of the mathematical modeling were provided by the computer simulation group formerly part of The Bendix Engineering Development Center and now part of the ICAT/Simulation Center in Teterboro, New Jersey. This effort was coordinated by Mr. William Gelbach. Mr. G. A. Cornell and Mr. Don Lipski of the Simulation Center produced a substantial portion of the mathematical modeling and computer simulation . Mr. Norman O. Tiffany, a former staff member of the simulation group, also made substantial contributions to the simulation of the control systems studied and analyses of their relative performances. The guidance of Drs. Michael Borelli and Henry Waites of MSFC during the course of this study is gratefully acknowledged.

*Presently a member of the technical staff of the Corporate Simulation Center, Teterboro, New Jersey.

ABSTRACT

A new hybrid multilevel-linear quadratic regulator (ML-LQR) approach was developed and applied to the attitude control of models of the rotational dynamics of a prototype flexible spacecraft and of a typical space platform. Three axis rigid body-flexible suspension models were developed for both the spacecraft and the space platform utilizing augmented body methods. Models of the spacecraft with hybrid ML-LQR attitude control and with LQR attitude control were simulated and their responses with the two different types of control were compared.

TABLE OF CONTENTS

LIST OF ILLUSTRATIONS

LIST OF ILLUSTRATIONS

LIST OF ILLUSTRATIONS

LIST OF TABLES

SECTION 1

1.0 INTRODUCTION

This report is submitted in compliance with the Scope of Work under contract NAS8-33979. The period of performance covered by the contract is from August 15, 1980 to October 15, 1981. The submission and approval of this report constitute the successful completion of the "Exhibit A" portion of the contract.

This report is a sequel to two others previously submitted under a different contract number. The two prior reports, references (1-1) and (1-2) were submitted in October 1978 and September, 1979 and covered the periods from July 27, 1977 to July 27, 1978 and from August 26, 1978 to August 26, 1979, respectively, in compliance with "Exhibit A" of contract NAS8-32660.

1 OBJECTIVES

The sections that follow summarize the effort expended on the Modular Design Attitude Control System Study contract. The primary objective of the study was to develop a new approach to applying attitude control to mathematical models of the rotational dynamics of a representative flexible spacecraft and of a representative space platform incorporating both the flexible spacecraft and a deployable truss. Since these rotational dynamics models were comprised of equations containing second order derivatives, it was necessary to develop a new control approach that could treat such a class of models effectively. A secondary objective was

the development of more efficient methods for generating the three axis discrete mass models of the rotational dynamics of the flexible spacecraft and space platform. These objectives led to the development and application of a new hybrid control approach combining the techniques of multilevel (ML) control and an extension of linear quadratic regulator (LQR) control and the application of augmented body techniques in the modeling of the rotational dynamics of the spacecraft and space platform.

1.2 SCOPE

Study effort was concentrated in five main areas.

a. Development of a new hybrid ML-LQR approach to applying optimal control to the mathematical models of the rotational dynamics of prototype flexible spacecraft and space platforms.

b. Improvement in the efficiency of developing three axis discrete mass models of the rotational dynamics of flexible spacecraft and platforms by utilizing augmented body techniques.

c. Development of three axis discrete mass models of the rotational dynamics of a prototype flexible spacecraft and of a prototype space platform incorporating the flexible spacecraft.

d. Application of the hybrid ML-LQR approach to the attitude control of models of the rotational dynamics of a prototype flexible spacecraft and the space platform.

e. Digital computer simulation of the rotational dynamics models of the prototype flexible spacecraft with hybrid ML-LQR attitude control and with LQR control for comparison of responses to disturbances.

1.3 GENERAL

This report is comprised of eight sections. Section 2 describes the application of a new hybrid ML-LQR approach to effecting attitude control of a single axis three body model of the rotational dynamics of a typical flexible spacecraft. Section 3 presents the development of a three axis five body linearized state variable model of the rotational dynamics of the flexible spacecraft treated in Section 2., utilizing augmented body (barycentric) techniques. Section 4 describes the extension of the hybrid ML-LQR approach to the attitude control of the three axis five body model and compares the responses of the model with this type of control with those obtained from the same model with LQR control alone. Section 5 reviews some specific aspects of the application of hybrid ML-LQR control to the three axis five body model. Section 6 treats the development of a three axis ten body model of the rotational dynamics of a typical space platform consisting of two spacecraft interconnected by a deployable truss described in Ivey (1-3). Section 7 presents the extension of the bybrid

ML-LQR approach to the attitude control of the three axis ten body model of the space platform. Section 9 lists a number of conclusions and recommendations. Three appendices appear at the end of the report. References are cited liberally and are listed at the end of each section.

The original RFQ requested that the International System of units (designated as SI) be used in the program and in any reporting. Torques, moments, angular momentum, moments of inertia and distances, however, are stated in English units since this was the system of units used in presenting all of the vehicle data in the RFQ and the truss data in Ivey (1-3).

1-4 REFERENCES

1-1 Guidance Systems Division, The Bendix Corporation, "Space Construction Base Control System, Final Report," Contract NAS8-32660 for George C. Marshall Space Flight Center, October 27, 1978.

1-2 Guidance Systems Division, The Bendix Corporaion, "Space Construction Base Control System, Final Report," Contract NAS8-32660 for George C. Marshall Space Flight Center, September 1, 1979.

1-3 Ivey, Wayne "Vibration Analysis of the MSFC/Hybrid Deployable Truss," MSFC memorandum, June 26, 1980.

SECTION 2

2.0 APPLICATION OF HYBRID MULTILEVEL-LQR ATTITUDE CONTROL TO A SINGLE AXIS TORSIONAL MODEL

In Porcelli (2-1)* an example of the application of multiple control in the design of an attitude control system for a simple flexible space vehicle comprised of three rigid bodies that could rotate about a common axis was presented. In Chichester (2-2) an approach to applying multilevel techniques to this control problem was described. This latter approach was based upon techniques developed in Wismer (2-3) and Chichester (2-4). In a later memorandum by Kaczynski (2-5) it was shown that single axis attitude control of the discrete mass model of Configuration 1 of the Space Construction Base could be reduced to the control of the three mass single axis torsional model treated in Porcelli's paper and linear quadratic regulator (LQR) techniques were applied to effect this control.

In the work reported here, an approach to applying multilevel control techniques to Porcelli's model is presented that is both more broadly applicable and more efficient than the one proposed earlier in Chichester (2-2). A combination of Gauss-Seidel multilevel control techniques and an extension of LQR techniques is applied to this model which contains second order time derivatives. The paper upon which this section is based,

*Numbers enclosed in parentheses refer to references listed at the end of this section.

Chichester (2-6), is believed to be the first publication of the application of this hybrid approach to the control of a flexible vehicle.

The overall approach followed here in applying the combination of multilevel and LQR control may be outlined as follows:

a. Express mathematical model of vehicle dynamics in (linear) state variable form.

b. Decompose model into a set of temporarily decoupled state equators by defining a suitable set of state coordination equations.

c. Construct correspondingly decomposed performance index.

d. Form decomposed Hamiltonian.

e. Derive constate equations with associated costate coordination equations from necessary conditions for minimization of Hamiltonian.

f. Derive control equations from additional necessary conditions for minimization of Hamiltonian.

g. Combine state, costate and control equations pertaining to the ith rigid body in the model into the ith two point boundary value (TPBV) subproblem.

h. Combine the state coordination and the costate coordination equations into an overall coordination subproblem.

i. Assemble the subproblems of the last two steps into a two level hierarchy with the coordination subproblem in the upper level.

j. Reduce the solution of each TPBV subproblem in the lower level of the hierarchy to the solution of the Riccati equation and an auxiliary equation.

2.1 STATE VARIABLE VEHICLE MODEL

In Figure 2-1, let:

$$\underline{u} = \left[u_1, \frac{T_o}{J_o}, u_3, \frac{T_1}{J_1}, u_5, \frac{T_2}{J_2} \right]^T \tag{2-1}$$

$$\underline{x} = (\underline{x}_1^T, \underline{x}_2^T, \underline{x}_3^T)^T \tag{2-2}$$

$$\underline{x}_1 = (\theta_o, \dot{\theta}_o)^T = (x_1, x_2)^T \tag{2-3}$$

$$\underline{x}_2 = (\theta_1, \dot{\theta}_1)^T = (x_3, x_4)^T \tag{2-4}$$

$$\underline{x}_3 = (\theta_2, \dot{\theta}_2)^T = (x_5, x_6)^T \tag{2-5}$$

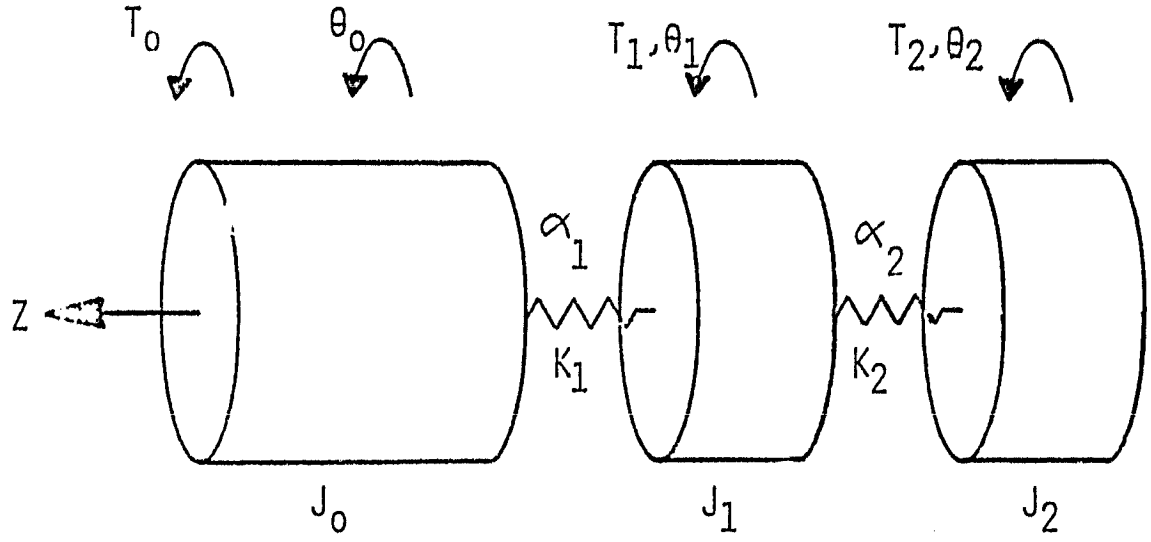

FIGURE 2-1: TORSIONAL MODEL OF VEHICLE

Then the normalized torque equations for this single axis torsional model may be written in state variable form as follows:

$$\begin{bmatrix} \dot{x}_1 \\ \dot{x}_2 \end{bmatrix} = \begin{bmatrix} 0 & 1 \\ \frac{-K_1}{J_o} & \frac{-\alpha_1}{J_o} \end{bmatrix} \begin{bmatrix} x_1 \\ x_2 \end{bmatrix} + \begin{bmatrix} 0 & 0 \\ \frac{K_1}{J_o} & \frac{\alpha_1}{J_o} \end{bmatrix} \begin{bmatrix} x_3 \\ x_4 \end{bmatrix}$$

$$+ \begin{bmatrix} 0 & 0 \\ 0 & 1 \end{bmatrix} \begin{bmatrix} u_1 \\ u_2 \end{bmatrix} \quad \text{or}$$

$$\dot{\underline{x}}_1 = A_{11}\underline{x}_1 + A_{12}\underline{x}_2 + B_{11}\underline{u}_1 \qquad (2\text{-}6)$$

$$\begin{bmatrix} \dot{x}_3 \\ \dot{x}_4 \end{bmatrix} = \begin{bmatrix} 0 & 1 \\ \frac{-(K_1 + K_2)}{J_1} & \frac{-(\alpha_1 + \alpha_2)}{J_1} \end{bmatrix} \begin{bmatrix} x_3 \\ x_4 \end{bmatrix}$$

$$+ \begin{bmatrix} 0 & 0 \\ \frac{K_1}{J_1} & \frac{\alpha_1}{J_1} \end{bmatrix} \begin{bmatrix} x_1 \\ x_2 \end{bmatrix} + \begin{bmatrix} 0 & 0 \\ \frac{K_2}{J_1} & \frac{\alpha_2}{J_1} \end{bmatrix} \begin{bmatrix} x_5 \\ x_6 \end{bmatrix}$$

$$+ \begin{bmatrix} 0 & 0 \\ 0 & 1 \end{bmatrix} \begin{bmatrix} u_3 \\ u_4 \end{bmatrix} \quad \text{or} \qquad (2\text{-}7)$$

$$\dot{\underline{x}}_2 = A_{22}\underline{x}_2 + A_{21}\underline{x}_1 + A_{23}\underline{x}_3 + B_{22}\underline{u}_2$$

$$\begin{bmatrix} \dot{x}_5 \\ \dot{x}_6 \end{bmatrix} = \begin{bmatrix} 0 & 1 \\ \frac{-K_2}{J_2} & \frac{-\alpha_2}{J_2} \end{bmatrix} \begin{bmatrix} x_5 \\ x_6 \end{bmatrix} +$$

$$\begin{bmatrix} 0 & 0 \\ \frac{K_1}{J_2} & \frac{\alpha_1}{J_2} \end{bmatrix} \begin{bmatrix} x_3 \\ x_4 \end{bmatrix} + \begin{bmatrix} 0 & 0 \\ 0 & 1 \end{bmatrix} \begin{bmatrix} u_5 \\ u_6 \end{bmatrix} \quad \text{or}$$

$$\dot{\underline{x}}_3 = A_{33}\underline{x}_3 + A_{32}\underline{x}_2 + B_{33}\underline{u}_3 \qquad (2\text{-}8)$$

2.2 DECOMPOSED STATE EQUATIONS

The above state equations may be decoupled temporarily by defining the following vector coordination variables.

$$\underline{s}_1^{\ell} = \underline{x}_2$$

$$\underline{s}_2^{u} = \underline{x}_1 \qquad (2\text{-}9)$$

State Coordination Equations

$$\underline{s}_2^{\ell} = \underline{x}_3$$

$$\underline{s}_3^{u} = \underline{x}_2$$

With these coordination relationships, the ith state equation assumes the following decomposed form:

$$\dot{\underline{x}}_i = A_{ii}\underline{x}_i + B_{ii}\underline{u}_i + \underline{a}_i(t);\ i=1,2,3 \tag{2-10}$$

where: $$\underline{a}_1 = A_{12}\underline{s}_1^{\ell} \tag{2-11}$$

$$\underline{a}_2 = A_{21}\underline{s}_2^{u} + A_{23}\underline{s}_2^{\ell} \tag{2-12}$$

$$\underline{a}_3 = A_{32}\underline{s}_3^{u} \tag{2-13}$$

2.3 DECOMPOSED PERFORMANCE INDEX

The corresponding decomposed performance index to minimize position and rate errors as well as control effort may be written in the following form:

$$P = \sum_{i=1}^{3} \int_{t_o}^{t_f} p_i\,dt \tag{2-14}$$

where

$$p_i = (\underline{x}_i - \underline{x}_{di})^T Q_i (\underline{x}_i - \underline{x}_{di}) + \underline{u}_i^T R_i \underline{u}_i \tag{2-15}$$

$$Q_1 = \begin{bmatrix} W_1 & 0 \\ 0 & W_2 \end{bmatrix} \qquad Q_2 = \begin{bmatrix} W_5 & 0 \\ 0 & W_6 \end{bmatrix}$$

$$Q_3 = \begin{bmatrix} W_9 & 0 \\ 0 & W_{10} \end{bmatrix} \tag{2-16}$$

$$R_1 = \begin{bmatrix} W_3 & 0 \\ 0 & W_4 \end{bmatrix} \qquad R_2 = \begin{bmatrix} W_7 & 0 \\ 0 & W_8 \end{bmatrix}$$

$$R_3 = \begin{bmatrix} W_{11} & 0 \\ 0 & W_{12} \end{bmatrix} \tag{2-17}$$

$\underline{x}_{d1} = \underline{x}_d$ = desired angular position and rate for all three bodies

2.4 DECOMPOSED HAMILTONIAN

The specific form of the Hamiltonian utilized depends upon the type of second level control that is to be employed. Feasible, nonfeasible and Gauss-Siedel* second level control formulations and their respective advantages and disadvantages are discussed on pp. 12-16

*Wismer's name for this approach.

of Wismer (2-3). Gauss-Seidel second level control was chosen because it does not require that each subsystem have at least as many controls as constraints and it does not require the use of gradient techniques. From Wismer, pp. 37-38, the decomposed Gauss-Seidel Hamiltonian may be written in the following form:

$$H = \sum_{i=1}^{3} H_i \tag{2-18}$$

$$H_1 = (\underset{-1}{x} - \underset{-d1}{x})^T \underset{1}{Q} (\underset{-1}{x} - \underset{-d1}{x}) + \underset{-1}{u}^T \underset{1-1}{R} \underset{-1}{u}$$

$$+ \underset{-1}{\lambda}^T (\underset{11-1}{A} \underset{-1}{x} + \underset{11-1}{B} \underset{-1}{u} + \underset{12-1}{A} \underset{-1}{s}^{\ell}) + \underset{-1}{\nu}^T (\underset{-1}{x} - \underset{-1}{s}^{u}) \tag{2-19}$$

$$H_2 = (\underset{-2}{x} - \underset{-d2}{x})^T \underset{2}{Q} (\underset{-2}{x} - \underset{-d2}{x}) + \underset{-2}{u}^T \underset{2-2}{R} \underset{-2}{u}$$

$$+ \underset{-2}{\lambda}^T (\underset{22-2}{A} \underset{-2}{x} + \underset{22-2}{B} \underset{-2}{u} + \underset{23-2}{A} \underset{-2}{s}^{\ell} + \underset{21-2}{A} \underset{-2}{s}^{u})$$

$$+ \underset{-2}{\mu}^T (\underset{-2}{x} - \underset{-1}{s}^{\ell}) + \underset{-2}{\nu}^T (\underset{-2}{x} - \underset{-3}{s}^{u}) \tag{2-20}$$

$$H_3 = (\underset{-3}{x} - \underset{-d3}{x})^T Q_3 (\underset{-3}{x} - \underset{-d3}{x}) + \underset{-3}{u}^T R_{33} \underset{-3}{u}$$

$$+ \underset{-3}{\lambda}^T (A_{33} \underset{-3}{x} + B_{33} \underset{-3}{u} + A_{32} \underset{-3}{s}^u) + \underset{-3}{\nu}^T (\underset{-3}{x} - \underset{-2}{s}^\ell) \qquad (2\text{-}21)$$

2.5 COSTATE EQUATIONS

The costate equations may be written as follows:

$$\dot{\underset{-1}{\lambda}} = - \frac{\partial H_1}{\partial \underset{-1}{x}}, \qquad i = 1,2,3 \qquad (2\text{-}22)$$

$$\dot{\underset{-1}{\lambda}} = -A_{11}^T \underset{-1}{\lambda} - 2Q_1 (\underset{-1}{x} - \underset{-d1}{x}) + \underset{-1}{b}(t) \qquad (2\text{-}23)$$

where:

$$\underset{-1}{\lambda}(t_f) = \underset{-}{0}$$

$$\underset{-1}{b} = - \underset{-1}{\nu} \qquad (2\text{-}24)$$

$$\underset{-2}{b} = -\underset{-2}{\mu} - \underset{-2}{\nu} \qquad (2\text{-}25)$$

$$\underset{-3}{b} = -\underset{-3}{\mu} \qquad (2\text{-}26)$$

$\underline{0}$ = null vector of appropriate dimension.

2.6 CONTROL EQUATIONS

The control equations are written in the following form:

$$\frac{\partial H_i}{\partial \underline{u}_i} = 2R_{ii}\underline{u}_i + B_{ii}^T \underline{\lambda}_i = \underline{0} \qquad (2\text{-}27)$$

$$\underline{u}_i = -\frac{1}{2} R_i^{-1} B_{ii}^T \underline{\lambda}_i \qquad i=1,2,3 \qquad (2\text{-}28)$$

2.7 TPBV FORMULATION OF FIRST LEVEL SUBPROBLEMS

Substitution of the control equations into the decomposed state equations yields the following:

$$\dot{\underline{x}} = A_{ii}\underline{x}_i - \frac{1}{2} B_{ii} R_i^{-1} B_{ii}^T \underline{\lambda}_i + \underline{a}_i(t); \qquad (2\text{-}29)$$

$$\underline{x}_i(t_o) = \underline{x}_{io} \qquad (i = 1,2,3)$$

First level subproblem i is formed by associating equation (2-23) with equation (2-29). The vector-matrix form of this subproblem is expressed as follows:

$$\begin{bmatrix} \dot{\underline{x}}_i \\ \dot{\underline{\lambda}}_i \end{bmatrix} = \begin{bmatrix} A_{ii} & -\frac{1}{2} R_i^{-1} \\ -2Q_i & -A_{ii}^T \end{bmatrix} \begin{bmatrix} \underline{x}_i \\ \underline{\lambda}_i \end{bmatrix} + \begin{bmatrix} \underline{a}_i(t) \\ \hat{\underline{b}}_i(t) \end{bmatrix}$$

$$i = 1,2,3 \qquad (2\text{-}30)$$

where: $\hat{R}_i^{-1} \triangleq B_{ii} R_i^{-1} B_{ii}^T$

$$\hat{\underline{b}}_i = \underline{b}_i + 2Q_i \underline{x}_{id}$$

$$\underline{x}_i^T(t_o) = \underline{x}_{io}^T$$

$$= [O_{i-1}(t_o), \dot{O}_{i-1}(t_o)]^T$$

$$\underline{\lambda}_i(t_f) = \underline{0} = [0, 0]^T$$

Equation (2-30) and its associated boundary conditions constitute a set of three vector two-point boundary value (TPBV) subproblems. They may be solved by an extension of the linear quadratic regulator (LQR) techniques that appears in Appendix A.

2.8 GAUSS-SEIDEL SECOND LEVEL COORDINATION SUBPROBLEM

The second level necessary conditions may be written as follows:

From $\frac{\partial H_i}{\partial \underline{\rho}_i} = 0$: $\underline{s}_i^u = \underline{x}_{i-1}$ $i=1,2,3$ (2-31)

$\frac{\partial H_i}{\partial \underline{\nu}_{i-1}} = 0$: $\underline{s}_{i-1}^{\ell} = \underline{x}_{i+1}$ $i = 1,2,3$ (2-32)

$\frac{\partial H}{\partial \underline{s}_{i-1}} = 0$: $\underline{\nu}_{i-1} = A_{21}^T \underline{\lambda}_{2-2}$ (2-33)

$\nu_2 = A_{32}^T \underline{\lambda}_3$ (2-34)

$\underline{\rho}_2 = A_{12}^T \underline{\lambda}_1$ (2-35)

$\underline{\rho}_3 = A_{23}^T \underline{\lambda}_2$ (2-36)

These equations are assembled into the coordination subproblem appearing at the apex of the subproblem hierarchy depicted in Figure 2-2.

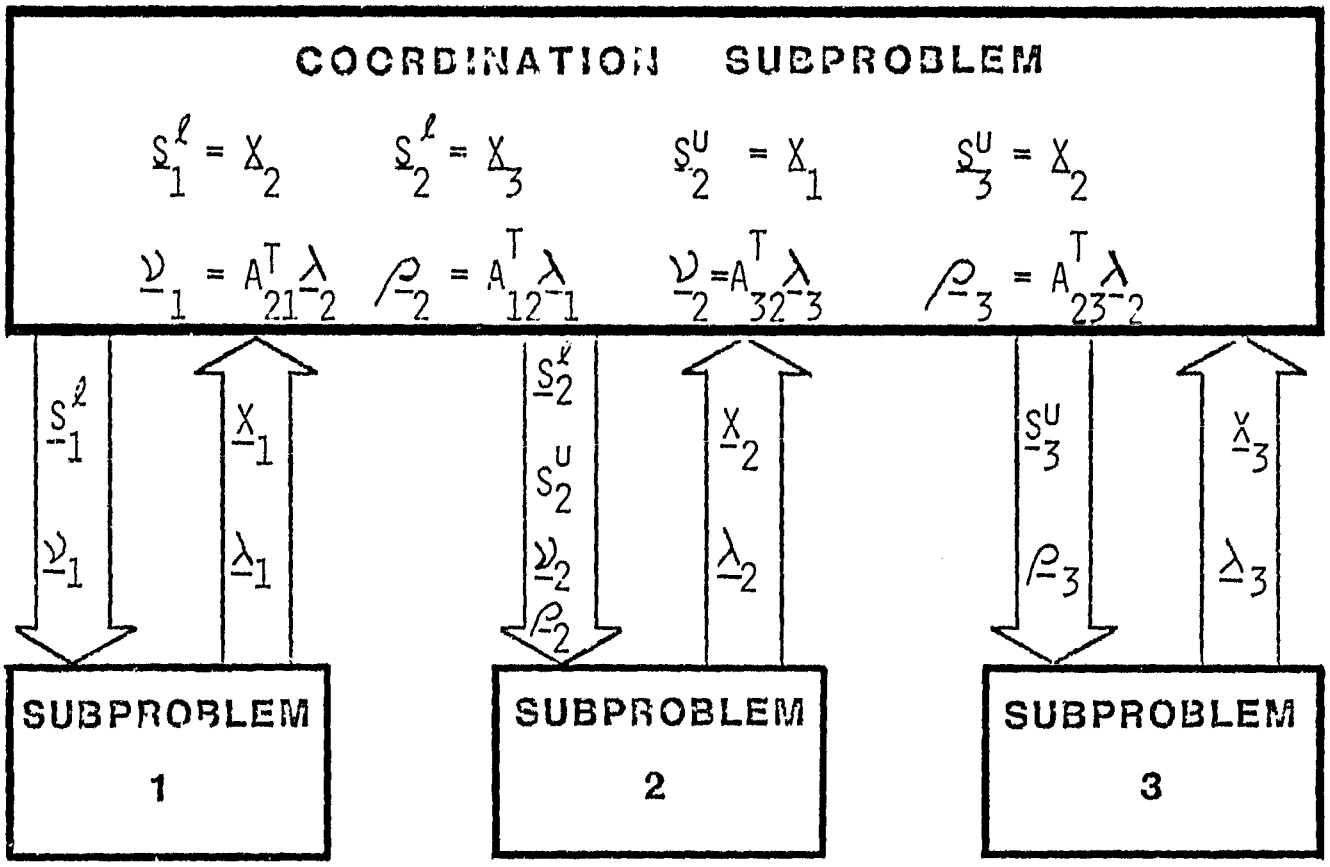

FIGURE 2-2: SUBPROBLEM HIERARCHY WITH GAUSS-SEIDEL SECOND LEVEL COORDINATION FOR SINGLE AXIS MODEL

2.9 REFERENCES

2-1. Porcelli, G. "Attitude Control of Flexible Space Vehicles," AIAA Journal, Vol. 10, No. 6, June, 1972, pp. 807-812.

2-2. Chichester, F.D., "Application of Multilevel Control to a Single Axis Torsional System." Bendix Corporation MT-40,808, Issue A, May 16, 1978.

2-3. Wismer, D.A., "Optimal Control of Distributed Parameter Systems Using Multilevel Techniques." Ph.D. dissertation, University of California, Los Angeles, California, 1966.

2-4. Chichester, F.D., "Application of Multilevel Control Techniques to Classes of Distribued Parameter Plants." Dr. Engineering Science dissertation, New Jersey Institute of Technology, Newark, New Jersey, 1976.

2-5. Kaczynski, R.F., "Attitude Control Using the Linear Quadratic Regulator (LQR) Technique." Bendix Corporation Technical Memorandum MT-40,815, January 21, 1980.

2-6. Chichester, F.D., "Application of Gauss-Seidel Multilevel Control to a Single Axis Torsional Model," Proceedings of the Space Transportation Symposium, 1980 SAE Aerospace Congress and Exposition, October, 1980. Los Angeles Convention Center, Los Angeles, California.

2-7. Sage, A.P., Optimum Systems Control, Englewood Cliffs, New Jersey. Prentice-Hall, 1968.

SECTION 3

3.0 DEVELOPMENT OF A THREE AXIS GAUSS-SEIDEL MULTILEVEL ROTATIONAL DYNAMIC MODEL OF A FLEXIBLE SPACECRAFT

INTRODUCTION

In the work presented in this section Gauss-Seidel multilevel modeling was applied to a three axis five body representative of the Space Construction Base (SCB). The general approach included augmented body techniques presented in Cornell (3-1), (3-2), and Lipski (3-3), (3-4) followed by multilevel modeling techniques described in the previous section and Wismer (3-5). The procedure utilized was as follows.

1) Approximate the flexible vehicle with rigid bodies interconnected by a spring-hinge suspension.

2) List any symmetry conditions that may apply to the elements of the model.

3) Determine the vector locating the center of mass of each rigid body with respect to its barycenter.

4) Determine the vectors locating each adjacent hinge with respect to the barycenter of each rigid body.

5) Derive augmented moment of inertia matrices equivalent to the effective moment of inertia of every rigid body in the model with respect to each barycenter.

6) Write the effective torque balance about each barycenter with rigid body angular rates, $\underline{\omega}_i$, as vector state variables.

7) Express the equations resulting from 6) in vector-matrix form.

8) Invert the coefficient matrix of $\underline{\omega}$ in the model of 7) to obtain the state variable rigid body angular rate model.

9) Express time rate of change of relative Euler angles in terms of rigid body angular rates to obtain the state variable Euler angle model.

10) Aggregate the state variable Euler angle model with the state variable rigid body angular rate model to obtain the state variable rotational dynamics model.

11) Decompose the state variable rotational dynamics model.

3.1 RIGID BODY-SUSPENSION APPROXIMATION OF FLEXIBLE VEHICLE

The typical flexible space vehicle depicted in Figure 3-1, Configuration 1 of the Space Construction Base, was approximated by an assembly of five rigid bodies interconnected by a spring hinge suspension as shown in Figure 3-2. The symmetry relationships for this model are as follows.

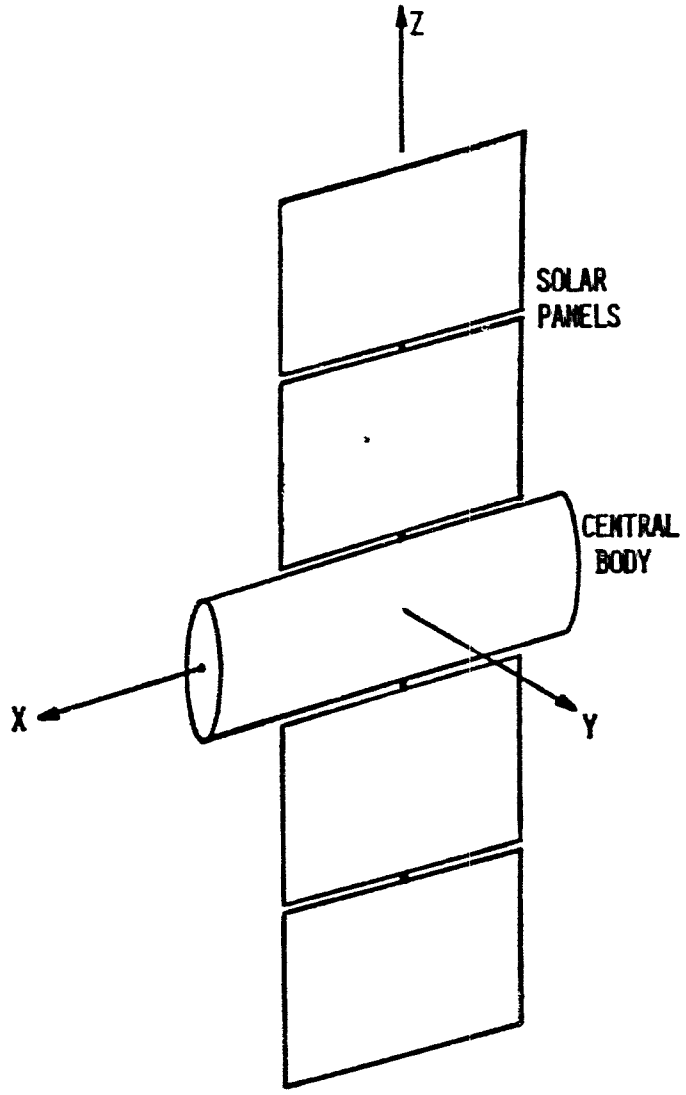

FIG. 3-1: A PROTOTYPE VEHICLE WITH APPENDAGES

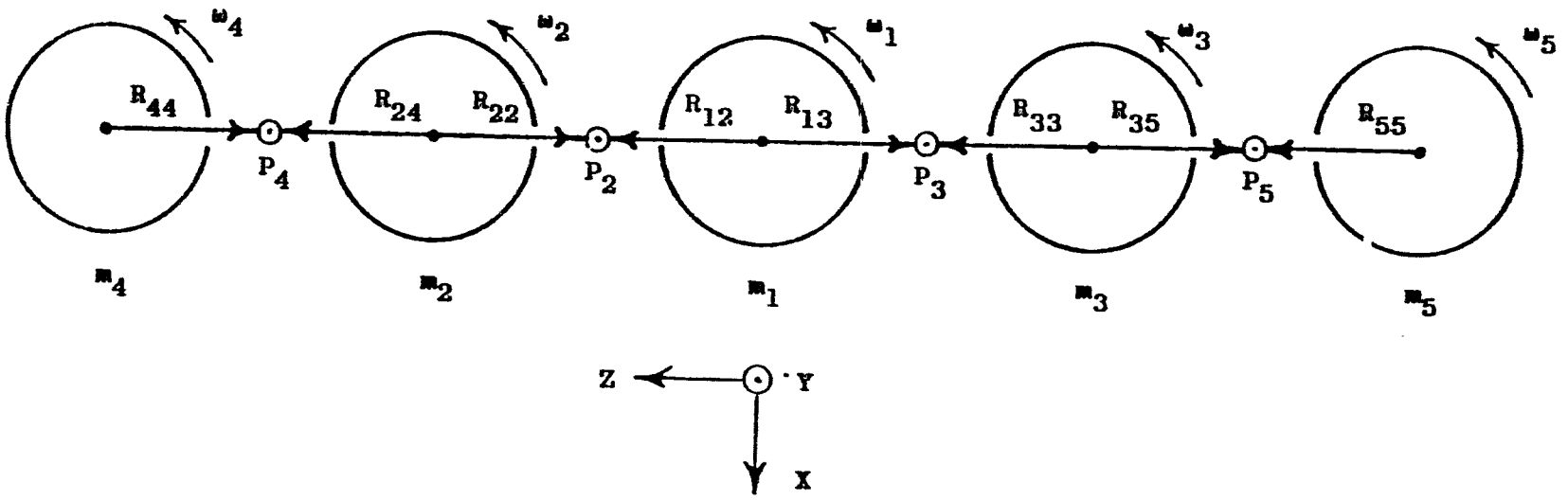

FIG. 3-2: TOPOLOGICAL DIAGRAM OF FIVE BODY MODEL OF FLEXIBLE VEHICLE

$$m_5 = m_4 = m_3 = m_2 \qquad I_5 = I_4 = I_3 = I_2 \qquad (3\text{-}1)$$

$$\underline{r}_{13} = -\underline{r}_{12} \qquad \underline{r}_{55} = \underline{r}_{33} = \underline{r}_{44} = -\underline{r}_{22} = -\underline{r}_{35}$$

3.2 LOCATION OF CENTER OF MASS WITH RESPECT TO BARYCENTER OF EACH RIGID BODY

Under these symmetry conditions the total mass of the model is given by:

$$M = \sum_{i=1}^{5} m_i = m_1 + 4m_2 \qquad (3\text{-}2)$$

$$\underline{d}_1 = \underline{0} \qquad \underline{d}_2 = -\frac{m_1 + m_2}{M}\,\underline{r}_{22} = -\underline{d}_3$$

$$\underline{d}_4 = -\frac{m_1 + 3m_2}{M}\,r_{22} = -\underline{d}_5 \qquad (3\text{-}3)$$

3.3 LOCATION OF ADJACENT HINGES WITH RESPECT TO BARYCENTER OF EACH BODY

$$\underline{d}_{12} = \underline{d}_1 + \underline{r}_{12} = \underline{r}_{12} = -\underline{d}_{13}$$

$$\underline{d}_{24} = \underline{d}_2 + \underline{r}_{24} - \frac{2m_1 + 5m_2}{M}\,\underline{r}_{22} = -\underline{d}_{35} \qquad (3\text{-}4)$$

$$\underline{d}_{22} = \underline{d}_2 + \underline{r}_{22} = \frac{3m_2}{M}\,\underline{r}_{22} = -\underline{d}_{33}$$

$$\underline{d}_{44} = \underline{d}_4 + \underline{r}_{44} = \frac{m_2}{M}\,\underline{r}_{22} = -\underline{d}_{55}$$

3.4 GENERATION OF AUGMENTED INERTIA SUBMATRICES

The effective moment of inertia matrix with respect to the barycenter of each rigid body may be expressed as follows:

$$I_1^* = I_1 - 4m_2\tilde{D}_{12}\tilde{D}_{12}$$

$$I_2^* = I_2 - m_2\tilde{D}_2\tilde{D}_2 - (m_1 + 2m_2)\tilde{D}_{22}\tilde{D}_{22} - m_2\tilde{D}_{24}\tilde{D}_{24} = I_3^*$$

$$I_4^* = I_4 - m_2\tilde{D}_4\tilde{D}_4 - (m_1 + 3m_2)\tilde{D}_{22}\tilde{D}_{22} = I_5^* \qquad (3\text{-}5)$$

where: for $\underline{a} = (a_x, a_y, a_z)^T$ and $\underline{b} = (b_x, b_y, b_z,)^T$

$$\underline{a} \times \underline{b} = \tilde{A}\underline{b}$$

and

$$\tilde{A} = \begin{bmatrix} 0 & -a_z & a_y \\ a_z & 0 & -a_x \\ -a_y & a_x & 0 \end{bmatrix} \qquad (3\text{-}6)$$

3.5 RIGID BODY ANGULAR RATE EQUATIONS

Equations in terms of the rigid body rates of angular rotation, $\underline{\omega}_i$, may be obtained by equating the rate of change of angular momentum of each rigid body comprising the model to the sum of torques acting on that body at its barycenter. Under the assumption of small angular displacements the linearized equation for the central rigid body in the model may be expressed as follows.

$$I_1^* \dot{\underline{\omega}}_1 + M\check{D}_{12}\,\check{D}_{22}(\dot{\underline{\omega}}_2 + \dot{\underline{\omega}}_3) + \check{D}_{44}(\dot{\underline{\omega}}_4 + \dot{\underline{\omega}}_5)$$

$$= \underline{t}_1 + \underline{t}_{12}^H + \underline{t}_{13}^H + \check{D}_1\underline{f}_1 - \check{D}_{12}\,(\underline{f}_2 + \underline{f}_4 - \underline{f}_3 - \underline{f}_5) \qquad (3\text{-}7)$$

where:

$\underline{t}_i$ = vector sum of external torques on ith rigid body.

$\underline{t}_{ij}^H$ = vector sum of torques from hinge j on ith rigid body.

$\underline{f}_i$ = vector sum of external forces on ith rigid body.

A corresponding equation was written for each of the other rigid bodies in the model. The entire group of rigid body angular rate equations may be expressed in vector state variable form as follows:

$$\dot{\underline{\omega}} = G(\underline{t} + \underline{t}^{H}) + GB\underline{t} \qquad (3\text{-}8)$$

where:

$\dot{\underline{\omega}} = (\dot{\underline{\omega}}_1^T, \dot{\underline{\omega}}_2^T, \ldots, \dot{\underline{\omega}}_5^T)^T$

$\underline{t}^{H} = \left[(\underline{t}_1^{H})^T, (\underline{t}_2^{H})^T, \ldots, (\underline{t}_5^{H})^T\right]^T$

$\underline{\omega}_1$ = angular rate of ith rigid body

$\underline{t}_1^{H}$ = total hinge torque on ith rigid body

$\underline{t} = (\underline{t}_1^T, \underline{t}_2^T, \ldots, \underline{t}_5^T)^T$

$\underline{t}_1^{H} = \underline{t}_{12}^{H} + \underline{t}_{13}^{H}$

$\underline{t} = (\underline{t}_1^T, \underline{t}_2^T, \ldots, \underline{t}_5^T)^T$

$\underline{t}_3^{H} = \underline{t}_{33}^{H} + \underline{t}_{35}^{H}$

$\underline{t}_1$ = total external torque on ith rigid body

$\underline{t}_4^{H} = \underline{t}_{44}^{H}$

t_{ij}^{H} = torque on body i from hinge j

$\underline{t}_5^{H} = \underline{t}_{55}^{H}$

$$G = A^{-1} = \begin{bmatrix} G_{11} & G_{12} & G_{13} & G_{14} & G_{15} \\ G_{21} & G_{22} & G_{23} & G_{24} & G_{25} \\ G_{31} & G_{32} & G_{33} & G_{34} & G_{35} \\ G_{41} & G_{42} & G_{43} & G_{44} & G_{45} \\ G_{51} & G_{52} & G_{53} & G_{54} & G_{55} \end{bmatrix} \qquad \text{where:} \quad G_{ji} = G_{ij}^{T} \tag{3-9}$$

$$A = \begin{bmatrix} I_1^* & A_{12} & A_{13} & A_{14} & A_{15} \\ A_{12}^T & I_2^* & A_{23} & A_{24} & A_{25} \\ - & - & I_3^* & A_{34} & A_{35} \\ - & - & - & I_4^* & A_{45} \\ A_{15}^T & - & - & A_{45}^T & I_5^* \end{bmatrix} \tag{3-10}$$

G_{ij} and A_{ij} = 3 x 3 submatrices within symmetric matricies.

The submatrices, A_{ij}, are derived from the original rigid body angular rate equations utilizing the symmetry properties derived for the hinge location vectors relative to the barycenter of each rigid body.

$$A_{ii} = I_i^* \quad i = 1,2,3,4,5$$

$$A_{12} = M\tilde{D}_{12}\tilde{D}_{22} = A_{13} = A_{21}^T = A_{31}^T \qquad A_{24} = M\tilde{D}_{24}\tilde{D}_{44} = A_{35} = A_{42}^T = A_{53}^T$$

$$A_{14} = M\tilde{D}_{12}\tilde{D}_{44} = A_{15} = A_{41}^T = A_{51}^T \qquad A_{25} = -M\tilde{D}_{22}\tilde{D}_{44} = A_{34} = A_{43}^T = A_{52}^T \tag{3-11}$$

$$A_{23} = -M\tilde{D}_{22}\tilde{D}_{22} = A_{32}^T = A_{23} \qquad A_{45} = -M\tilde{D}_{44}\tilde{D}_{44} = A_{54}^T = A_{45}$$

3.6 SUSPENSION EQUATIONS

The suspension equations express the torque acting upon each rigid body due to the vector sum of the forces acting on the hinge joints adjacent to the body. They may be expressed in vector matrix form as follows.

$$\underline{t}^H = LC_s\underline{\omega} + LK_s\hat{\underline{\alpha}} \qquad (3\text{-}12)$$

where:

$$\underline{t}^H = \left[-(\underline{t}_{s12} + \underline{t}_{s13})^T,\ (\underline{t}_{s12} - \underline{t}_{s24})^T,\ (\underline{t}_{s13} - \underline{t}_{s35})^T,\ \underline{t}_{s24}^T,\ \underline{t}_{s35}^T\right]^T$$

$$\underline{\omega} = (\underline{\omega}_1^T, \underline{\omega}_2^T, \ldots, \underline{\omega}_5^T)^T \qquad \underline{\omega}_1 = (\omega_{ix}, \omega_{iy}, \omega_{iz})^T \qquad \hat{\underline{\alpha}} = (\hat{\underline{\alpha}}_1^T, \hat{\underline{\alpha}}_2^T, \ldots, \hat{\underline{\alpha}}_5^T)^T$$

$$\hat{\underline{\alpha}}_1 = \underline{\alpha}_{24} \qquad \hat{\underline{\alpha}}_2 = \underline{\alpha}_{35} \qquad \hat{\underline{\alpha}} = \underline{\alpha}_{12} \qquad \hat{\underline{\alpha}}_4 = \underline{\alpha}_{13} \qquad \hat{\underline{\alpha}}_5 = \underline{\alpha}_1$$

$$\underline{\alpha}_i = (\phi_1, \theta_1, \psi_1)^T \qquad \underline{\alpha}_{ij} = (\Delta\phi_{ij}, \Delta\theta_{ij}, \Delta\psi_{ij})^T$$

$$\underline{t}^H = L\underline{ts} \qquad (3\text{-}13)$$

$$\underline{t}^H = \left[(\underline{t}_1^H)^T, (\underline{t}_2^H)^T, \ldots, (\underline{t}_5^H)^T\right]^T \qquad \underline{ts} = (\underline{t}_{s12}^T, \underline{t}_{s13}^T, \underline{t}_{s24}^T, \underline{t}_{35}^T)^T$$

$$L = \begin{bmatrix} I & -I & 0 & 0 \\ -I & 0 & -I & 0 \\ 0 & I & 0 & -I \\ 0 & 0 & I & 0 \\ 0 & 0 & 0 & I \end{bmatrix} \qquad (3\text{-}14)$$

where: $0 = \begin{bmatrix} 0 & 0 & 0 \\ 0 & 0 & 0 \\ 0 & 0 & 0 \end{bmatrix}$ and $I = \begin{bmatrix} I & 0 & 0 \\ 0 & I & 0 \\ 0 & 0 & I \end{bmatrix}$

$$\underline{ts} = K_s \hat{\underline{\alpha}} + C_s \underline{\omega} \qquad (3\text{-}15)$$

$$K_s = \begin{bmatrix} 0 & 0 & -K_{s12} & 0 & 0 \\ 0 & 0 & 0 & -K_{s13} & 0 \\ -K_{s24} & 0 & 0 & 0 & 0 \\ 0 & -K_{s35} & 0 & 0 & 0 \end{bmatrix}$$

$$C_s = \begin{bmatrix} C_{s12} & -C_{s12} & 0 & 0 & 0 \\ C_{s13} & 0 & -C_{s13} & 0 & 0 \\ 0 & C_{s24} & 0 & -C_{s24} & 0 \\ 0 & 0 & C_{s35} & 0 & -C_{s35} \end{bmatrix} \qquad (3\text{-}16)$$

3.7 EULER ANGLE RATE EQUATIONS

The Euler angle rate equations express the first time derivatives of the Euler angles of body 1 and the relative Euler angles between adjacent bodies of the vehicl model in terms of angular rates of rotation of the rigid bodies comprising the vehicle. For small angular displacements the linearized Euler angle equations are written in the following form.

$$\dot{\underline{\alpha}} = K\underline{\omega} \tag{3-17}$$

where:
$$K = \begin{bmatrix} 0 & -I & 0 & I & 0 \\ 0 & 0 & -I & 0 & I \\ -I & I & 0 & 0 & 0 \\ -I & 0 & I & 0 & 0 \\ I & 0 & 0 & 0 & 0 \end{bmatrix} \tag{3-18}$$

3.8 STATE VARIABLE ROTATIONAL DYNAMICS MODEL

The linearized rigid body angular rate equations and the linearized Euler angle rate equations may be combined into a state variable rotational dynamic model of the following form.

$$\begin{aligned} \dot{\underline{\omega}} &= GLC_g\underline{\omega} + GLK_g\hat{\underline{\alpha}} + G\underline{u} \\ \dot{\underline{\alpha}} &= K\underline{\omega} \end{aligned} \tag{3-19}$$

where $\underline{u} = \underline{t} = (\underline{u}_1^T, \underline{u}_2^T, \ldots, \underline{u}_5^T)^T$ = actuator torque vector and the remaining vector variables were defined earlier in this paper. If these vectors and matrices are expanded in terms of their scalar components and elements, respectively, they may be rearranged in such a way that scalars associated with a specific axis of the model are grouped into the same subvector. Each coefficient matrix appearing in the resulting state variable model possesses a high concentration of non-zero elements on or near its principal diagonal and few non-zero elements distant from this diagonal. This lightly coupled state variable model may be written in the following form.

$$\dot{\underline{x}}_j = \sum_{k=1}^{3} (A_{jk}\underline{x}_k + B_{jk}\underline{u}_k) \qquad j = 1,2,3 \qquad k = 1,2,3 \qquad (3\text{-}20)$$

where:

$$\underline{x}_k = (\underline{\omega}_k^T, \underline{\alpha}_k^T)^T$$

$$A_{jk} = \left[\begin{array}{c|c} \hat{G}_{jk}L_kC_{sk} & \hat{G}_{jk}L_kK_{sk} \\ \hline K_{jk} & [0] \end{array}\right] \qquad B_{jk} = \left[\begin{array}{c} \hat{G}_{jk} \\ \hline [0] \end{array}\right]$$

$[0]$ = 5X5 zero matrix

$$\underline{\omega}_1 = (\omega_{1x}, \omega_{2x}, \ldots, \omega_{5x})^T \quad \underline{\omega}_2 = (\omega_{1y}, \omega_{2y}, \ldots, \omega_{5y})^T$$

$$\underline{\omega}_3 = (\omega_{1z}, \omega_{2z}, \ldots, \omega_{5z})^T$$

$\underline{u}_k$ and $\underline{t}_k^H$ $(k = 1,2,3)$ have scalar expansions of the same form as $\underline{\omega}_k$

$$\underline{\alpha}_1 = (\Delta\phi_{2,4}, \Delta\phi_{3,5}, \Delta\phi_{1,2}, \Delta\phi_{1,3}, \phi_1)^T$$

$$\underline{\alpha}_2 = (\Delta\Theta_{2,4}, \Delta\Theta_{3,5}, \Delta\Theta_{1,2}, \Delta\Theta_{1,3}, \Theta_1)^T$$

$$\underline{\alpha}_3 = (\Delta\psi_{2,4}, \Delta\psi_{3,5}, \Delta\psi_{1,2}, \Delta\psi_{1,3}, \psi_1)^T$$

$$\underline{ts}_1 = (t_{sl2x}, t_{sl3x}, t_{s24x}, t_{s35x})^T$$

$\underline{ts}_2$ and $\underline{ts}_3$ have scalar expansions of the same form as that of $\underline{ts}_1$ with the subscripts y and z in the place of x, respectively.

L_k is a 5 x 4 matrix of the same form as the 5 x 4 partitioned matrix, L, with "1" in the place of each 3 x 3 submatrix, "I". K_{s1} is a 4 x 5 matrix of the same form as the 4 x 5 partitioned matrix, K_s, with k_{12x} in the place of each 3 x 3 submatrix, K_{s12}, and similar substitutions for the remaining submatrices. C_{s1} is a 4 x 5 matrix similarly developed from the 4 x 5 partitioned matrix, C_s. The matrices K_{s2} and C_{s2} are similarly expanded with the subscript, y, in the place of x as are the matrices K_{s3} and C_{s3} with the subscript, z, in the place of x.

$K_{jk} = 0$ for $k \neq j$. For $k = j$, it is a 5 x 5 matrix of the same form as the 5 x 5 partitioned matrix, K, with "1" in the place of each 3 x 3 submatrix, "I".

$$\hat{G} = \begin{bmatrix} \hat{G}_{11} & \hat{G}_{12} & \hat{G}_{13} \\ \hat{G}_{21} & \hat{G}_{22} & \hat{G}_{23} \\ \hat{G}_{31} & \hat{G}_{32} & \hat{G}_{33} \end{bmatrix} \qquad G = \begin{bmatrix} g_{11} \cdots g_{1,15} \\ \vdots \quad\quad \vdots \\ g_{15,1} \cdots g_{15,15} \end{bmatrix} = A^{-1}$$

$$\hat{G}_{1k}^T = \left[\underline{g}_{1k}, \underline{g}_{4k}, \underline{g}_{7k}, \underline{g}_{10k}, \underline{g}_{13k} \right]$$

$$\hat{G}_{2k}^T = \left[\underline{g}_{2k}, \underline{g}_{5k}, \underline{g}_{8k}, \underline{g}_{11k}, \underline{g}_{14k} \right]$$

$$\hat{G}_{3k}^T = \left[\underline{g}_{3k}, \underline{g}_{6k}, \underline{g}_{9k}, \underline{g}_{12k}, \underline{g}_{15k} \right]$$

$$\underline{g}_{j1}^T = (g_{j1}, g_{j4}, g_{j7}, g_{j10}, g_{j13})$$

$$\underline{g}_{j2}^T = (g_{j2}, g_{j5}, g_{j8}, g_{j11}, g_{j14})$$

$$\underline{g}_{j3}^T = (g_{j3}, g_{j6}, g_{j9}, g_{j12}, g_{j15})$$

3.9 MULTILEVEL STATE VARIABLE MODEL

The subscripts appearing in the state variable rotational dynamics model, equation (3-20) correspond to the axes of the model. The matrix coefficients, A_{jk} and B_{jk}, represent interaxial coupling when $k \neq j$. This model may be recast into multilevel form by decomposing it into a series of submodels. Decomposition temporarily supresses the interaxial coupling in the overall model producing three single axis submodels and a coordination submodel. It is effected by writing the following coordination equations which constitute the coordination subproblem.

$$\underline{a}_j = \sum_{\substack{k=1 \\ k\neq j}}^{3} (A_{jk}\underline{d}_{jk-j}^{k} + B_{jk}\underline{s}_{jk-j}^{k}) \qquad j = 1,2,3 \qquad (3\text{-}21)$$

$$\underline{d}_j^k = \underline{x}_k \qquad \underline{s}_j^k = \underline{u}_k \qquad k\neq j = 1,2,3 \qquad (3\text{-}22)$$

Equation set (3-22) is in the form of Gauss-Seidel coordination as presented in Wismer (3-5).

Substitution of equation sets (3-21) and (3-22) into the state variable rotational dynamics model of equation (3-20) yields three submodels of the following form.

$$\dot{\underline{x}}_j = A_{jj}\underline{x}_j + B_{jj}\underline{u}_j + \underline{a}_j(t) \qquad j = 1,2,3 \qquad (3\text{-}23)$$

The four submodels developed in this section may be assembled into the two level hierarchy shown in Figure 3-3.

When the relatively light coupling between the axes of the above model was neglected, it could be written in the following form.

$$\dot{\underline{x}}_j = A_{jj}\underline{x}_j + B_{jj}\underline{u}_j \qquad j = 1,2,3 \qquad (3\text{-}24)$$

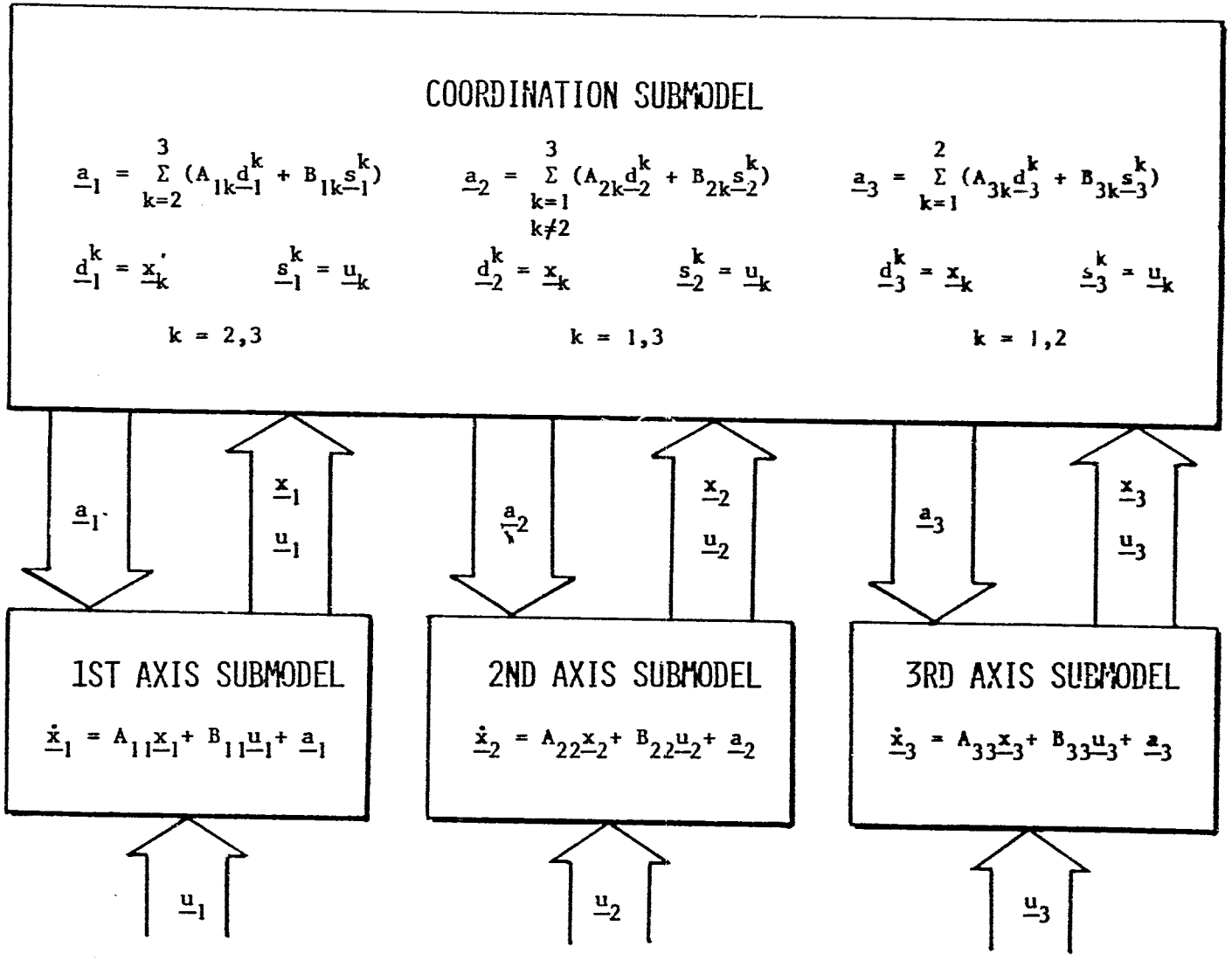

FIG. 3-3: SUBMODEL HIERARCHY FOR LINEARIZED DECOMPOSED STATE VARIABLE ROTATIONAL MODEL OF VEHICLE

3.10 REFERENCES

3-1. Cornell, G.A., "Derivation of the Equations of Motion of the Space Base Configurations I through XII." Bendix Research Laboratories Internal Memorandum, November 3, 1977.

3-2. Cornell, G.A., "Space Base Mathematical Model," Bendix Research Laboratories Internal Memorandum, December 14, 1977.

3-3. Lipski, D.B., "Linearized Five Body Space Base Simulation Model," Bendix Research Laboratories Internal Memorandum, April 23, 1979.

3-4. Lipski, D.B., "Discrete Coordinate Modeling of Flexible Bodies," Engineering Development Center Internal Memorandum, January 12, 1981.

3-5. Wismer, D.A., "Optimal Control of Distributed Parameter Systems Using Multilevel Techniques." Ph.D. dissertation, University of California, Los Angeles, California, 1966.

3-6. Chichester, F.D., "Application of Gauss-Seidel Multilevel Control to a Single Axis Torsional Model," Proceedings of the Space Transportation System Symposium, 1980 SAE Aerospace Congress and Exposition, October, 1980, Los Angeles Convention Center, Los Angeles, California.

SECTION 4

4.0 COMPARISON BETWEEN HYBRID MULTILEVEL-LQR AND LQR CONTROL APPROACHES APPLIED TO THREE AXIS FIVE BODY MODEL

4.1 COMPARISON OF SIMULATION RESPONSES

When the scalar equations comprising the original linearized state variable model were rearranged so that all equations pertaining to the same axis were grouped into the same submodel, the resulting overall model contained three submodels with light coupling between them. LQR control was applied to a model obtained by ignoring the coupling between the submodels associated with each of the three axes. Hybrid ML-LQR control was applied to a vehicle model that retained the interaxial coupling. Both controlled vehicle models were simulated on a digital computer. Their responses to an initial small angular displacement of one unit about the x axis and .1 unit about both the y axis and the z axis were plotted.

Responses of the decoupled model with LQR control appear in Figures 4-1 and 4-2. Angular displacement of the central body and angular displacement of the outer body of the solar panel relative to the body representing the inner portion of the solar panel are plotted on common axes in both figures. From the plots, it appears that the oscillations of the solar panels are reflected in the transient responses of the central body.

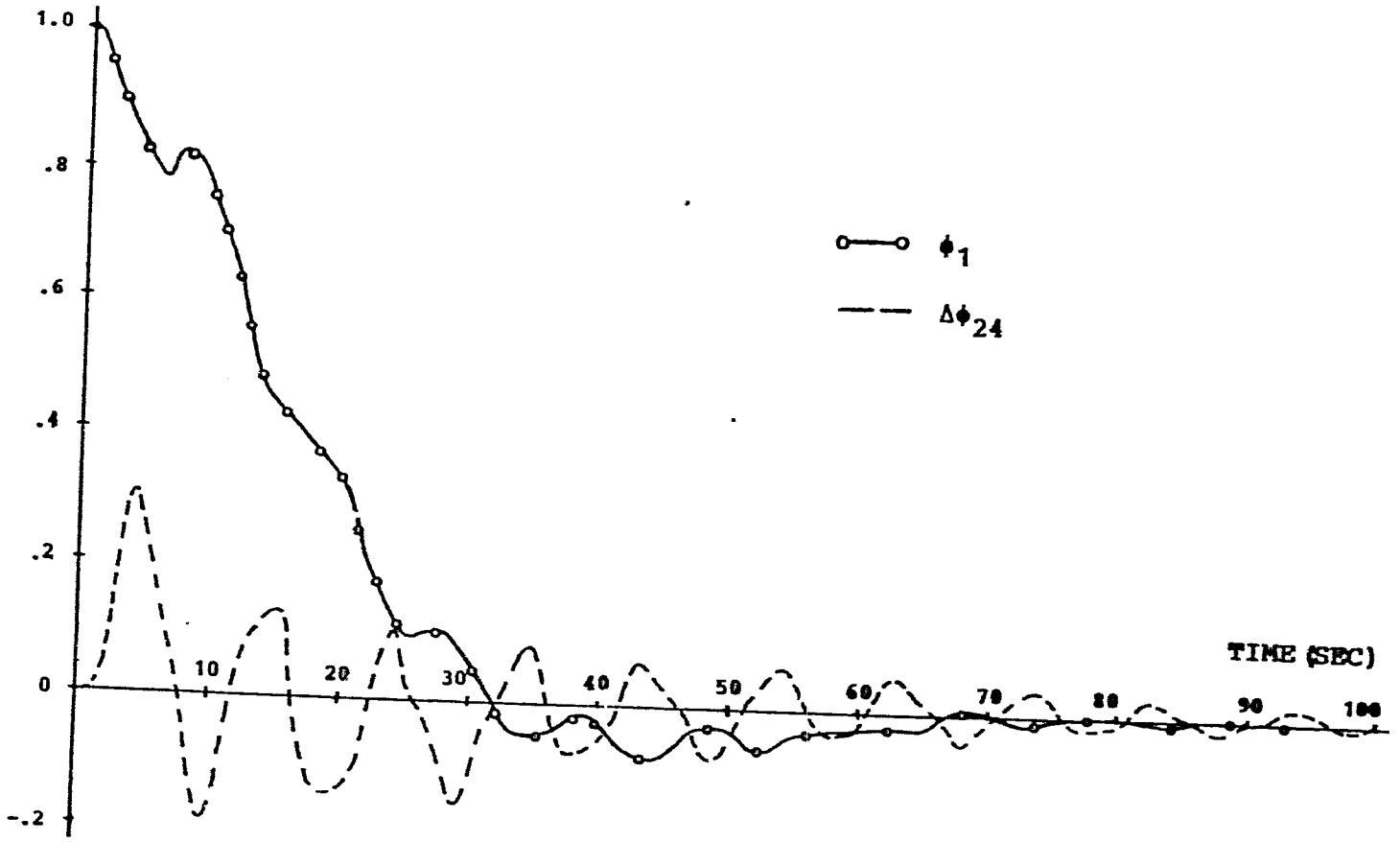

FIG. 4-1: RESPONSES OF THREE AXIS FIVE BODY MODEL WITH LQR CONTROL (X AXIS)

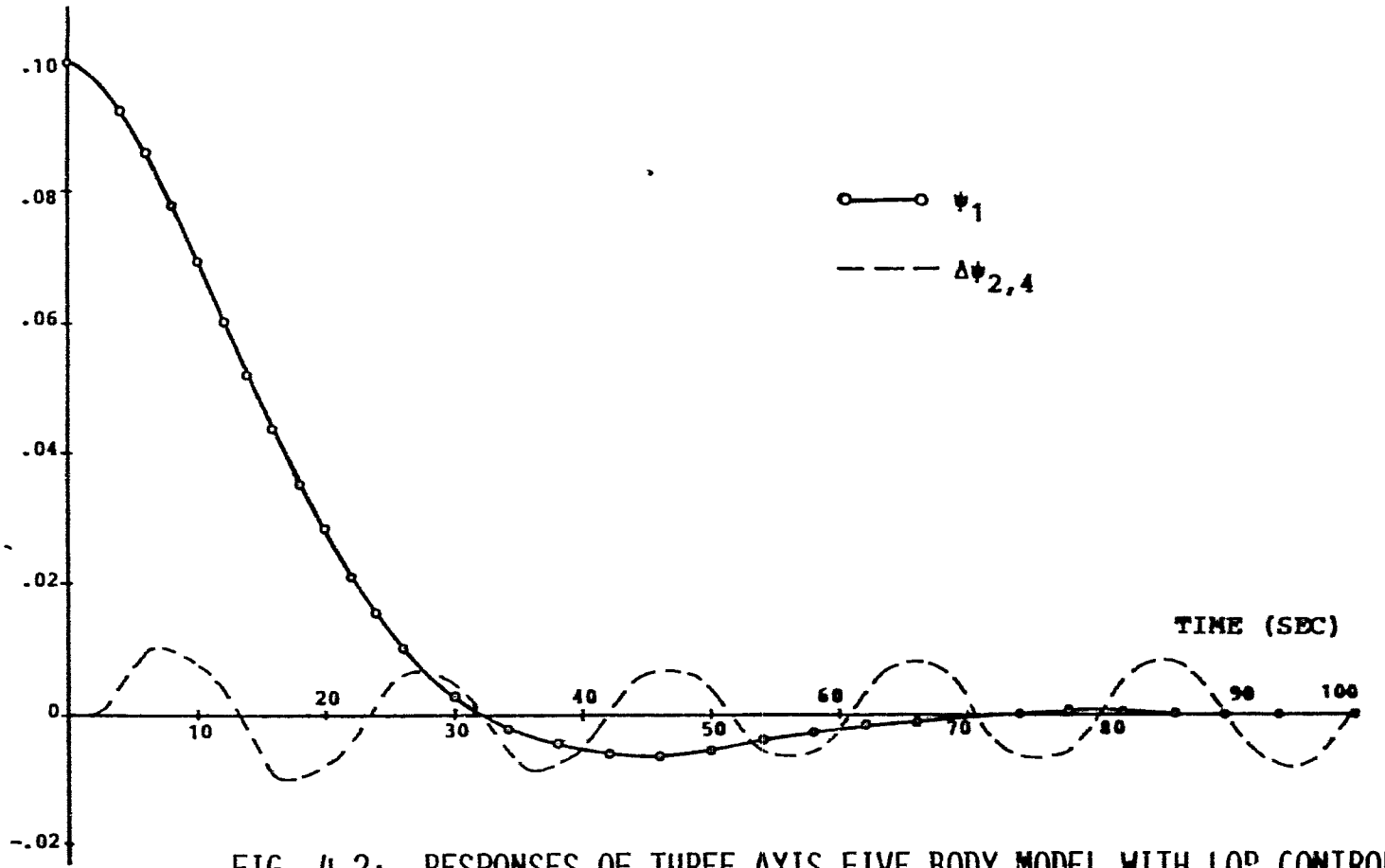

FIG. 4-2: RESPONSES OF THREE AXIS FIVE BODY MODEL WITH LQR CONTROL (Z AXIS)

Responses of the coupled model with hybrid ML-LQR control appear in Figures 4-3 through 4-6. In this series of plots the relative displacement of the outer body of the solar panel is separated from the plot of the angular displacement of the central body to facilitate direct comparison between the responses for LQR control and hybrid ML-LQR control. From these plots it is evident that the two control approaches produce very nearly the same responses to the same initial displacements.

The LQR control approach has been compared with that of hybrid ML-LQR control on the basis of the responses of the digital simulation of the two controlled systems to the same set of initial angular displacements. In the sequel, each of these control approaches is summarized to facilitate comparison of the two. Each approach is applied to one of the models previously presented and developed from techniques presented in Lipski (4-1), (4-2), Hooker and Margulies (4-3) and Chichester (4-4). Comparison of the analyses associated with the two control approaches is based in part upon Tiffany (4-5).

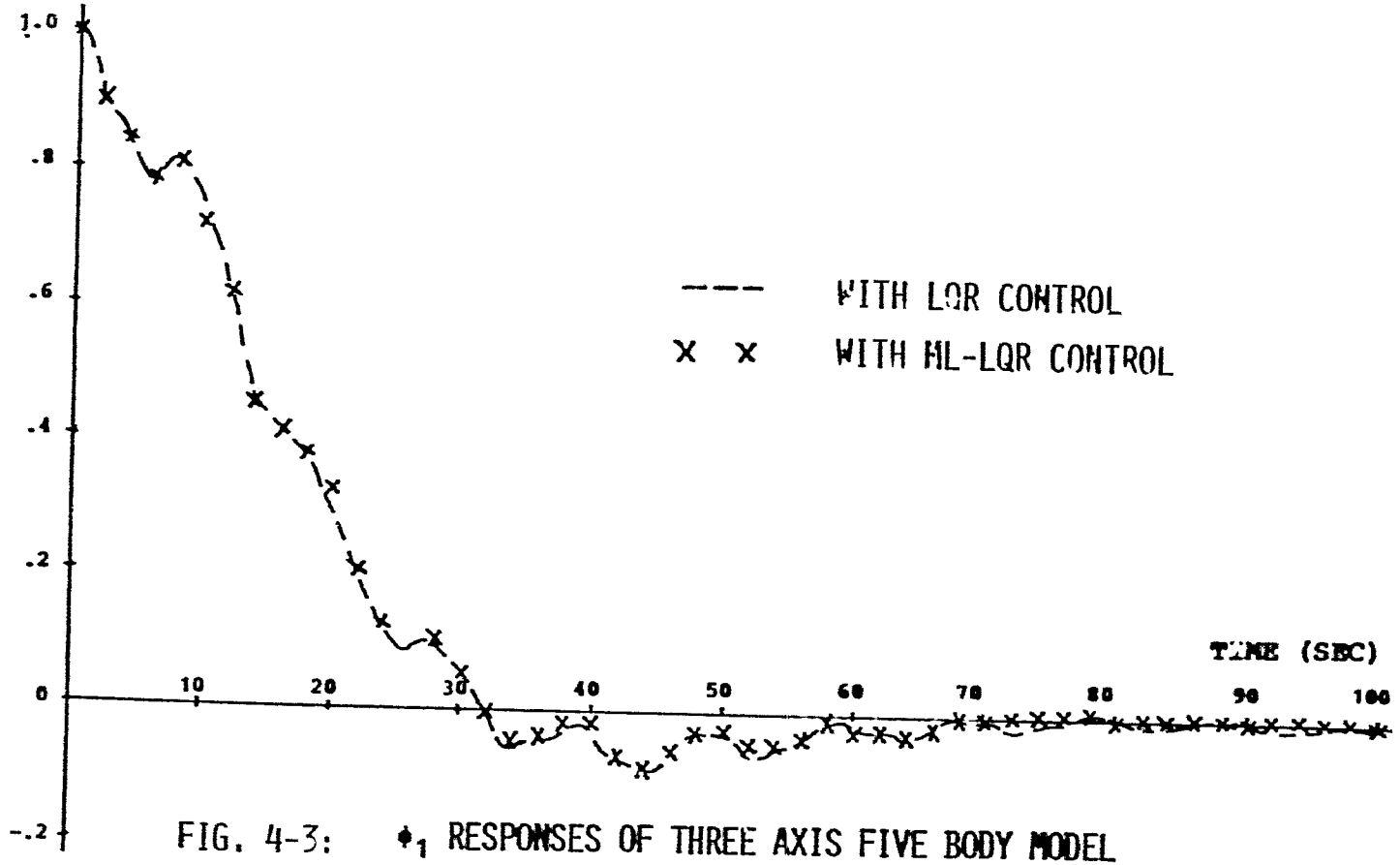

FIG. 4-3: ϕ_1 RESPONSES OF THREE AXIS FIVE BODY MODEL

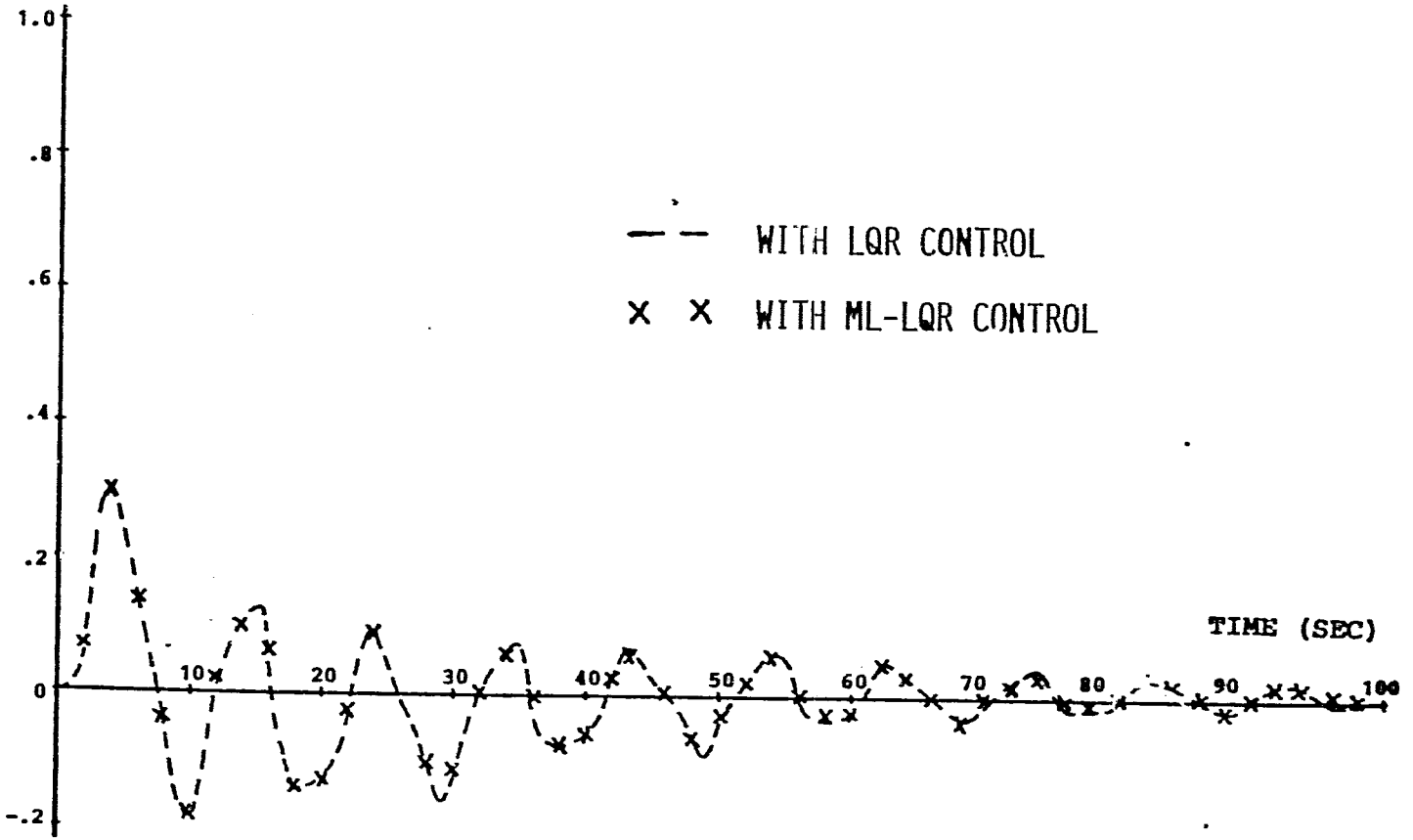

FIG. 4-4: $\Delta\phi_{24}$ RESPONSES OF THREE AXIS FIVE BODY MODEL

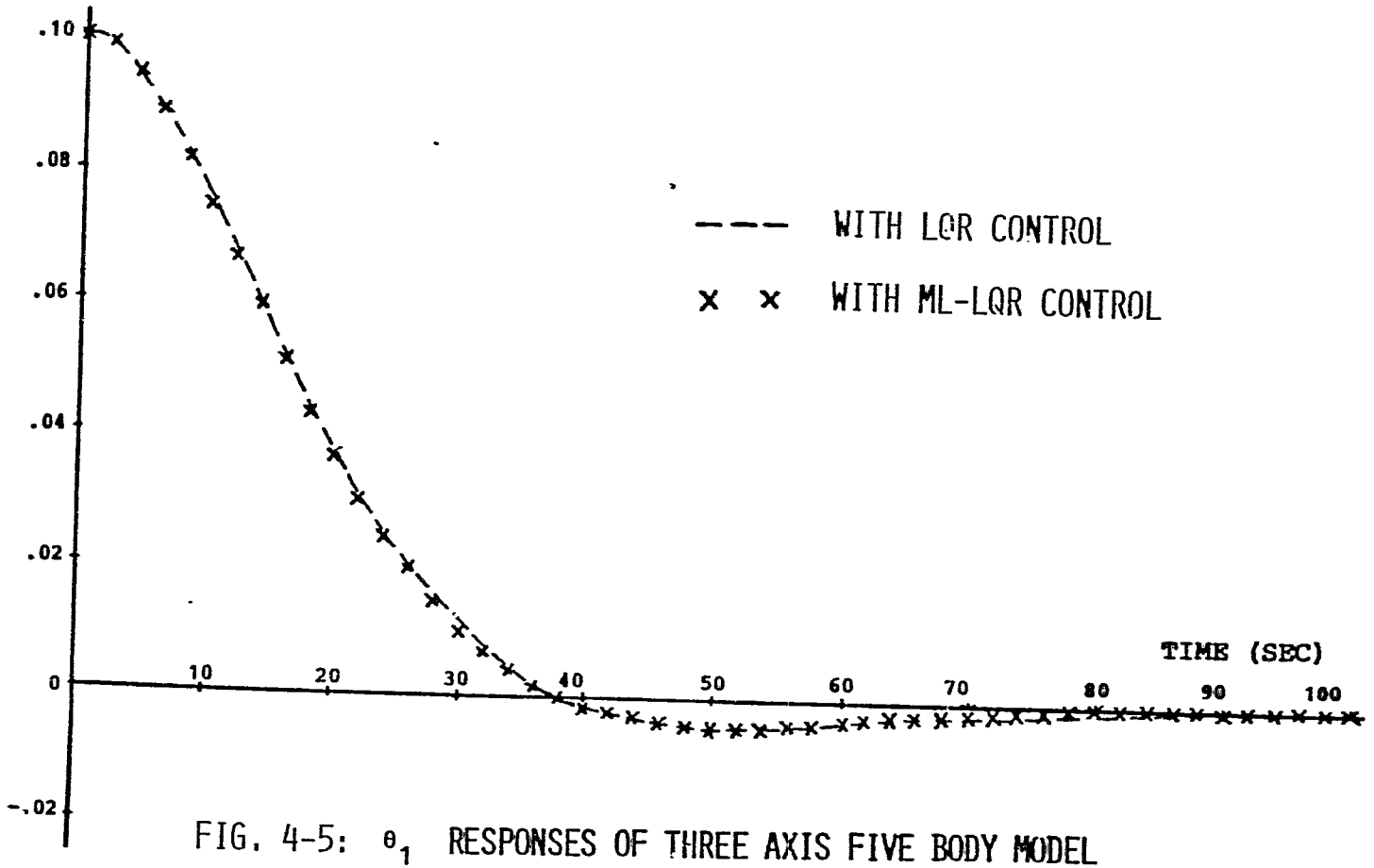

FIG. 4-5: θ_1 RESPONSES OF THREE AXIS FIVE BODY MODEL

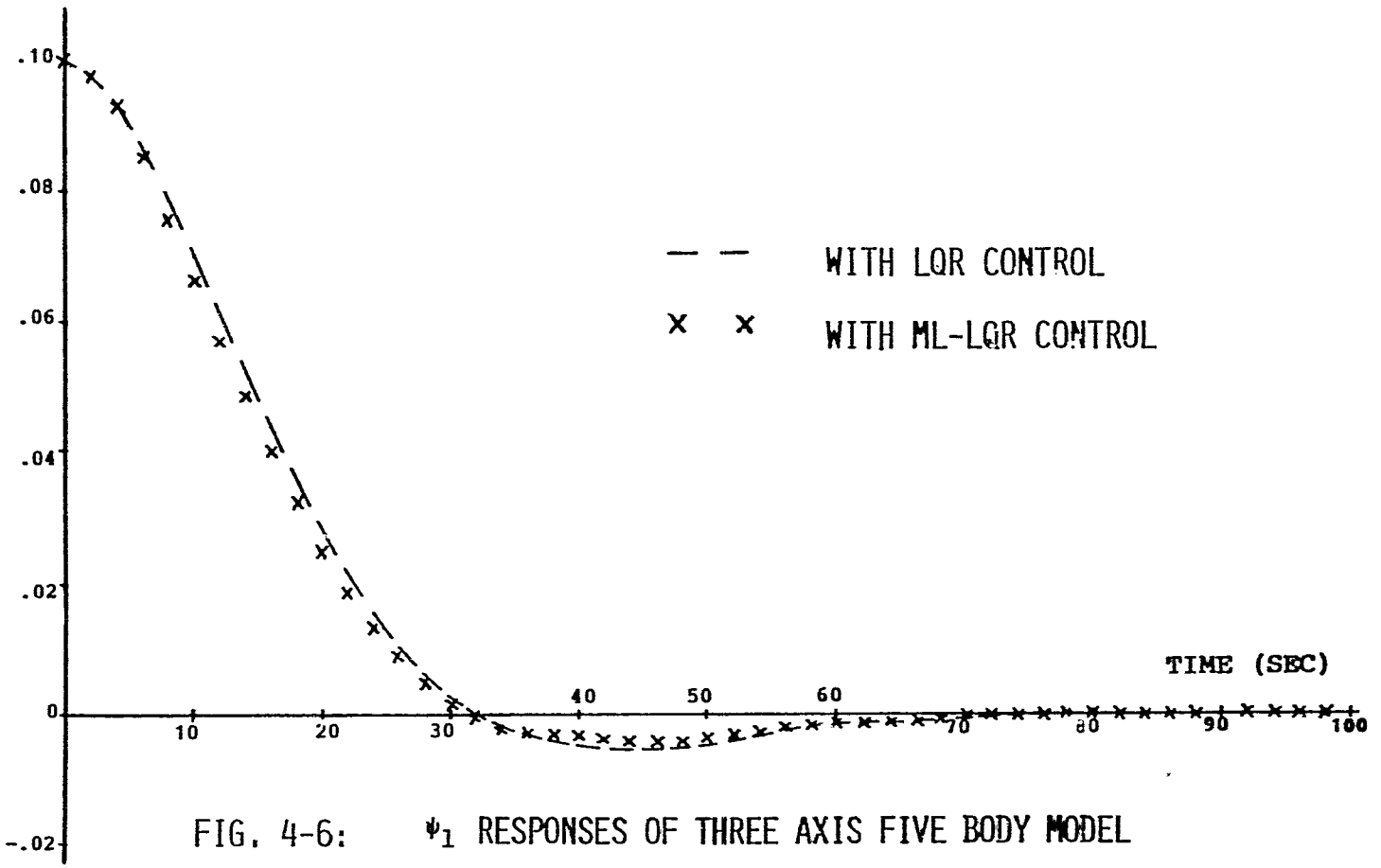

FIG. 4-6: ψ_1 RESPONSES OF THREE AXIS FIVE BODY MODEL

4.2 LQR CONTROL OF THE AXIALLY DECOUPLED THREE AXIS FIVE BODY MODEL OF A FLEXIBLE SPACECRAFT.

4.2.1 Decoupled State Variable Model

The axially decoupled rotational dynamic model of Space Construction Base Configuration 1 was represented by equation (3-24). It may be written more compactly as follows:

$$\dot{\underline{x}}_j = A_j \underline{x}_j + B_j \underline{u}_j \qquad j=1,2,3$$

where: (4-1)

$$\underline{x}_j = (\underline{\omega}_j^T, \underline{\alpha}_j^T)^T$$

$$\underline{x}_j(t_o) = \underline{x}_{j0} \text{ (initial boundary conditions)}$$

$$\underline{u}_j = \underline{T}\underline{A}_j$$

$$A_j = \left[\begin{array}{c|c} \hat{G}_{jj} L_j C_{sj} & \hat{G}_{jj} L_j K_{sj} \\ \hline \hat{K}_{jj} & [0] \end{array}\right]$$

$$B_j = \left[\begin{array}{c} \hat{G}_{jj} \\ \hline [0] \end{array}\right]$$

4.2.2 Generation of Three Hamiltonians and Their Minimization

Since the axes of the state variable model of the vehicle are decoupled from each other, optimal control is applied to each axis independently. Optimal linear quadratic regulator control of the attitude of the vehicle with respect to its jth axis corresponds to minimization of the jth Hamiltonian which incorporates the integrand of the quadratic performance index pertaining to control about the jth axis. This Hamiltonian may be expressed as follows:

$$H_j = P_j + \underline{\lambda}_j^T(A_j\underline{x}_j + B_j\underline{u}_j) \qquad (4\text{-}2)$$

where: P_j = the integrand of the jth quadratic performance index

$$= \frac{1}{2}(\underline{x}_j - \underline{x}_{jd})^T Q_J(\underline{x}_j - \underline{x}_{jd}) + \frac{1}{2}\underline{u}_j^T W_{ju}^{-1}\underline{u}_j$$

$\underline{x}_{jd}$ = specified value of $\underline{x}_j$

Q_j = state variable error weighting coefficient matrix

W_{ju} = control energy weighting coefficient matrix

$\underline{\lambda}_j$ = jth costate vector

The jth costate equation is obtained from a necessary condition for minimization of the jth Hamiltonian.

$$\dot{\underline{\lambda}}_j = \frac{\partial H_j}{\partial \underline{x}_j} = -Q_j \underline{x}_j - A_j^T \underline{\lambda}_j \tag{4-3}$$

Another necessary condition for minimization of the Hamiltonian yields the control equation,

$$\underline{u}_j = - W_{ju}^{-1} B_j^T \underline{\lambda}_j \tag{4-4}$$

4.2.3 Formulation and Solution of jth TPBV Sub-Problem

Substitution of the control equation into the state equation (4-1) and association of the costate equation given by equation (4-3) with the resulting equation yields a two point boundary value (TPBV) problem to be solved of the following form.

$$\begin{aligned} \dot{\underline{x}}_j &= A_j \underline{x}_j + R_j \underline{\lambda}_j \\ \dot{\underline{\lambda}}_j &= -Q_j \underline{x}_j - A_j^T \underline{\lambda}_j \end{aligned} \tag{4-5}$$

where:

$$R_j = -B_j W_{ju}^{-1} B_j^T$$

$\underline{x}_j(t_o) = \underline{x}_{jo}$ (initial boundary condition)

$\underline{\lambda}_j(t_f) = \underline{0}$ (final boundary condition)

Solution of this TPBV problem is effected by assuming that:

$$\underline{\lambda}_j = K_j(t)\underline{x}_j \tag{4-6}$$

Differentiation of equation (4-6) with respect to time and substitution of the resulting expressions for $\underline{\lambda}_j$ and $\dot{\underline{\lambda}}_j$ into equation set (4-5) transforms solution of the jth TPBV subproblem to solution of the jth Riccati equation for K_j.

$$\dot{K}_j = -(K_jA_j + A_j^TK_j + K_jR_jK_j + Q_j) \quad j = 1,2,3 \tag{4-7}$$

where:

$$R_j = B_jW_{ju}^{-1}B_j^T \tag{4-8}$$

$$\underline{u}_j = W_{ju}^{-1}B_j^TK_j\underline{x}_j = F_j\underline{x}_j \tag{4-9}$$

$$K_j(t_f) = [0]$$

Substitution of equation (4-6) into the control equation yields the relationship for obtaining the optimal feedback control utilizing the solution to the jth Riccati equation.

4.3 HYBRID ML-LQR CONTROL OF THE THREE AXIS FIVE BODY MODEL OF A FLEXIBLE SPACE VEHICLE WITH INTERAXIAL COUPLING.

4.3.1 State Variable Model with Coupling

The axially coupled state variable rotational dynamic model of Space Construction Base Configuration 1 was presented in equation set (3-20). In this set of equations, the subscripts identify the axes of the model and terms involving both subscripts in which $k \neq j$ represent interaxial coupling.

4.3.2 Decomposed Model

Application of Gauss-Seidel multilevel control to this system begins with decomposition of the state variable model to temporarily suppress this coupling. The resulting coordination equations were presented in equation sets (3-21) and (3-22). The corresponding decomposed model of the rotational dynamics is represented by equation set (3-23). Comparison of equation set (3-23) with equation set (3-24) for the decoupled model reveals that the decomposed model has additional terms on the right hand side due to interaxial coupling.

4.3.3 Generation of Decomposed Hamiltonian and Its Minimization

Optimal control may be applied to this decomposed state variable model by extension of the procedure described above for applying LQR control to the model in which the three axes are decoupled.

The modified procedure involves the generation of a decomposed performance index and a decomposed Hamiltonian

corresponding to the decomposed form of the state equations. The application of necessary conditions for the minimization of the decomposed Hamiltonian yields a set of costate equations and costate coordionation equations as well as a set of control and control coordination equations.

The state, costate and control coordination equations are combined into an overall coordination subproblem. Inputs to this subproblem are the state, costate and control vectors while its outputs are the various coordination vectors.

4.3.4 Formulation of TPBV Subproblems

When the control equations are substituted into the corresponding state equations and each costate equation is associated with its corresponding state equation, the resulting set of two-point boundary value subproblems to be solved is written in the following form:

$$\begin{aligned} \dot{\underline{x}}_j &= A_{jj}\underline{x}_j + R_j\underline{\lambda}_j + \hat{\underline{a}}_j(t) \\ \dot{\underline{\lambda}}_j &= Q_j\underline{x}_j - A_{jj}^T\underline{\lambda}_j + \hat{\underline{b}}_j(t) \end{aligned} \qquad j = 1,2,3 \qquad (4\text{-}10)$$

where:

$R_j = -B_{jj}W_{uj}^{-1}B_{jj}^T$

$\hat{\underline{a}}_j(t)$, $\hat{\underline{b}}_j(t)$ = functions of the coordination variables

$\underline{x}_j(t_o) = \underline{x}_{jo}$ (initial boundary condition)

$\underline{\lambda}_j(t_f) = \underline{0}$ (final boundary condition)

4.3.5 Extended LQR Solution of TPBV Subproblem

The presence of additional terms on the right hand side of the TPBV problem represented by equation set (4-10) compared with the TPBV problem represented by equation set (4-5) requires an extension of the LQR approach. In this extension of LQR control, it is assumed that the costate variables may be written in the following form.

$$\underline{\lambda}_j = K_j(t)\underline{x}_j + \underline{m}_j(t) \qquad (4\text{-}11)$$

where:

$K_j(t)$ = time varying matrix to be determined.

$\underline{m}_j(t)$ = time varying vector to be determined.

Differentiating equation (4-11) with respect to time and substituting the resulting expressions for $\underline{\lambda}_j$ and $\dot{\underline{\lambda}}_j$ in equation set (4-10) transforms the jth TPBV subproblem to a pair of Riccati-type equations to be solved for K_j and $\underline{m}_j$.

$$\dot{K}_j = -(K_j A_{jj} + A_{jj}^T K_j + K_j R_j K_j + Q_j) \qquad j = 1,2,3 \qquad (4\text{-}12)$$

$$\dot{\underline{m}}_j + (K_j R_j + A_{jj}^T)\underline{m} + K_j \hat{\underline{a}}_j + \hat{\underline{b}}_j = \underline{0} \qquad (4\text{-}13)$$

where

$$K_j(t_f) = [0]$$

$$\underline{m}_j(t_f) = \underline{0}$$

Solution of this pair of equations along with equation (4-11) leads to generation of the feedback control needed to minimize the portion of the overall performance index associated with the jth axis subject to values of the coordination variables obtained from the coordination subproblem. Other outputs obtained from the jth TPBV subproblem include the state vector, $\underline{x}_j$, and the costate vector, $\underline{\lambda}_j$.

4.3.6 Construction of Subproblem Hierarchy

Due to the relationship between their respective inputs and outputs, the coordination subproblem and the TPBV subproblems may be assembled into the subproblem hierarchy shown in Figure 4-7. Solution of the overall optimal attitude control problem is then attained by iteration between the subproblems in the hierarchy.

4.4 COMPARISON BETWEEN THE TWO APPROACHES

Had the LQR control techniques been applied directly to the coupled model, each of the coefficient matrices would have had dimensions three times as large as they are for the coefficient matrices associated with either the application of LQR control to the axially decoupled model or the application of hybrid ML-LQR techniques to the coupled model. Hybrid ML-LQR control, therefore, reduces the problem of optimally controlling the attitude of the coupled vehicle model to a form closely approximating the control of its attitude with respect to each of its axes independently with periodic adjustments by the coordination subproblem to account for the effects of

interaxial coupling. Part of the price of attaining this result is greater complexity in the control system and the addition of iteration between the subproblems of the hierarchy in the generation of the optimal control solution. However, this iterative model of solution implies an adaptive capability not present in the conventional LQR control approach.

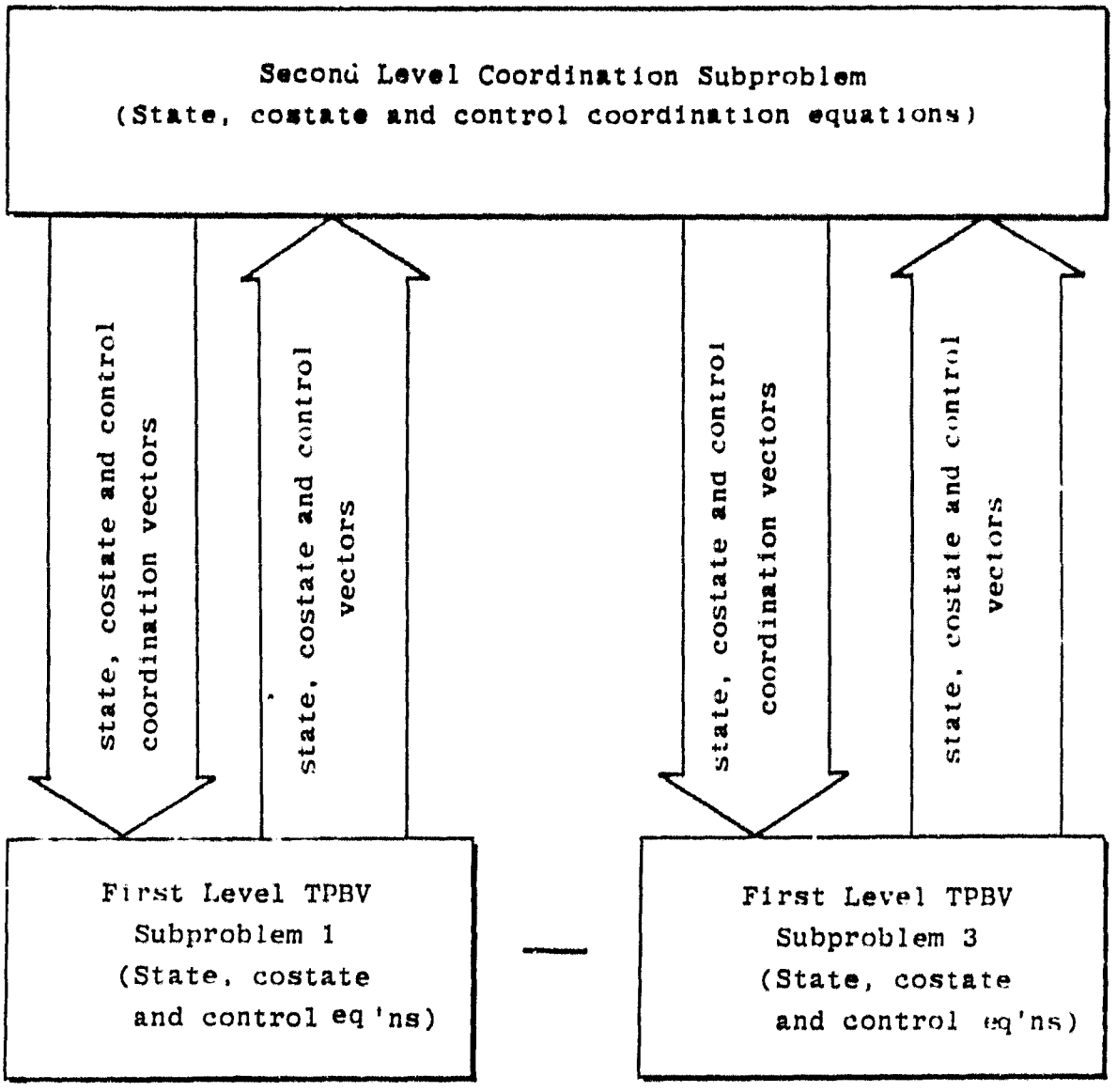

FIG. 4-7: SUBPROBLEM HIERARCHY FOR HYBRID MULTILEVEL-LQR ATTITUDE CONTROL OF FIVE BODY MODEL

4.5 REFERENCES

4-1. Lipski, D.P., "State Variable Representation of the Five Body Linearized Space Construction Base," Bendix Engineering Development Center Internal Memorandum, September 5, 1980.

4-2. Lipski, D.P., "Discrete Coordinate Modeling of Flexible Bodies," Bendix Engineering Development Center Internal Memorandum, January 12, 1981.

4-3. Hooker, W.W. and G.J. Margulies, "The Dynamical Equations for an n-Body Satellite", J. Astronaut Science., Vol. 12, 1965, pp. 123-128.

4-4. Chichester, F.D., "Application of Gauss-Seidel Multilevel Control to a Single Axis Torsional Model", Proceedings of the Space Transportation System Symposium, SAE Aerospace Congress and Exposition, Los Angeles, California,October 15, 1980.

4-5. Tiffany, N.O., "Comparison of Multilevel and LQR Control for Spacecraft Stabilization and Control", Bendix Engineering Development Center Internal Memorandum, October 23, 1980.

SECTION 5

5.0 REVIEW OF SIMULATION RESULTS OF THREE AXIS FIVE BODY MODEL OF A FLEXIBLE SPACECRAFT

An internal memorandum by N.O. Tiffany (5-1) was reviewed and is summarized herein. The purpose of this report was to document the results obtained to date with the simulations of multilevel and LQR control at the Bendix Engineering Development Center in support of this study contract and to outline fruitful areas for further work.

Plots of the controlled responses of uncoupled and lightly coupled forms of the linearized five body state variable rotational model of a flexible space vehicle to initial angular displacements were generated on the Bendix Engineering Development Center digital computer. The prototype vehicle whose attitude was controlled is depicted in Figure 3-1 while its corresponding topological diagram in which each flexible appendage was approximated by two rigid bodies interconnected by a spring hinge suspension appears in Figure 3-2. The subproblem hierarchy developed for the application of a combination of multilevel and an extension of LQR control techniques to the coupled form of the model is shown in Figure 4-7. The uncoupled linearized five body model was derived from the coupled model by ignoring the light coupling between its three spatial axes. LQR attitude

control was then applied to each axis independently. In the application of hybrid ML-LQR attitude control the coupled model was partitioned by spatial axes and the coupling between these axes was temporarily suppressed as explained in Section 3.9.

Plots of responses of the central body of the vehicle to angular displacements about the x, y and z axes appear in Figures 5-1, 5-2 and 5-3 respectively. The responses of the uncoupled model with LQR attitude control applied independently about each axis and of the coupled model with hybrid ML-LQR of control to the same initial angular displacements are plotted with common sets of coordinates. Those responses pertaining to the uncoupled model are distinguished by small circles. It is evident that the angular responses of the central body of the coupled model with hybrid ML-LQR control compare very closely with the corresponding responses for the uncoupled model with LQR control applied to each axis independently.

Multilevel control temporarily suppresses interaxial coupling effectively reducing the problem of controlling the coupled model to the problem of controlling the decoupled model with later coordination.

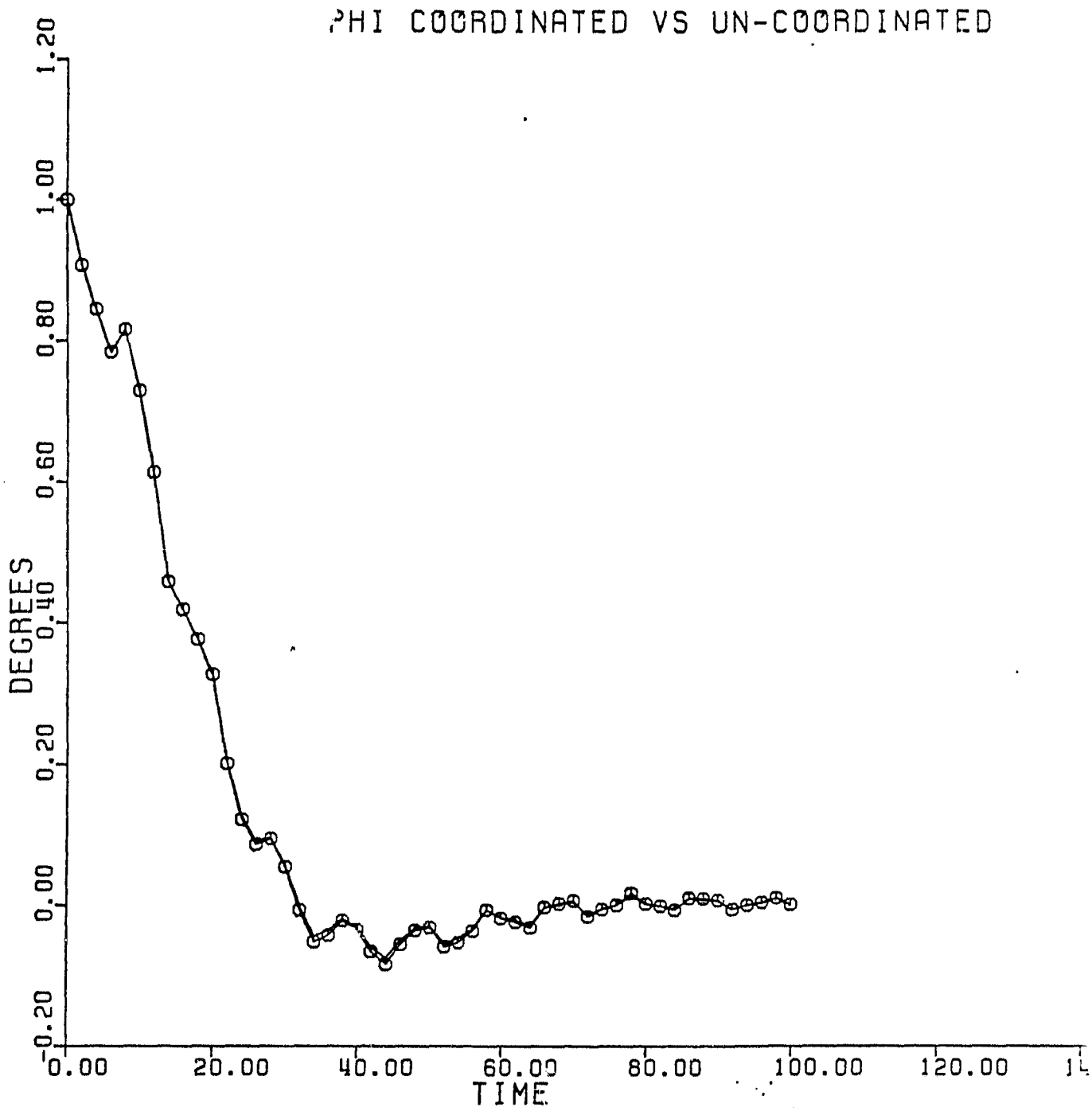
PHI COORDINATED VS UN-COORDINATED
DEGREES
1.20
1.00
0.80
0.60
0.40
0.20
0.00
-0.20
0.00
20.00
40.00
60.00
80.00
100.00
120.00
TIME

FIGURE 5-1

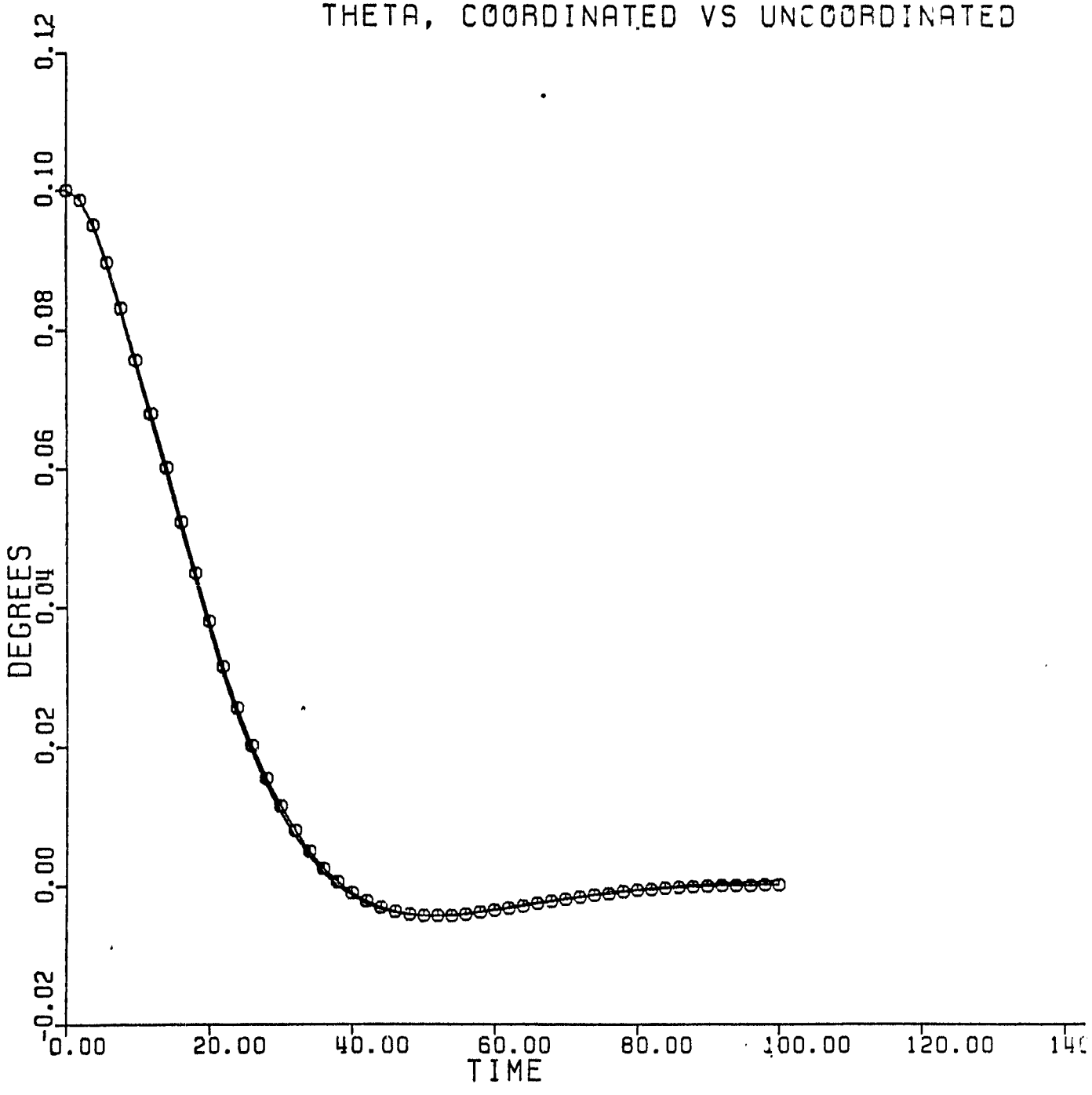
THETA, COORDINATED VS UNCOORDINATED
DEGREES
0.12
0.10
0.08
0.06
0.04
0.02
0.00
-0.02
0.00
20.00
40.00
60.00
80.00
100.00
120.00
TIME

FIGURE 5-2

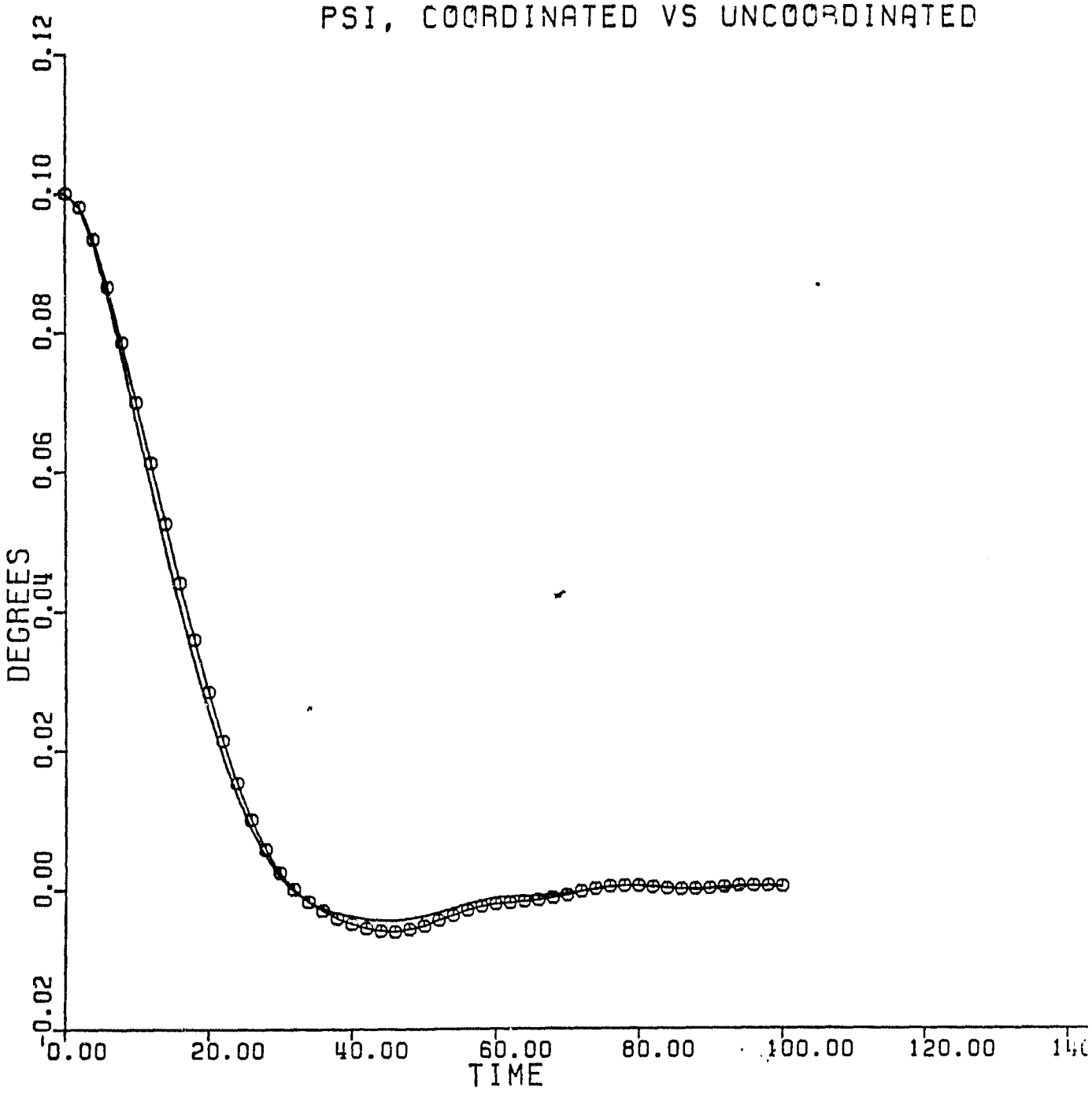
PSI, COORDINATED VS UNCOORDINATED
0.12
0.10
0.08
0.06
0.04
0.02
0.00
-0.02
DEGREES
0.00
20.00
40.00
60.00
80.00
100.00
120.00
TIME

FIGURE 5-3

Additional response plots were drawn for cases in which the control laws generated for the nominal controlled system were applied to a system in which the values of damping coefficients and the spring constants of the model were changed. Plots of the angular attitude responses of the central body of the model about its x axis appear in Figures 5-4, 5-5 and 5-6 in order of increasing perturbation of these parameters. In each figure the response of the perturbed system is identified by small triangles with the responses of the unperturbed system included to facilitate comparison. The principal differences between the two classes of responses are slightly increased damping and phase shift for the responses of the perturbed system. In general, however, the control of the vehicle appears quite insensitive to such mismatches between the model upon which the generation of the control law was based and the system to which it was applied.

5.1 SENSITIVITY OF CONTROL LAW TO SYSTEM PARAMETERS

The use of a control law depends upon a suitable model of the system to be controlled. Suppose that the system to be controlled is represented by the state equation

$$\dot{\underline{x}} = A\underline{x} + B\underline{u} \qquad (5\text{-}1)$$

while the control law is based on a model of this system represented by

$$\dot{\underline{x}}' = A'\underline{x}' + B'\underline{u} \qquad (5\text{-}2)$$

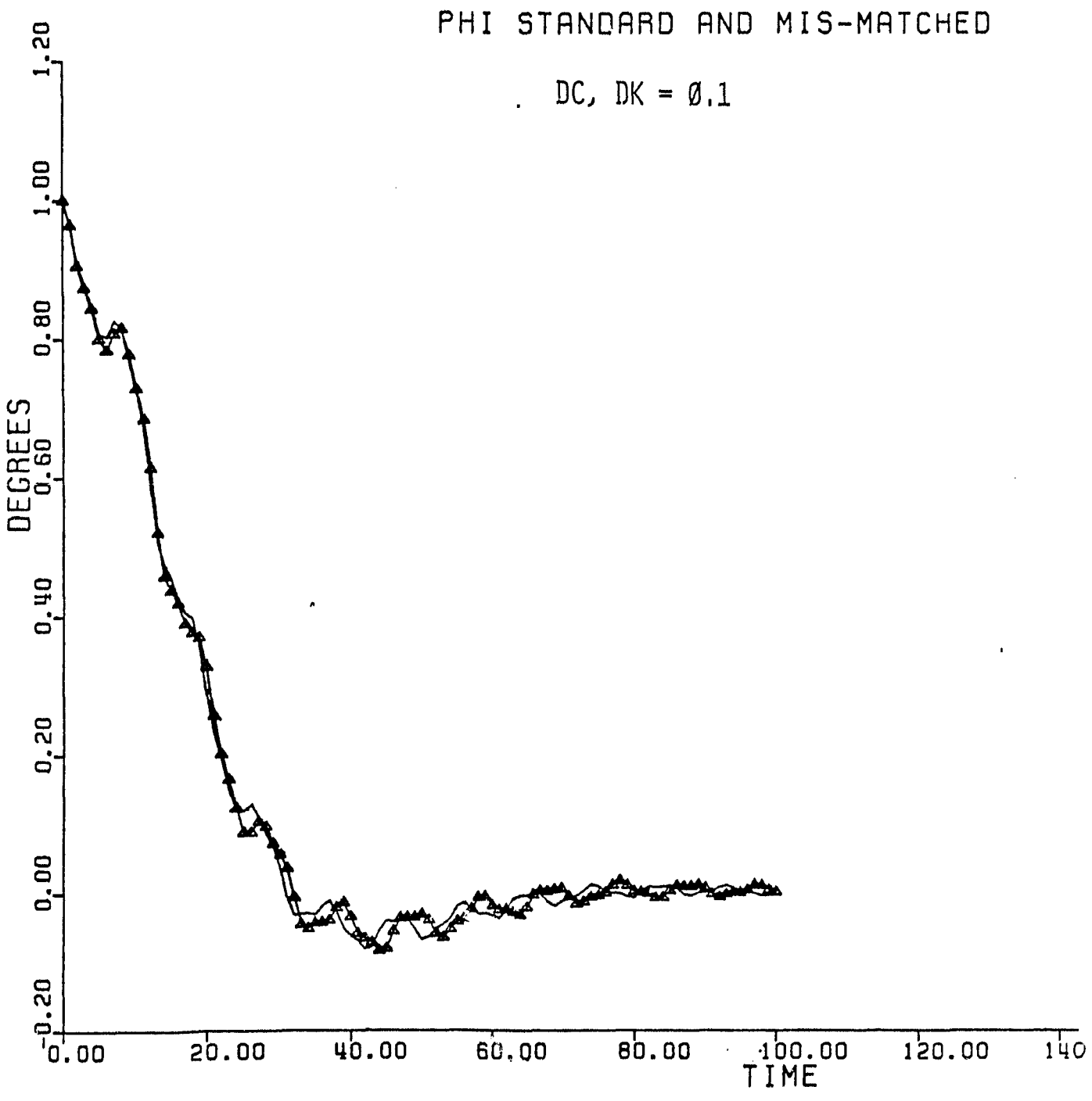
PHI STANDARD AND MIS-MATCHED
DC, DK = Ø.1
DEGREES
1.20
1.00
0.80
0.60
0.40
0.20
0.00
-0.20
0.00
20.00
40.00
60.00
80.00
100.00
120.00
140
TIME

FIGURE 5-4

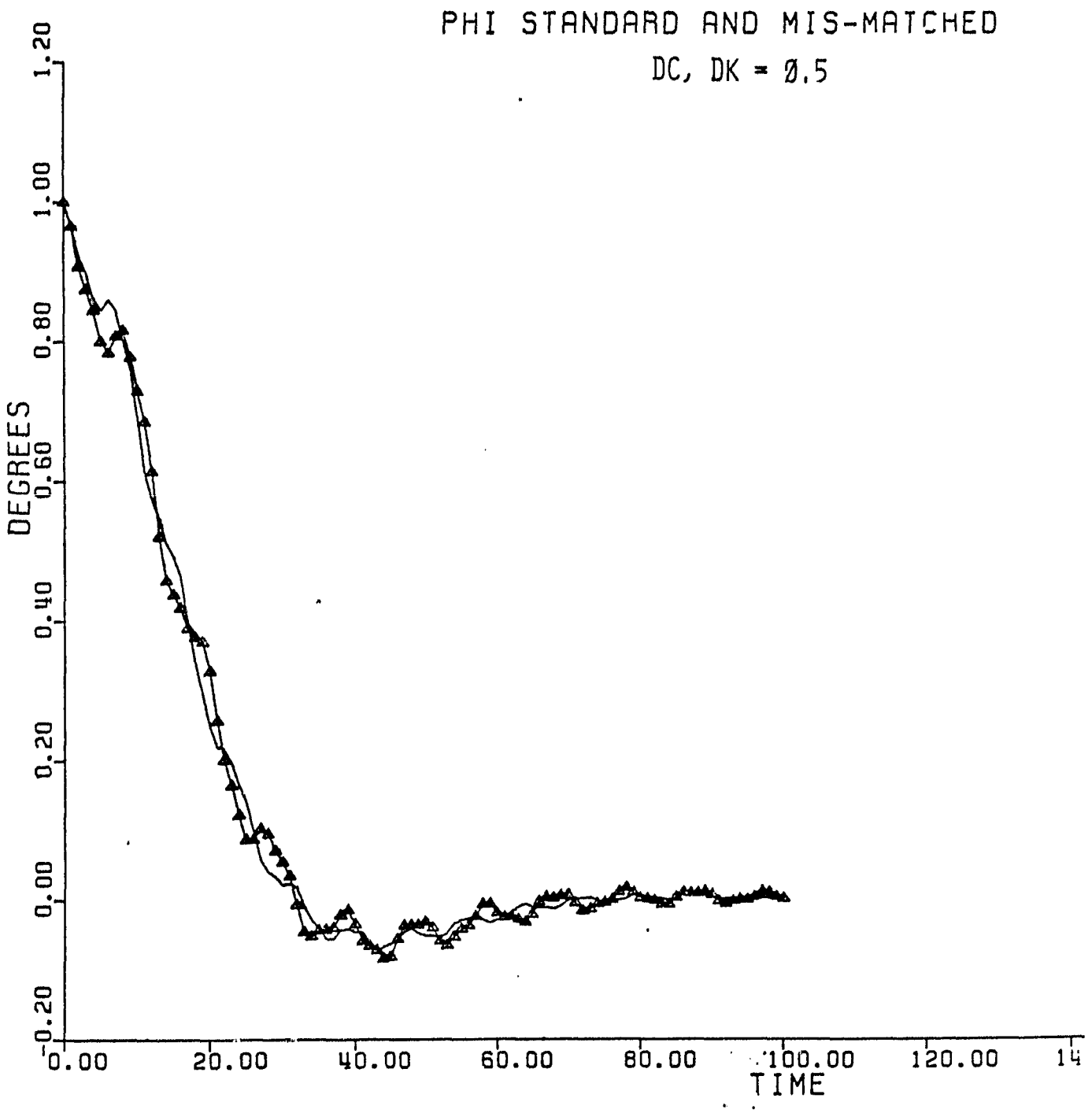
PHI STANDARD AND MIS-MATCHED
DC, DK = Ø.5
DEGREES
1.20
1.00
0.80
0.60
0.40
0.20
0.00
-0.20
0.00
20.00
40.00
60.00
80.00
100.00
120.00
14
TIME

FIGURE 5-5

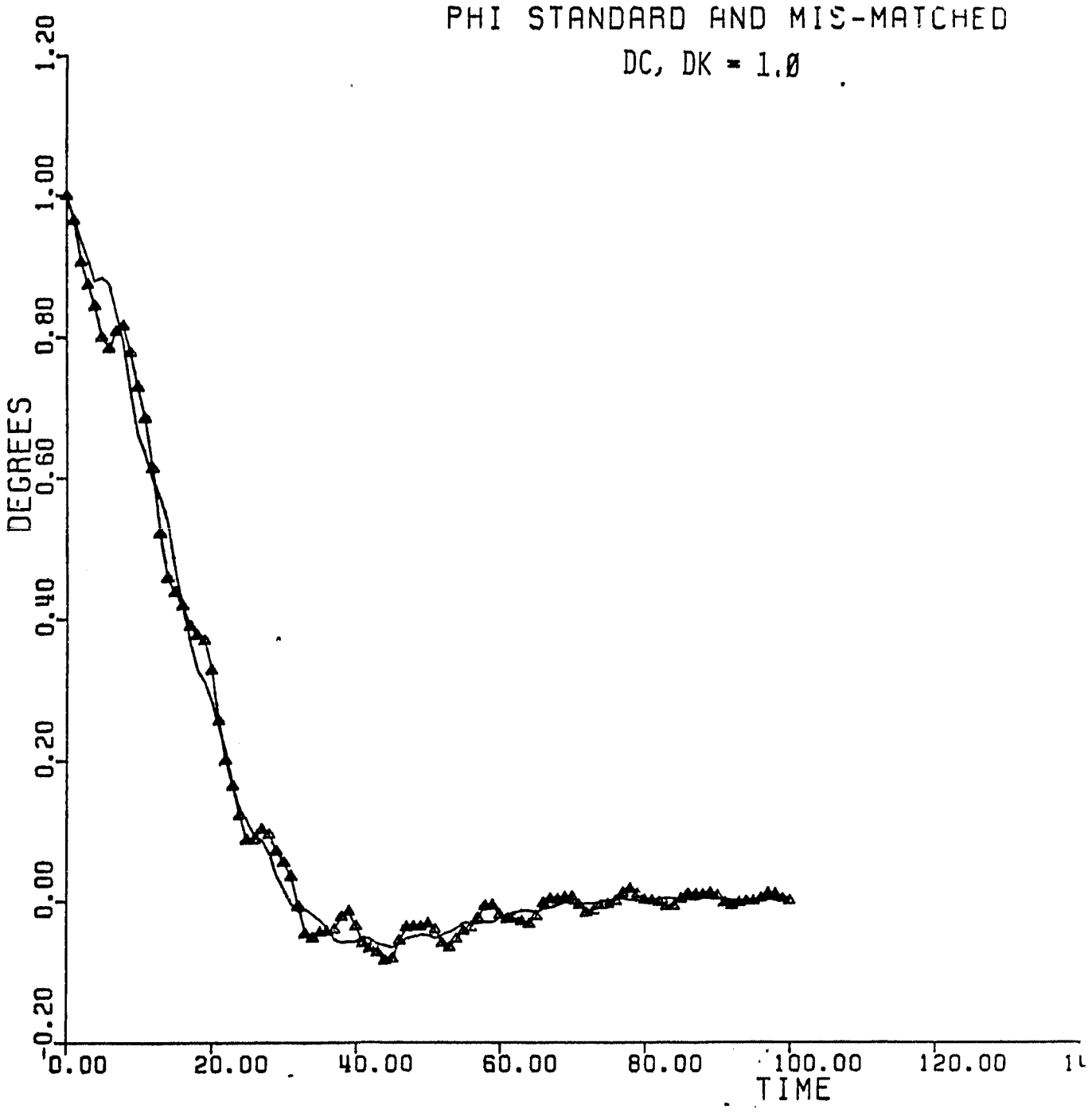
PHI STANDARD AND MIS-MATCHED
DC, DK = 1.Ø
DEGREES
1.20
1.00
0.80
0.60
0.40
0.20
0.00
-0.20
0.00
20.00
40.00
60.00
80.00
100.00
120.00
TIME

FIGURE 5-6

The question arises as to the effect of differences between equations (5-1) and (5-2). These may differ in many ways including the dimensionality of the system. In the case of the five body model, the sensitivity of the control to some of the parameters involved was investigated. From equation (3-20), the A matrix is of the form

$$A = \begin{bmatrix} GLC_s & GLK_s \\ K & O \end{bmatrix} \qquad (5-3)$$

Here, K_s involves spring constants, C_s involved damping, and G involves mass distribution and geometry. B depends upon G only, and the K in equation (5-3) is independent of system parameters.

An investigation was conducted, in which the spring constants and damping constants were subjected to variations, and the control law as developed without those variations was applied. That is, A' in equation (5-2) was fixed, and A in equation (5-1) was varied. Each damping constant c' contributing to A' was modified to $c = (1 + DC)c'$, and similarly, $k = (1 + DK)k'$. The effects on the central body angle ϕ_1 for variations of DC, DK = 0.1, 0.5 and 1.0 are shown in Figures 5-4, 5-5 and 5-6, respectively. The conclusion is that the control law is quite insensitive to these parameters, in a macro sense. This study was conducted on the uncoordinated control only, but the results are applicable to the partitioned control also, since the coupling is weak.

5.2 CHOICE OF PARTITIONING

The five body three axis partitioned control converged after two iterations, due to the weak coupling between axes. The 5 body control system must operate on 10x10 matrices, with a resulting penalty in computation time. The choice of partitioning was guided by intuition and insight. A more systematic approach is desirable. The choice made with the five body model attempts to increase convergence by satisfying the following independence conditions. If $\hat{\underline{a}}_j \equiv \underline{0}$ and $\hat{\underline{b}}_j \equiv \underline{0}$, then $\underline{m}_j = 0$ and the jth subsystem is completely controlled by K_j alone, and is independent of $\underline{x}_j$. This condition will occur if A_{ij}, R_{ij} and Q_{ij} are zero for $j \neq i$. Further partitioning may be desirable.

5.3 CENTRAL BODY CONTROL

In the studies discussed here, control was applied to the central body only. Furthermore, for the five body model no constraint tending to control flexible appendage motion was utilized. The investigation so far has been concerned with the practicality and implementation of multilevel control via partitioning in general, and has not addressed the question of its effectiveness in controlling the flexible vehicle. The tools required to investigate that aspect of the problem are now developed, except for the means for selecting the weights necessary to best accomplish the desired control of those states representing the flexible behavior. This study assumes that all states are available.

5.4 REFERENCES

5-1. Tiffany, N.O., "Multilevel Control by Partitioning," Bendix Engineering Development Center Internal Memorandum, April 14, 1981.

5-2. Chichester, F.D., "Application of Gauss Seidel Multilevel Control to a Single Axis Torsional Model," Proceedings of the Space Transportation System Symposium, 1980 SAE Aerospace Congress and Exposition, Los Angeles Convention Center, Los Angeles, California, October 13, 1980.

5-3. Chichester, F.D., "Modular Design Attitude Control System Study Monthly Progress Report." Contract NAS-33979, April, 1981.

SECTION 6

6.0 THREE AXIS TEN BODY MODELING OF THE ROTATIONAL DYNAMICS OF A FLEXIBLE SPACE PLATFORM

6.1 RIGID BODY-FLEXIBLE SUSPENSION APPROXIMATION OF MODULAR SPACE PLATFORM

The typical platform consisting of two spacecraft interconnected by a deployable truss* was approximated by an assembly of ten rigid bodies interconnected by a spring hinge suspension as shown in the topological diagram of Figure 6-1. From this figure, the following symmetry relationships between the rigid bodies of the model were written.

$$m_5 = m_4 = m_3 = m_2 \qquad \underline{r}_{13} = -\underline{r}_{12}$$

$$I_5 = I_4 = I_3 = I_2 \qquad \underline{r}_{55} = \underline{r}_{33} = \underline{r}_{24} = -\underline{r}_{21} = -\underline{r}_{35}$$

Additional symmetry conditions were obtained by comparing the truss portion of Figure 6-1 with the description of the truss appearing in Ivey (6-1).

$$m_8 = m_6 \quad I_8 = I_6 \qquad \underline{r}_{88} = \underline{r}_{66} = -\underline{r}_{89} = -\underline{r}_{67}$$

$$m_9 = m_7 \quad I_9 = I_7 \qquad \underline{r}_{99} = \underline{r}_{77} = -\underline{r}_{9,10} = -\underline{r}_{78}$$

*A more detailed development of the rigid body spring hinge suspension approximation of the deployable truss appears in Appendix B.

Selected masses of rigid bodies comprising the model were related to each other by ratios as follows:

$$m_6 = a_r m_2 \qquad m_7 = b_r m_1 \qquad m_{10} = c_r m_1$$

Then the total mass of the model was expressed in the following form

$$M = \sum_{i=1}^{10} m_i = (1+2b_r+c_r)m_1+(4+2a_r)m_2$$

6.2 LOCATION OF CENTER OF MASS WITH RESPECT TO CONNECTION BARYCENTER OF EACH RIGID BODY

The connection barycenter of a rigid body may be defined, following Hooker and Margulies (6-6), as "the new center of mass obtained by 'loading' each joint of the body with the residual mass of the system connected to that joint." With the aid of the topological diagram of Figure 6-1, the symmetry conditions and the ratios between the masses defined above, the vectors representing the location of the center of mass of each rigid body with respect to its barycenter are written as follows.

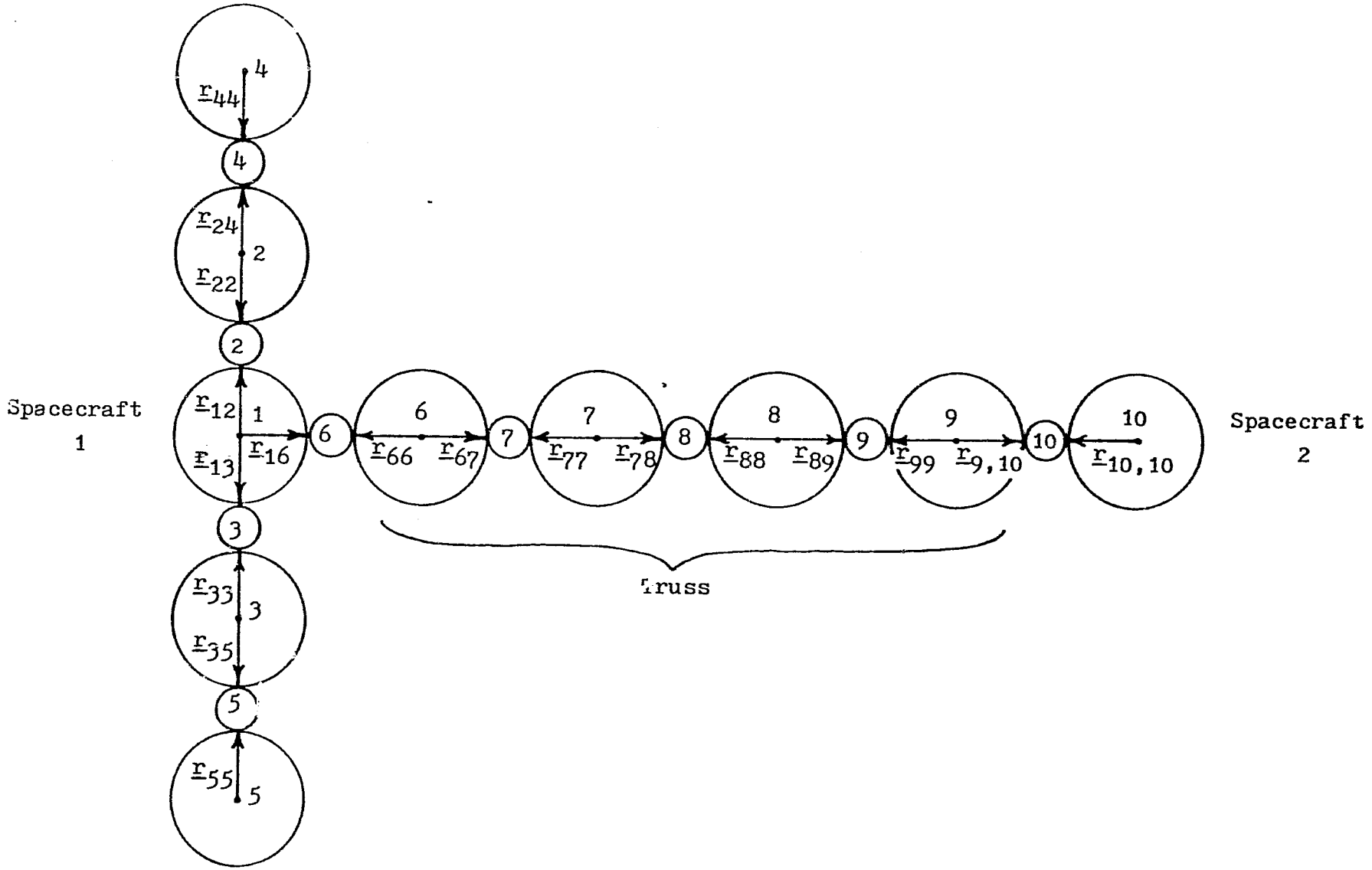

FIG. 6-1: TOPOLOGICAL DIAGRAM OF DISCRETE MASS MODEL OF TWO SPACECRAFT INTERCONNECTED BY DEPLOYABLE TRUSS

$$\underline{d}_1 = -(1 - \frac{m_1+4m_2}{M})\underline{r}_{16} = -\frac{(2b_r+c_r)m_1+2a_rm_2}{M}\underline{r}_{16} > -\frac{2b_r+c_r}{1+2b_r+c_r}\underline{r}_{16}$$

$$\underline{d}_2 = -(1-\frac{3m_2}{M})\underline{r}_{22} = -\frac{(1+2b_r+c_r)m_1 + (1+2a_r)m_2}{M}\underline{r}_{22} = -\underline{d}_3 > -\underline{r}_{22}$$

$$\underline{d}_4 = -\underline{d}_5 = -(1-\frac{m_2}{M})\underline{r}_{22} = -\frac{(1+2b_r+c_r)m_1 + (3+2a_r)m_2}{M}\underline{r}_{22} > -\underline{r}_{22}$$

$$\underline{d}_6 = -\left[1 - \frac{(4b_r+2c_r)m_1 + 3a_rm_2}{M}\right]\underline{r}_{66} = -\frac{(1-2b_r-c_r)m_1 + (4-a_r)m_2}{M}\underline{r}_{66} \qquad (6\text{-}1)$$

$$> -\frac{1-2b_r-c_r}{1+2b_r+c_r}\underline{r}_{66}$$

$$\underline{d}_7 = -\left[1-\frac{(3b_r+2c_r)m_1+2a_rm_2}{M}\right]\underline{r}_{77} = -\frac{(1-b_r-c_r)m_1+4m_2}{M}\underline{r}_{77}$$

$$> \frac{1-b_r-c_r}{1+2b_r+c_r}\underline{r}_{77}$$

$$\underline{d}_8 = -\left[1 - \frac{2b_rm_1 + a_rm_2}{M}\right]\underline{r}_{66} = -\frac{(1+c_r)m_1+(4+a_r)m_2}{M}\underline{r}_{66}$$

$$> -\frac{1+c_r}{1+2b_r+c_r}\underline{r}_{66}$$

$$\underline{d}_9 = -(1 - \frac{2b_r m_1}{M})\underline{r}_{77} = -\frac{(1+c_r)m_1 + (4+2a_r)m_2}{M}\underline{r}_{77}$$

$$> -\frac{1+c_r}{1+2b_r+c_r}\underline{r}_{77}$$

$$\underline{d}_{10} = -(1 - \frac{c_r m_1}{M})\underline{r}_{10,10} = -\frac{(1+2b_r)m_1 + (4+2a_r)m_2}{M}\underline{r}_{10,10}$$

$$> -\frac{1+2b_r}{1+2b_r+c_r}\underline{r}_{10,10}$$

6.3 LOCATION OF ADJACENT HINGES WITH RESPECT TO BARYCENTER OF EACH RIGID BODY

The vectors representing the location of adjacent hinges with respect to the connection barycenter of each rigid body were expressed in terms of the location vectors with respect to the center of mass of the same body as follows:

$$\underline{d}_{12} = \underline{d}_1 + \underline{r}_{12} = \underline{r}_{12} - \frac{(2b_r+c_r)m_1+2a_r m_2}{M}\underline{r}_{16}$$

$$\underline{d}_{13} = \underline{d}_1 + \underline{r}_{13} = \underline{r}_{13} - \frac{(2b_r+c_r)m_1+2a_r m_2}{M}\underline{r}_{16}$$

$$\underline{d}_{16} = \underline{d}_1 + \underline{r}_{16} = \frac{m_1+4m_2}{M}\underline{r}_{16} > \frac{1}{1+2b_r+c_r}\underline{r}_{16} \qquad (6\text{-}2)$$

$$\underline{d}_{22} = \underline{d}_2 + \underline{r}_{22} = \frac{3m_2}{M}\underline{r}_{22} = -\underline{d}_{33} << 1$$

$$\underline{d}_{-24} = \underline{d}_{-2} + \underline{r}_{-24} = -(2 - \frac{3m_2}{M})\underline{r}_{-22} = -\underline{d}_{-35} > -2\underline{r}_{-22}$$

$$\underline{d}_{-44} = \underline{d}_{-4} + \underline{r}_{-44} = \frac{m_2}{M}\underline{r}_{-22} = -\underline{d}_{-55} << 1$$

$$\underline{d}_{66} = \underline{d}_6 + \underline{r}_{66} = \frac{(4b_r+2c_r)m_1+3a_r m_2}{M}\,\underline{r}_{66} < \frac{2(2b_r+c_r)}{1+2b_r+c_r}\,\underline{r}_{66}$$

$$\underline{d}_{67} = \underline{d}_6 + \underline{r}_{67} = \underline{d}_6 - \underline{r}_{66} = -\frac{2m_1+(8+a_r)m_2}{M}\,\underline{r}_{66} > \frac{-2}{1+2b_r+c_r}\,\underline{r}_{66}$$

$$\underline{d}_{77} = \underline{d}_7 + \underline{r}_{77} = \frac{(3b_r+2c_r)m_1+2a_r m_2}{M}\,\underline{r}_{77} < \frac{3b_r+2c_r}{1+2b_r+c_r}\,\underline{r}_{77}$$

$$\underline{d}_{78} = \underline{d}_7 + \underline{r}_{78} = \underline{d}_7 - \underline{r}_{77} = -\frac{(2+b_r)m_1+(8+2a_r)m_2}{M}\,\underline{r}_{77} > \frac{-(2+b_r)}{1+2b_r+c_r}\,\underline{r}_{77}$$

$$\underline{d}_{88} = \underline{d}_8 + \underline{r}_{88} = \underline{d}_8 + \underline{r}_{66} = \frac{(2b_r m_1+a_r m_2)}{M}\,\underline{r}_{66} < \frac{2b_r}{1+2b_r+c_r}\,\underline{r}_{66}$$

$$\underline{d}_{89} = \underline{d}_8 - \underline{r}_{66} = -\frac{(2+2b_r+2c_r)m_1+(8+3a_r)m_2}{M}\,\underline{r}_{66} > \frac{-2(1+b_r+c_r)}{1+b_r+c_r}\,\underline{r}_{66}$$

$$\underline{d}_{99} = \underline{d}_9 + \underline{r}_{99} = \underline{d}_9 + \underline{r}_{77} = \frac{2b_r m_1}{M}\,\underline{r}_{77} < \frac{2b_r}{1+2b_r+c_r}\,\underline{r}_{77}$$

$$\underline{d}_{9,10} = \underline{d}_9 + \underline{r}_{9,10} = \underline{d}_9 - \underline{r}_{77} = -\frac{(2+2b_r+c_r)m_1+(8+4a_r)m_2}{M}\,\underline{r}_{77}$$

$$> \frac{-2(1+b_r+c_r)}{1+2b_r+c_r}\,\underline{r}_{77}$$

$$\underline{d}_{10,10} = \underline{d}_{10} + \underline{r}_{10,10} + \frac{c_r m_1}{M}\,\underline{r}_{10,10} > \frac{c_r}{1+2b_r+c_r}\,\underline{r}_{10,10}$$

The relative locations of the barycenters, centers of mass and hinge locations along the axis of the truss were estimated for four sets of values of the mass ratios b_r and c_r. The corresponding sketches, including the location vectors, appear in Figures 6-2, 6-3 6-4 and 6-5.

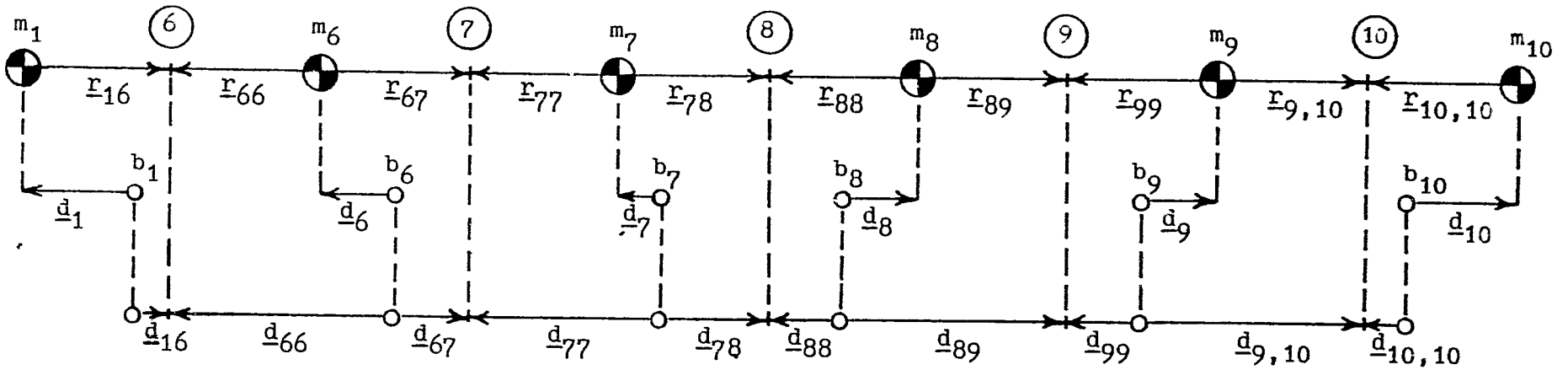

m_i = location of center of mass of ith body.

b_i = location of connection barycenter of ith augmented body.

(j) = location of jth hinge.

$\underline{r}_{ij}$ = vector from center of mass of ith body to jth hinge.

$\underline{d}_{ij}$ = vector from connection barycenter of ith augmented body to jth hinge.

$\underline{d}_i$ = vector from barycenter of ith augmented body to center of mass of ith body.

FIG. 6-2: Relationships Between Barycenters, Centers of Mass and Hinge Locations Along Truss Axis for $b_r = 1$, $c_r = 1$.

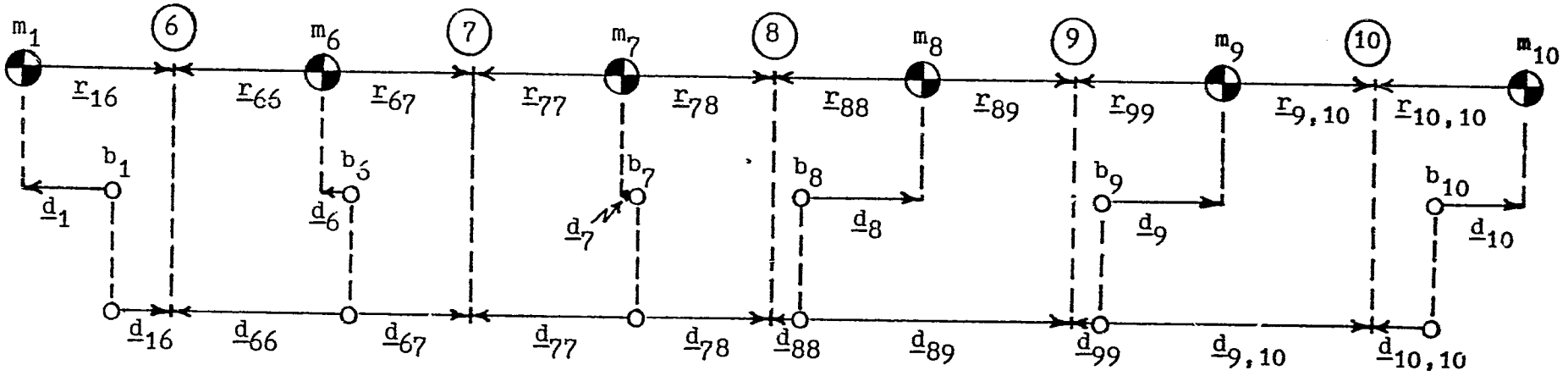

FIG. 6-3: Relationships Between Barycenters, Centers of Mass and Hinge Locations Along Truss Axis for $b_r = \frac{1}{4}$, $c_r = 1$.

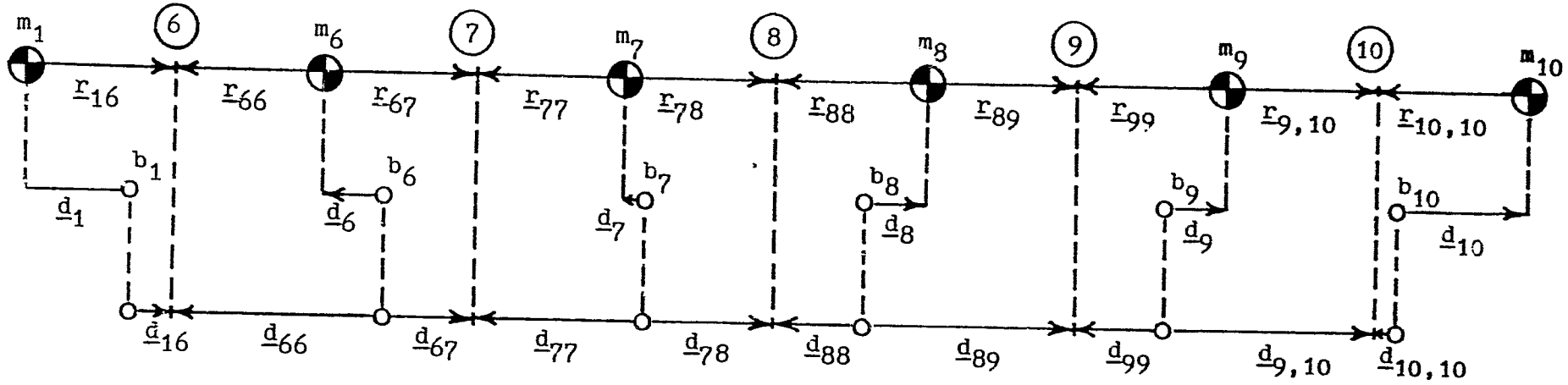

FIG. 6-4: Relationships Between Barycenters, Centers of Mass and Hinge Locations Along Truss Axis for $b_r = 1$, $c_r = \frac{1}{2}$.

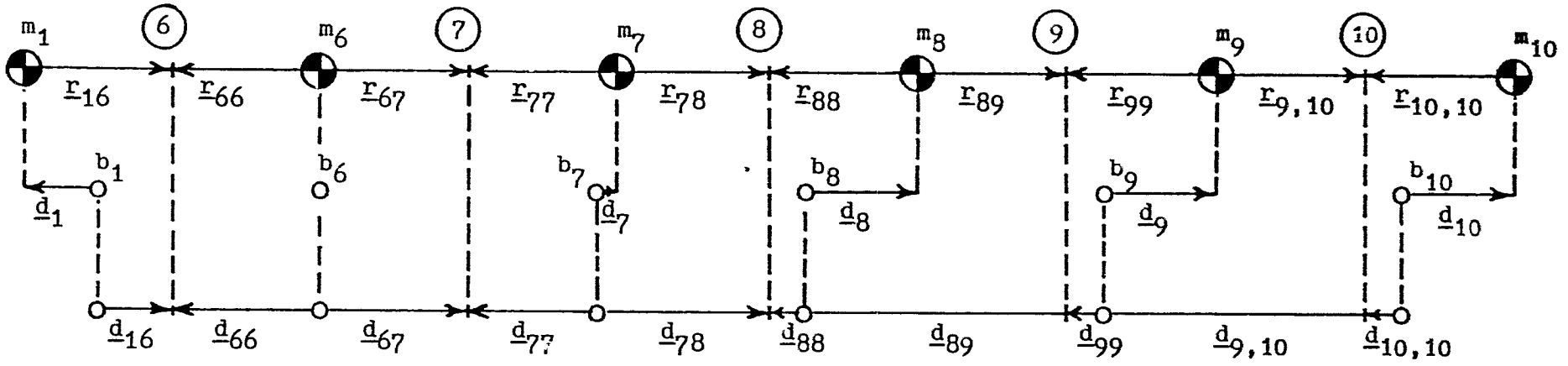

FIG. 6-5: Relationships Between Barycenters, Centers of Mass and Hinge Locations Along Truss Axis for $b_r = \frac{1}{4}$, $c_r = \frac{1}{2}$.

In the first two sketches $c_r = 1$ which corresponds to the two spacecraft having approximately the same mass since $m_1 >> m_2$, $b_r = 1$ corresponds to the total mass of two of the bodies attached along the truss being approximately equal to the mass of the central body in spacecraft 1. The $b_r = 1/4$ condition corresponds to the total mass of this pair of bodies being about 25% of that of the central body. The same sequence of values of b_r was repeated in Figures 6-4 and 6-5 for $c_r = 1/2$ which corresponds to the mass of spacecraft 2 being about 1/2 that of spacecraft 1.

Inspection of Figures 6-2 through 6-5 reveals certain common patterns. For both values of c_r when $b_r = 1/4$ the centers of mass of bodies 6 and 7 remain close to their respective connection barycenters. In fact, for $b_r = 1/4$ and $c_r = 1/2$, the center of mass and the barycenter of body 6 coincide while the center of mass remains very close to the connection barycenter for body 7. The greater distances between the centers of mass and their corresponding barycenters generally occur close to the extreme ends of the truss in each case. Decreasing the ratio of the mass of the second spacecraft to that of the first, c_r, reduces the distance between the barycenter and the center of mass of the central body of the first spacecraft and increases the distance between the barycenter and the center of mass of the second spacecraft. These effects agree with physical reasoning since reduction of this ratio reduces the influence of the combined mass of the truss and the second spacecraft compared with that of the first spacecraft while it increases the influence of the combined mass of the first spacecraft and the truss compared with that of the second spacecraft.

6.4 AUGMENTED INERTIA MATRICES

In the sequel the following form of the vector cross product is utilized frequently. Let

$$\underline{a} = (a_x, a_y, a_z)^T \text{ and } \underline{b} = (b_x, b_y, b_z)^T \text{ then } \underline{a} \times \underline{b} = \tilde{A}\underline{b}$$

where:

$$\tilde{A} = \begin{bmatrix} 0 & -a_z & a_y \\ a_z & 0 & -a_x \\ -a_y & a_x & 0 \end{bmatrix} \qquad (6-3)$$

With the aid of the symmetry conditions and the sets of vectors developed in the preceeding sections and the augmented body techniques presented in Lipski (6-4), (6-5) the effective moment of inertia matrix with respect to the connection barycenter of each rigid body in the model is expressed in terms of the above listed mass ratios as follows:

$$I_1^* = I_1 - m_1\tilde{D}_1\tilde{D}_1 - 4m_2\tilde{D}_{12}\tilde{D}_{12} - \{ (2b_r+c_r)m_1+2a_rm_2 \}\tilde{D}_{16}\tilde{D}_{16}$$

$$I_2^* = I_2 - m_2\tilde{D}_2\tilde{D}_2 - \{ (1+2b_r+ c_r)m_1+(2+2a_r)m_2 \}\tilde{D}_{22}\tilde{D}_{22} - m_2\tilde{D}_{24}\tilde{D}_{24} = I_3^*$$

$$I_4^* = I_4 - m_2\tilde{D}_4\tilde{D}_4 - \{ (1+2b_r+c_r)m_1+(3+2a_r)m_2 \}\tilde{D}_{44}\tilde{D}_{44} = I_5^* \qquad (6-4)$$

$$I_6^* = I_6 - a_rm_2\tilde{D}_6\tilde{D}_6 - (m_1+4m_2)\tilde{D}_{66}\tilde{D}_{66} - \{ (2b_r+c_r)m_1+a_rm_2 \}\tilde{D}_{67}\tilde{D}_{67}$$

$$I_7^* = I_7 - b_r m_1 \tilde{D}_7 \tilde{D}_7 - \left[m_1 + (4+a_r) m_2 \right] \tilde{D}_{77} \tilde{D}_{77}$$

$$- \left[(b_r+c_r) m_1 + a_r m_2 \right] \tilde{D}_{78} \tilde{D}_{78}$$

$$I_8^* = I_8 - a_r m_2 \tilde{D}_8 \tilde{D}_9 - \left[(1+b_r) m_1 + (4+a_r) m_2 \right] \tilde{D}_{88} \tilde{D}_{88}$$

$$- (b_r+c_r) m_1 \tilde{D}_{89} \tilde{D}_{89}$$

$$I_9^* = I_9 - b_r m_1 \tilde{D}_9 \tilde{D}_9 - \left[(1+b_r) m_1 + (4+2a_r) m_2 \right] \tilde{D}_{99} \tilde{D}_{99} - c_r m_1 \tilde{D}_{9\ 10} \tilde{D}_{9,10}$$

$$I_{10}^* = I_{10} - c_r m_1 \tilde{D}_{10} \tilde{D}_{10}$$

Under the assumption that the mass of body 1 is much larger than the mass of each rigid body in the model of the solar panels, $m_1 >> m_2$ and the differences between the rotational moments of inertia for each rigid body are bounded as follows:

$$I_1 - I_1^* \leq \frac{2b_r + c_r}{1 + 2b_r + c_r} m_1 \tilde{R}_{16} \tilde{R}_{16}$$

$$I_2 - I_2^* = I_3 - I_3^* \leq 5 m_2 \tilde{R}_{22} \tilde{R}_{22}$$

$$I_4 - I_4^* = I_5 - I_5^* \leq m_2 \tilde{R}_{22} \tilde{R}_{22}$$

$$I_6 - I_6^* \leq \frac{4(2b_r + c_r)(4 + 2b_r + c_r)}{(1 + 2b_r + c_r)^2} m_1 \tilde{R}_{66} \tilde{R}_{66}$$

(6-5)

$$I_7 - I_7^* \leq \left[\left(\frac{1 - b_r - c_r}{1 + 2b_r + c_r} \right)^2 b_r + \left(\frac{3b_r + 2c_r}{1 + 2b_r + c_r} \right)^2 + \left(\frac{2b_r}{1 + 2b_r + c_r} \right)^2 b_r \right] m_1 \tilde{R}_{77} \tilde{R}_{77}$$

$$I_8 - I_8^* \leq \left[\left(\frac{2b_r}{1 + 2b_r + c_r} \right)^2 (1 + b_r) + \left(\frac{1 + b_r + c_r}{1 + 2b_r + c_r} \right)^2 4(b_r + c_r) \right] m_1 \tilde{R}_{66} \tilde{R}_{66}$$

$$I_9 - I_9^* \leq \left[\left(\frac{1 + c_r}{1 + 2b_r + c_r} \right)^2 b_r + \left(\frac{2b_r}{1 + 2b_r + c_r} \right)^2 (1 + b_r) \right.$$

$$\left. + \left(\frac{1 + b_r + c_r}{1 + 2b_r + c_r} \right)^2 4c_r \right] m_1 \tilde{R}_{77} \tilde{R}_{77}$$

$$I_{10} - I_{10}^* \leq \left(\frac{1 + b_r}{1 + 2b_r + c_r} \right)^2 c_r m_1 \tilde{R}_{10,10} \tilde{R}_{10,10}$$

In earlier sections the relative locations of the barycenters, centers of mass and hinge locations along the axis of the truss were estimated for four sets of values of the mass ratios b_r and c_r. In the present section the differences between the rotational inertia matrices with respect to the center of mass and with respect to the connection barycenter for each rigid body in the model are obtained for the same four sets of values of b_r and c_r. The normalized differences between the inertia matrices for the rigid bodies along the axis of the truss appear in Table 6-1. Since R_{jj} may differ considerably from R_{ii} for $j \neq i$, comparisons between rows along a given column have more validity than do comparisons between columns of a given row of the table.

TABLE 6-1

NORMALIZED DIFFERENCES BETWEEN ROTATIONAL INERTIA MATRICES FOR BODIES ALONG TRUSS AXIS

b_r	c_r	$\frac{I_6 - I_6^*}{m_1 \tilde{R}_{66} \tilde{R}_{66}}$	$\frac{I_7 - I_7^*}{m_1 \tilde{R}_{77} \tilde{R}_{77}}$	$\frac{I_8 - I_8^*}{m_1 \tilde{R}_{66} \tilde{R}_{66}}$	$\frac{I_9 - I_9^*}{m_1 \tilde{R}_{77} \tilde{R}_{77}}$	$\frac{I_{10} - I_{10}^*}{m_1 \tilde{R}_{10,10} \tilde{R}_{10,10}}$
1	1	$\frac{21}{4}$	$\frac{35}{16}$	5	3	$\frac{1}{4}$
$\frac{1}{4}$	1	$\frac{132}{25}$	$\frac{283}{200}$	$\frac{41}{10}$	$\frac{69}{25}$	$\frac{1}{4}$
1	$\frac{1}{2}$	$\frac{260}{49}$	$\frac{101}{49}$	$\frac{182}{49}$	$\frac{91}{49}$	$\frac{8}{49}$
$\frac{1}{4}$	$\frac{1}{2}$	5	$\frac{9}{8}$	$\frac{19}{8}$	$\frac{29}{16}$	$\frac{25}{128}$

6.5 RIGID BODY ANGULAR RATE EQUATIONS

Equations in terms of the rigid body angular rates of rotation, $\underline{\omega}_i$, were obtained by equating the rate of change of angular momentum of each rigid body in the model to the vector sum of torques acting on that body at its connection barycenter. Under the assumption of small angular displacements, the symmetry conditions, the vectors developed in equation sets (6-1) and (6-2) and the moment of inertia matrices developed in equation set (6-4), the rigid body angular rate equations were written as follows:

$$I^{*}_{1-1}\dot{\omega}_{1-1} + M\left(\tilde{D}_{12}\tilde{D}_{22}\dot{\omega}_{2-2} + \tilde{D}_{13}\tilde{D}_{33}\dot{\omega}_{3-3} + \tilde{D}_{12}\tilde{D}_{44}\dot{\omega}_{4-4} + \tilde{D}_{13}\tilde{D}_{55}\dot{\omega}_{5-5} + \tilde{D}_{16}\sum_{j=6}^{10}\left(\tilde{D}_{jj}\dot{\omega}_{j-j}\right)\right)$$

$$= t^{H}_{-1} + t^{H}_{-12} + t^{H}_{-13} + t^{H}_{-16} + \tilde{D}_{1-1}f - \tilde{D}_{13-3}f - \tilde{D}_{12-4}f - \tilde{D}_{13-5}f - \tilde{D}_{16}\sum_{j=6}^{10}f_{-j} - \tilde{D}_{12-2}f$$

$$I^{*}_{2-2}\dot{\omega}_{2-2} + M\left(\tilde{D}_{22}\tilde{D}_{12}\dot{\omega}_{1-1} + \tilde{D}_{22}\sum_{\substack{j=3\\ j\neq 4}}^{10}\left(\tilde{D}_{jj}\dot{\omega}_{j-j}\right) + \tilde{D}_{24}\tilde{D}_{44}\dot{\omega}_{4-4}\right)$$

$$= t^{H}_{-2} + t^{H}_{-22} + t^{H}_{-24} + \tilde{D}_{2-2}f - \tilde{D}_{22}\sum_{\substack{j=1\\ j\neq 2,4}}^{10}f_{-j} - \tilde{D}_{24-4}f$$

$$I^{*}_{3-3}\dot{\omega}_{3-3} + M\left(\tilde{D}_{33}\tilde{D}_{13}\dot{\omega}_{1-1} + \tilde{D}_{33}\sum_{\substack{j=2\\ j=3,5}}^{10}\left(\tilde{D}_{jj}\dot{\omega}_{j-j}\right) + \tilde{D}_{35}\tilde{D}_{55}\dot{\omega}_{5-5}\right)$$

$$= \underset{-3}{t} + \underset{-33}{\overset{H}{t}} + \underset{-35}{\overset{H}{t}} + \tilde{D}_{3-3}\underset{-3}{\dot{t}} - \tilde{D}_{33}\sum_{\substack{j=1\\ j\neq 3,5}}^{10} \underset{-j}{t} - \tilde{D}_{35}\underset{-5}{\dot{f}}$$

(6-6)

$$\underset{4-4}{I^{*}}\dot{\omega} + M\Big(\tilde{D}_{44}\tilde{D}_{12-1}\dot{\omega} + \tilde{D}_{44}\tilde{D}_{24-2}\dot{\omega} + \tilde{D}_{44}\sum_{\substack{j=3\\ j\neq 4}}^{10} (\tilde{D}_{jj-j}\dot{\omega}) \Big)$$

$$= \underset{-4}{t} + \underset{-44}{\overset{H}{t}} + \tilde{D}_{4-4}\underset{-4}{\dot{t}} + \tilde{D}_{44}\sum_{\substack{j=1\\ j\neq 4}}^{10} \underset{-j}{t}$$

$$\underset{5-5}{I^{*}}\dot{\omega} + M\Big(\tilde{D}_{55}\tilde{D}_{13-1}\dot{\omega} + \tilde{D}_{55}\tilde{D}_{35-3}\dot{\omega} + \tilde{D}_{55}\sum_{\substack{j=2\\ j\neq 3,5}}^{10} (\tilde{D}_{jj-j}\dot{\omega}) \Big)$$

$$= \underset{-5}{t} + \underset{-55}{\overset{H}{t}} + \tilde{D}_{5-5}\underset{-5}{\dot{f}} - \tilde{D}_{55}\sum_{\substack{j=1\\ j\neq 5}}^{10} \underset{-j}{f}$$

$$\underset{i-i}{I^{*}}\dot{\omega} + M\Big(\tilde{D}_{ii}\tilde{D}_{16-1}\dot{\omega} + \tilde{D}_{ii}\sum_{j=2}^{5} (\tilde{D}_{jj-j}\dot{\omega}) + \tilde{D}_{ii}\sum_{j=6}^{i-1} (D_{j,j+1-j}\dot{\omega}) + \tilde{D}_{i,i+1}\sum_{j=i+1}^{10} (\tilde{D}_{jj-j}\dot{\omega}) \Big)$$

$$= \underset{-i}{t} + \underset{-i,i}{\overset{H}{t}} + \underset{-i,i+1}{\overset{H}{t}} + \tilde{D}_{i-i}\underset{-i}{\dot{f}} - \tilde{D}_{ii}\sum_{j=1}^{i-1} (\underset{-j}{f}) - \tilde{D}_{i,i+1}\sum_{j=i+1}^{10} (\underset{-j}{f})$$

$i = 6,7,8,9$

$$\underline{I}^{*}_{10,10}\dot{\underline{\omega}}_{10} + M\left(\tilde{D}_{10,10}\tilde{D}_{16}\dot{\underline{\omega}}_{1} + \tilde{D}_{10,10}\sum_{j=2}^{5}(\tilde{D}_{jj}\dot{\underline{\omega}}_{j}) + \tilde{D}_{10,10}\sum_{j=6}^{9}(\tilde{D}_{j,j+1}\dot{\underline{\omega}}_{j})\right)$$

$$= \underline{t}_{10} + \underline{t}^{H}_{10,10} + \tilde{D}_{10}\underline{t}_{10} - \tilde{D}_{10,10}\sum_{j=1}^{9}\underline{f}_{j}$$

where $M = \sum_{i=1}^{10} m_i = m_1 + 4m_2 + 2m_6 + 2m_7 + m_{10} =$

$$= (1+2b_r+c_r)m_1 + (4+2a_r)m_2$$

6.6 VECTOR STATE VARIABLE FORM OF RIGID BODY ANGULAR RATE EQUATIONS

The rigid body angular rate equations of equation set (6-6) were recast into the following vector matrix state variable form.

$$A\dot{\underline{\omega}} = \underline{t} + \underline{t}^{H} + B\underline{f} \rightarrow \dot{\underline{\omega}} = A^{-1}(\underline{t} + \underline{t}^{H}) + A^{-1}B\underline{f} \qquad (6\text{-}7)$$

where:

$$\dot{\underline{\omega}} = (\dot{\underline{\omega}}_1^T, \dot{\underline{\omega}}_2^T, \ldots, \dot{\underline{\omega}}_{10}^T)^T$$

$\underline{\omega}_i$ = angular rotation rate of ith rigid body

$\underline{\omega} = (\underline{\omega}_1^T, \underline{\omega}_2^T, \ldots, \underline{\omega}_{10}^T)^T$

$\underline{f}_i$ = net force acting on ith rigid body

$\underline{f} = (\underline{f}_1^T, \underline{f}_2^T, \ldots, \underline{f}_{10}^T)^T$

$\underline{t}_i$ = vector sum of control and disturbance torques on ith rigid body.

$$\underline{t}^H = ((\underline{t}^H_{12})^T + (\underline{t}^H_{13})^T + (\underline{t}^H_{16})^T, (\underline{t}^H_{22})^T + (\underline{t}^H_{24})^T$$

$$(\underline{t}^H_{33})^T + (\underline{t}^H_{35})^T, (\underline{t}^H_{44})^T, (\underline{t}^H_{55})^T, (\underline{t}^H_{66})^T + (\underline{t}^H_{67})^T,$$

$$(\underline{t}^H_{77})^T + (\underline{t}^H_{78})^T, (\underline{t}^H_{88})^T + (\underline{t}^H_{89})^T, (\underline{t}^H_{99})^T + (\underline{t}_{9,10})^T, (\underline{t}^H_{10,10})^T)^T$$

$\underline{t}^H_{ij}$ = torque of jth hinge on ith rigid body.

$$A = \begin{bmatrix} A_{11} \cdots A_{1,10} \\ \vdots \quad\quad \vdots \\ A_{10,1} \cdots A_{10,10} \end{bmatrix}$$

= 10 x 10 partitioned coefficient matrix

$$B = \begin{bmatrix} B_{11} & \cdots & B_{1,10} \\ \vdots & & \vdots \\ B_{10,1} & \cdots & B_{10,10} \end{bmatrix} = 10 \times 10 \text{ partitioned coefficient matrix}$$

A_{ij}, B_{ij} are 3 x 3 submatrices

6.7 EXPANSION OF COEFFICIENT SUBMATRICES IN TERMS OF AUGMENTED MOMENT OF INERTIA MATRICES AND LOCATION VECTORS WITH RESPECT TO CONNECTION BARYCENTERS

The following matrices within the coefficient matrices, A and B, were expanded with the aid of the left hand sides of the rigid body angular rate equations listed in equation set (6-6).

$$A_{ii} = I^*_i, \quad i = 1,2,\ldots,10$$

$$A_{12} = M\tilde{D}_{12}\tilde{D}_{22} = A^T_{21} \qquad A_{13} = M\tilde{D}_{13}\tilde{D}_{33} = A^T_{31}$$

$$A_{14} = M\tilde{D}_{12}\tilde{D}_{44} = A^T_{41} \qquad A_{15} = M\tilde{D}_{13}\tilde{D}_{55} = A^T_{51}$$

$$A_{1j} = M\tilde{D}_{16}\tilde{D}_{jj} = A^T_{j1}, \quad j=6,7,8,9,10$$

$$A_{23} = M\tilde{D}_{22}\tilde{D}_{33} = A^T_{32} \qquad A_{24} = M\tilde{D}_{24}\tilde{D}_{44} = A^T_{42}$$

$$A_{2j} = M\tilde{D}_{22}\tilde{D}_{jj} = A^T_{j2}, \quad j=5,6,7,8,9,10$$

$$A_{34} = M\tilde{D}_{33}\tilde{D}_{44} = A^T_{43} \qquad A_{35} = M\tilde{D}_{35}\tilde{D}_{55} = A^T_{53}$$

$$A_{3j} = M\tilde{D}_{33}\tilde{D}_{jj} = A_{j3}^T, \qquad j=6,7,8,9,10$$

$$A_{4j} = M\tilde{D}_{44}\tilde{D}_{jj} = A_{j4}^T, \qquad j=5,6,7,8,9,10 \tag{6-8}$$

$$A_{5j} = M\tilde{D}_{55}\tilde{D}_{jj} = A_{j5}^T, \qquad j=6,7,8,9,10$$

$$A_{ij} = M\tilde{D}_{i,i+1}\tilde{D}_{jj} = A_{ji}^T; \quad i=6,7,8,9, \quad j=i+1,i+2,\ldots,10$$

$$B_{ii} = -\tilde{D}_i, \quad i=1,2,\ldots,10$$

$$B_{12} = -\tilde{D}_{12} = B_{14} \quad B_{13} = -\tilde{D}_{13} = B_{15} \quad B_{1j} = -\tilde{D}_{16}; j=6,7,8,9,10$$

$$B_{21} = -\tilde{D}_{22} = B_{23} \quad B_{24} = -\tilde{D}_{24} \quad B_{2j} = -D_{22}; \; j=5,6,7,8,9,10$$

(6-9)

$$B_{31} = -\tilde{D}_{33} = B_{32} = B_{34} \quad B_{35} = -\tilde{D}_{35} \quad B_{3j} = -\tilde{D}_{33}; \; j=6,7,8,9,10$$

$$B_{41} = -\tilde{D}_{44} = B_{42} = B_{43} \quad B_{4j} = -\tilde{D}_{44}; \; j=5,6,7,8,9,10$$

$$B_{51} = -\tilde{D}_{55} = B_{52} = B_{53} = B_{54} \quad B_{5j} = -\tilde{D}_{55}; \; j=6,7,8,9,10$$

$$B_{ij} = -\tilde{D}_{ii}; \; i=6,7,8,9,10 \quad j=1,2,\ldots,i-1 \qquad B_{ij} = -\tilde{D}_{i,i+1}; \; i=6,7,8,9 \quad j=i+1,i+2,\ldots,10$$

6.8 SUSPENSION EQUATIONS

The suspension equations represent the torque acting upon each rigid body due to the vector sum of the forces applied at the hinge joints adjacent to the body. They were expressed in vector matrix form as follows.

$$\underline{t}^H = LC_s\underline{\omega} + LK_s\hat{\underline{\alpha}} \qquad (6\text{-}10)$$

where:

$$\underline{t}^H = \left[(\underline{t}_1^H)^T, (\underline{t}_2^H)^T, \ldots, (\underline{t}_{10}^H)^T \right]^T \qquad (6\text{-}11)$$

$\underline{t}_1^H$ = vector sum of hinge torques acting on ith rigid body.

$$\underline{\omega} = (\underline{\omega}_1^T, \underline{\omega}_2^T, \ldots, \underline{\omega}_{10}^T)^T$$

$\underline{\omega}_1$ = rate of rotation of ith rigid body.

$$\underline{\omega}_1 = (\omega_{1x}, \omega_{1y}, \omega_{1z})^T$$

$$\hat{\underline{\alpha}} = (\underline{\alpha}_1^T, \underline{\alpha}_{12}^T, \underline{\alpha}_{13}^T, \underline{\alpha}_{24}^T, \underline{\alpha}_{35}^T, \underline{\alpha}_{16}^T, \underline{\alpha}_{67}^T, \underline{\alpha}_{78}^T, \underline{\alpha}_{89}^T, \underline{\alpha}_{9,10}^T)^T$$

$$\underline{\alpha}_1 = (\phi_1, \theta_1, \psi_1)^T$$

ϕ_1, θ_1, ψ_1 = inertially referenced Euler attitude angles of body 1.

$$\underline{\alpha}_{ij} = (\Delta\phi_{ij}, \Delta\theta_{ij}, \Delta\psi_{ij})^T$$

$\Delta\phi_{ij}, \Delta\theta_{ij}, \Delta\psi_{ij}$ = relative Euler angles of body j with respect to body i.

Coefficient matrices, L, C_s and K_s are expressed in terms of 3 x 3 submatrices in Appendix C.

6.9 EULER ANGLE RATE EQUATIONS

The Euler angle rate equations express the first time derivatives of the inertially referenced Euler attitude angles of body 1 and the relative Euler attitude angles between adjacent bodies of the model in terms of angular rates of rotation of the bodies comprising the model. For small angular displacements, the linearized Euler angle equations were written in the following form..

$$\dot{\underline{\alpha}} = K\underline{\omega} \tag{6-12}$$

where:

$$\underline{\alpha} = (\underline{\alpha}_1^T, \underline{\alpha}_{12}^T, \underline{\alpha}_{13}^T, \underline{\alpha}_{24}^T, \underline{\alpha}_{35}^T, \underline{\alpha}_{16}^T, \underline{\alpha}_{67}^T, \underline{\alpha}_{78}^T, \underline{\alpha}_{89}^T, \underline{\alpha}_{9,10}^T)^T$$

$$\dot{\underline{\alpha}}_1 = \underline{\omega}_1$$

$$\dot{\underline{\alpha}}_{1j} = \underline{\omega}_j - \underline{\omega}_1$$

6.10 STATE VARIABLE ROTATIONAL DYNAMICS MODEL

The linearized rigid body angular rate equations, linearized suspension equations and linearized Euler angle rate equations were combined into a state variable rotational dynamics model of the following form.

$$\dot{\underline{\omega}} = GLC_s\underline{\omega} + GLK_s\underline{\alpha} + G\underline{u} \qquad (6\text{-}13)$$

$$\dot{\underline{\alpha}} = K\underline{\omega}$$

where:

$\underline{\omega}$ = rigid body angular rate vector.

$\underline{\alpha}$ = Euler angle vector.

$\underline{u}$ = actuator torque vector.

and the matrices G, L, K, C_s and K_s are expanded in terms of 3 x 3 submatrices in Appendix C.

When these vectors and matrices were expanded in terms of their scalar components and elements, respectively, they were rearranged in such a way that scalars associated with a specific axis of the model were grouped into the same subvector. Each coefficient matrix appearing in the resulting state variable model was written in the following form.

$$\dot{\underline{x}}_j = \sum_{k=1}^{3} (A_{jk}\underline{x}_k + B_{jk}\underline{u}_k) \qquad j=1,2,3 \quad k = 1,2,3 \qquad (6\text{-}14)$$

where:

$$\underline{x}_k = (\underline{\omega}_k^T, \underline{\alpha}_k^T)^T \qquad (6\text{-}15)$$

$$A_{jk} = \left[\begin{array}{c|c} \hat{G}_{jk} L_k C_{sk} & \hat{G}_{jk} L_k K_{sk} \\ \hline K_{jk} & [0] \end{array}\right] \qquad B_{jk} = \left[\begin{array}{c} \hat{G}_{jk} \\ \hline [0] \end{array}\right] \qquad [0] = 10 \times 10 \text{ zero matrix}$$

$$\underline{u}_1 = (u_{1x}, u_{2x}, \ldots, u_{10x})^T \qquad \underline{u}_2 = (u_{1y}, u_{2y}, \ldots, u_{10y})^T$$

$$\underline{u}_3 = (u_{1z}, u_{2z}, \ldots, u_{10z})^T$$

$\underline{u}_k$ (k = 1,2,3) has scalar expansion of the same form as $\underline{\omega}_k$.

$$\underline{\alpha}_1 = (\phi_1, \Delta\phi_{12}, \Delta\phi_{13}, \Delta\phi_{24}, \Delta\phi_{35}, \Delta\phi_{16}, \Delta\phi_{67}, \Delta\phi_{78}, \Delta\phi_{89}, \Delta\phi_{9,10})^T$$

$$\underline{\alpha}_2 = (\theta_1, \Delta\theta_{12}, \Delta\theta_{13}, \Delta\theta_{24}, \Delta\theta_{35}, \Delta\theta_{16}, \Delta\theta_{67}, \Delta\theta_{78}, \Delta\theta_{89}, \Delta\theta_{9,10})^T$$

$$\underline{\alpha}_3 = (\psi_1, \Delta\psi_{12}, \Delta\psi_{13}, \Delta\psi_{24}, \Delta\psi_{35}, \Delta\psi_{16}, \Delta\psi_{67}, \Delta\psi_{78}, \Delta\psi_{89}, \Delta\psi_{9,10})^T$$

Using the definitions of $\hat{G}$, L, K, C_s, and K_s as given in Appendix C, L_k is a 10 x 9 matrix of the same form as the 10 x 9 partitioned matrix, L, with "1" in the place of each submatrix "I" and "0" in place of each submatrix "[0]". K_{s1} is a 9 x 10 matrix of the same form as the 9 x 10 partitioned matrix, K_s, with "k_{12x} in the place of submatrix "K_{12}" and similar substitutions for the remaining submatrices. C_{s1} is a 9 x 10 matrix similarly developed from the 9 x 10 partitioned matrix C_s. The matrices K_{s2} are similarly expanded with the subscript, y, in the place of x as are the submatrices K_{s3} and C_{s3} with the subscript, z, in place of x. $K_{jk} = [0]$ for $k \neq j$. For k = j, it is a 10 x 10 matrix of the same form as the partitioned matrix K, with "1" in the place of each "I" and "0" in the place of each "[0]".

6.11 REFERENCES

6-1. Ivey, Wayne, "Vibration Analysis of the MSFC/Hybrid Deployable Truss," MSFC Memorandum, June 26, 1980.

6-2. Cornell, G.A., "Derivation of the Equations of Motion of the Space Base Configurations I through XII," Bendix Research Laboratories Internal Memorandum, November 3, 1977.

6-3. Cornell, G.A., "Space Base Mathematical Model," Bendix Research Laboratoeies Internal Memorandum, December 14, 1977.

6-4. Lipski, D.B., "Linearized Five Body Space Base Simulation Model," Bendix Research Laboratories Internal Memorandum, April 23, 1979.

6-5. Lipski, D.B., "Discrete Coordinate Modeling of Flexible Bodies," Bendix Engineering Development Center Internal Memorandum, January 12, 1981.

6-6. Hooker, W.W. and G. Margulies, "The Dynamical Equations for an n-Body Satellite," Journal of the Astronautical Sciences, Vol. XII, No. 4, Winter 1965, pp. 123-128.

SECTION 7

7.0 HYBRID MULTILEVEL-LQR ATTITUDE CONTROL OF THE ROTATIONAL DYNAMICS MODEL OF THE SPACE PLATFORM

7.1 DECOMPOSED STATE VARIABLE MODEL

The subscripts appearing in the state variable rotational dynamics model, equation (6-14), correspond to the axes of the model. The matrix coefficients, A_{jk} and B_{jk}, represent interaxial coupling with $k \neq j$. This model was recast into multilevel form by decomposing it into a series of submodels. Decomposition temporarily suppresses the interaxial coupling in the overall model producing three single axis submodels and a coordination submodel. It is effected by writing the following coordination equations which constitute the coordination subproblem.

$$\underset{-j}{a} = \sum_{\substack{k=1 \\ k\neq 1}}^{3} \left(A_{jk} \underset{jk-j}{d}^{k} + B_{jk} \underset{jk-j}{s}^{k} \right) \qquad j = 1,2,3 \qquad (7\text{-}1)$$

$$\underset{-j}{d}^{k} = \underset{-k}{x} \qquad \underset{-j}{s}^{k} = \underset{-k}{u} \qquad k \neq j = 1,2,3 \qquad (7\text{-}2)$$

Equation set (7-2) is in the form of Gauss-Seidel coordination as presented in Wismer (7-1).

Substitution of equation sets (7-1) and (7-2) into the state variable rotational dynamics model of equation (6-14) yields three submodels of the following form:

$$\dot{\underline{x}}_j = A_{jj}\underline{x}_j + B_{jj}\underline{u}_j + \underline{a}_j(t) \qquad j = 1,2,3$$

The four submodels developed in this section were assembled into the two level hierarchy shown in Figure 7-1.

Corresponding to the decomposed state variable equations of this model, a decomposed performance index and a decomposed Hamiltonian were constructed.

7.2 DECOMPOSED PERFORMANCE INDEX AND HAMILTONIAN

The decomposed performance index for the application of optimal attitude control to this vehicle may be written as follows:

$$J = \sum_{j=1}^{3} \int_{t_o}^{t_f} P_j \, dt \tag{7-4}$$

where:

$$P_j = \tfrac{1}{2}(\underline{x}_j - \underline{x}_{jd})^T Q_j (\underline{x}_j - \underline{x}_{jd}) + \tfrac{1}{2}\underline{u}_j^T W_{ju} \underline{u}_j$$

$\underline{x}_{jd}$ = prespecified desired value of $\underline{x}_j$.

Q_j = symmetric positive semidefinite state variable error weighting coefficient matrix.

W_{ju} = symmetric positive definite control energy weighting coefficient matrix.

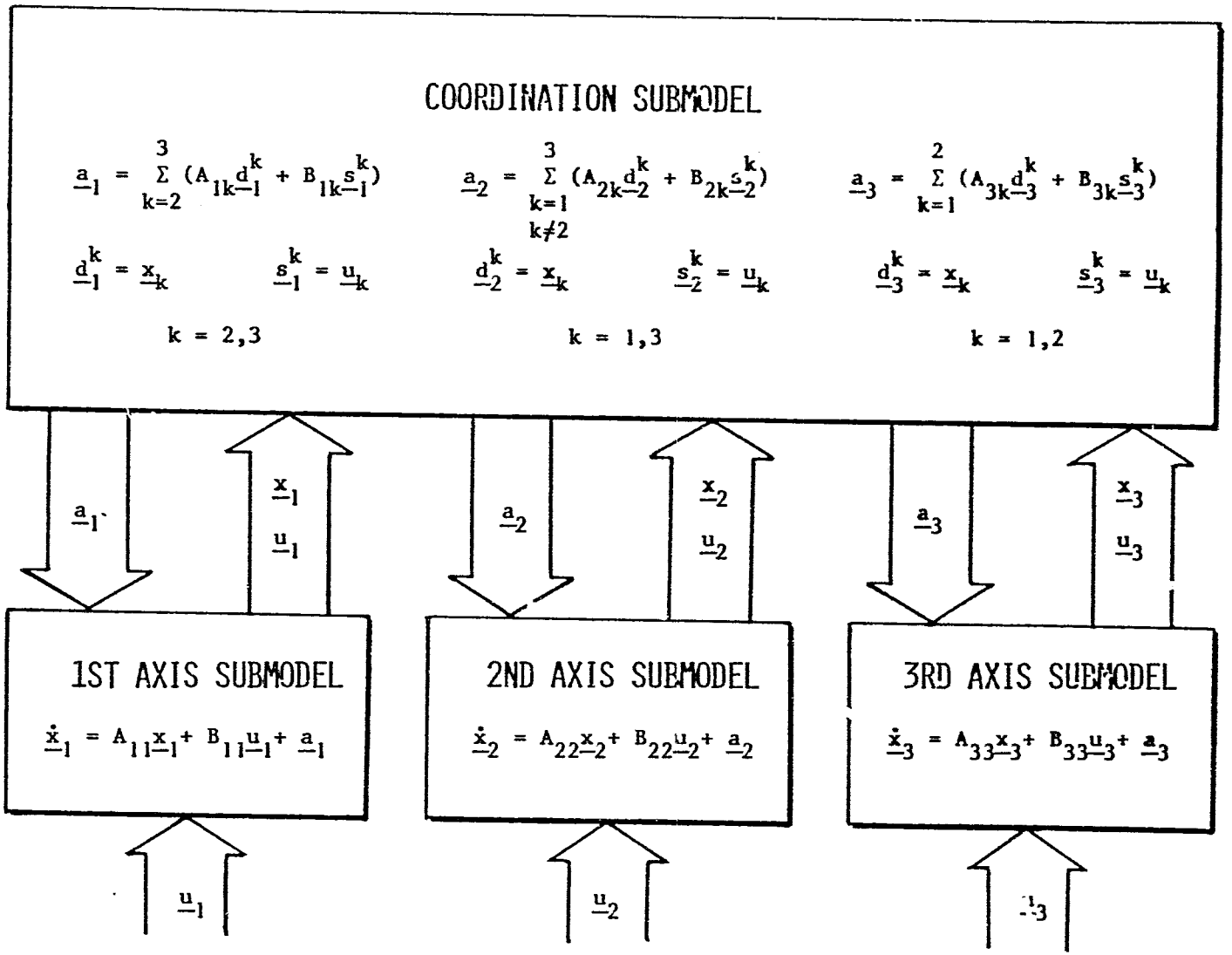

FIG. 7-1: SUBMODEL HIERARCHY FOR LINEARIZED DECOMPOSED STATE VARIABLE ROTATIONAL MODEL OF VEHICLE

The corresponding decomposed Hamiltonian expressing the energy state of the system is written as follows.

$$H = \sum_{j=1}^{3} H_j \tag{7-5}$$

where:

$$H_j = P_j + \underline{\lambda}_j^T \left[A_{jj} \underline{x}_j + B_{jj} \underline{u}_j + \sum_{\substack{k=1 \\ k \neq j}}^{3} \left(A_{jk} \underline{d}_j^k + B_{jk} \underline{s}_j^k \right) \right] + \sum_{\substack{k=1 \\ k \neq j}}^{3} \left[(\underline{\rho}_j^k)^T (\underline{x}_j - \underline{d}_k^j) + (\underline{\nu}_j^k)^T (\underline{u}_j - \underline{s}_k^j) \right] \tag{7-6}$$

$\underline{\lambda}_j$ = jth vector costate variable (Lagrange multiplier)

$\underline{d}_j^k$, $\underline{s}_j^k$, $\underline{\rho}_j^k$, and $\underline{\nu}_j^k$ = Gauss-Seidel type vector coordination variables

7.3 COSTATE EQUATIONS

The costate equations result from application of the following necessary condition for minimization of the decomposed Hamiltonian:

$$\dot{\underline{\lambda}}_j = - \frac{\partial H}{\partial \underline{x}_j} = - A_{jj}^T \underline{\lambda}_j - Q_j (\underline{x}_j - \underline{x}_{jd}) + \underline{b}_j(t) \tag{7-7}$$

where:

$$\underline{b}_j(t) = - \sum_{\substack{k=1 \\ k \neq j}}^{3} \underline{\rho}_j^k \qquad \underline{\lambda}_j(t_f) = \underline{0} \text{ (final boundary conditions)} \tag{7-8}$$

7.4 CONTROL EQUATIONS

The control equations result from application of the following necessary condition for minimization of the Hamiltonian:

$$\frac{\partial H}{\partial \underline{u}_j} = \underline{0} \rightarrow \underline{u}_j = -W_{ju}^{-1}\left(B_{jj}^{T}\underline{\lambda}_j + \sum_{\substack{k=1 \\ k\neq j}}^{3} \underline{\nu}_j^k\right) \tag{7-9}$$

7.5 COMBINATION OF jTH STATE, CONTROL, AND COSTATE EQUATIONS INTO THE jTH TPBV SUBPROBLEM

Substitution of the jth control equation into the jth state equation yields a new state equation in terms of $\underline{x}_j$ and λ_j. Association of the jth costate equation with the equation representing the combination of the state equation and the control equation results in the jth two-point boundary value (TPBV) subproblem.

$$\dot{\underline{x}}_j = A_{jj}\underline{x}_j + R_j\underline{\lambda}_j + \hat{\underline{a}}_j(t) \qquad \dot{\underline{\lambda}}_j = -Q_j\underline{x}_j - A_{jj}^{T}\underline{\lambda}_j + \hat{\underline{b}}_j(t)$$

where:

(7-10)

$$\hat{\underline{a}}_j(t) = \sum_{\substack{k=1 \\ k\neq j}}^{3}\left(A_{jk}\underline{d}_j^k + B_{jk}\underline{a}_j^k - B_{jj}\underline{\nu}_j^k\right) \qquad \hat{\underline{b}}_j(t) = Q_j\underline{x}_{jd} - \sum_{\substack{k=1 \\ k\neq j}}^{3}\underline{\rho}_j^k$$

$$R_j = -B_{jj}W_{ju}^{-1}B_{jj}^{T}$$

$\underline{x}_j(t_o) = \underline{x}_{jo}$ (initial boundary conditions)

$\underline{\lambda}_j(t_f) = \underline{0}$ (final boundary conditions)

Solution of the subproblems requires an extension of the LQR techniques to reflect the presence of the additional terms on the right hand side of the corresponding TPBV subproblems. This extension, which was presented in Chichester (7-2), begins with generalizing the assumed form of $\underline{\lambda}_j$ in terms of $\underline{x}_j$ to the following.

$$\underline{\lambda}_j(t) = K_j(t)\underline{x}_j(t) + \underline{m}_j(t)$$

where $K_j(t)$ and $\underline{m}_j(t)$ are a time variable matrix and vector, respectively, to be determined. The assumed form of $\underline{\lambda}_j$ results in the generation of two simultaneous Riccati type equations to be solved for $K_j(t)$ and $\underline{m}_j(t)$. Substitution of these solutions into equation (7-11) yields the feedback control to minimize the performance index at time t_f. It should be noted that the corresponding solutions to the TPBV subproblems are obtained subject to the value of the coordination variables $\underline{d}_j^k$, $\underline{s}_j^k$, $\underline{\rho}_j^k$, and $\underline{\nu}_j^k$.

7.6 ASSEMBLY OF COORDINATION EQUATIONS INTO THE COORDINATION SUBPROBLEM

The remaining necessary conditions for minimization of the Hamiltonian result in additional coordination equations to be satisfied.

$$\frac{\partial H_j}{\partial \underline{\rho}_j^k} = \underline{0} \rightarrow \underline{d}_j^k = \underline{x}_j \qquad \frac{\partial H_j}{\partial \underline{\nu}_j^k} = \underline{0} \rightarrow \underline{s}_j^k = \underline{u}_j \tag{7-12}$$

$$\frac{\partial H}{\partial \underline{d}_j^k} = \underline{0} \rightarrow \underline{\rho}_j^k = A_{kj}^T \underline{\lambda}_k \qquad \frac{\partial H}{\partial \underline{s}_j^k} = \underline{0} \rightarrow \underline{\nu}_j^k = B_{kj}^T \underline{\lambda}_k$$

The top two of the above coordination equations are associated with the state equations while the bottom two are associated with the costate equations. All of the coordination equations are assembled into an overall coordination subproblem. Inputs for this coordination subproblem are state vectors, $\underline{x}_j$, control vectors, $\underline{u}_j$, and costate vectors, $\underline{\lambda}_k$, obtained as solutions of the jth and kth TPBV of the hierarchy respectively.

7.7 CONSTRUCTION OF THE SUBPROBLEM HIERARCHY

The original problem of generating the optimal attitude control contours for the prototype flexible space vehicle has been transformed into a series of interrelated subproblems to be solved. Due to these interconnections it is evident that these subproblems can be assembled into a hierarchy with the coordination subproblem at its apex. This hierarchy is depicted in Figure 7-2. Solution of the overall optimal attitude control problem is attained by iteration between the levels of the hierarchy. The modification of the space platform's configuration by adding or removing modules is treated at the first level of the hierarchy as presented in Chichester
(7-2).

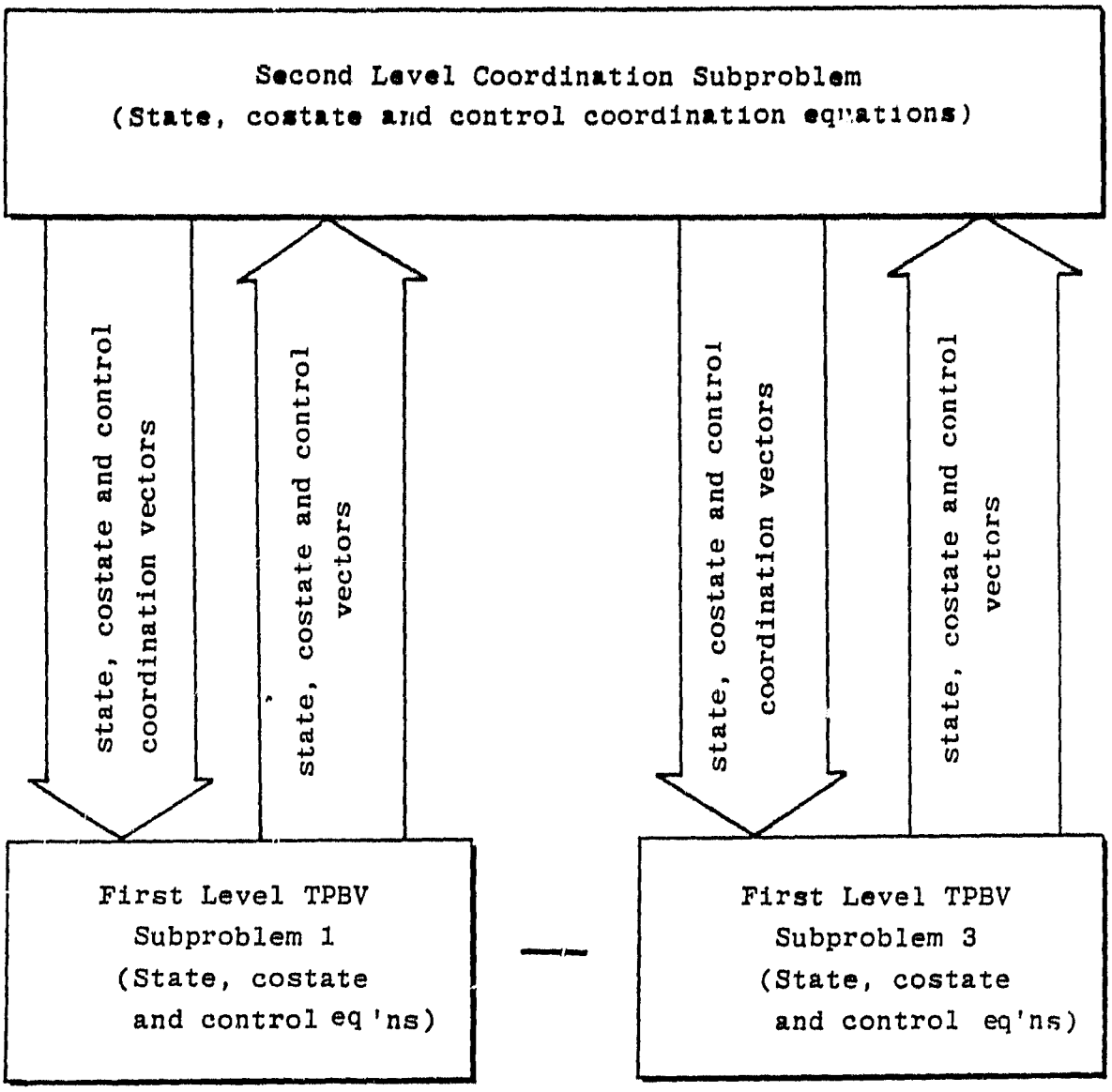

FIG. 7-2: SUBPROBLEM HIERARCHY FOR HYBRID MULTILEVEL-LQR ATTITUDE CONTROL OF TEN BODY MODEL

7.8 REFERENCES

7-1. Wismer, D.A., "Optimal Control of Distributed Parameter Systems Using Multilevel Techniques," Ph.D. dissertation, University of California, Los Angeles, California, 1966.

7-2. Chichester, F.D., "Application of Gauss-Seidel Multilevel Control to a Single Axis Torsional Model," Proceedings of the Space Transportation System Symposium, 1980 SAE Aerospace Congress and Exposition, October 1980, Los Angeles Convention Center, Los Angeles, California.

7-3. Chichester, F.D., "Application of Gauss-Seidel Multilevel and LQR Control to a Three Axis Rotational Model of a Flexible Space Vehicle", Proceedings of the Twelfth Annual Pittsburgh Conference on Modeling and Simulation, April 1981, University of Pittsburgh, Pittsburgh, Pennsylvania.

7-4. Chichester, F.D., and M.T. Borelli, "A Multilevel Control Approach for a Modular Structured Space platform, "AGARDograph on Spacecraft Pointing and Position Control, No. 260, November, 1981, Paper No. 10.

SECTION 8

8.0 CONCLUSIONS AND RECOMMENDATIONS

During FY'81 a new hybrid approach to the application of multilevel control techniques was developed and utilized in the attitude control of a series of prototypical models of flexible space vehicles. This hybrid approach consists of a combination of the techniques of multilevel hierarchical (ML) control and an extension of linear quadratic regulator (LQR) techniques to treat the modified two point boundary value subproblems resulting from the application of multilevel techniques.

This combination of ML and extended LQR techniques was first applied to a single axis model of the rotational dynamics of a prototype flexible spacecraft. The resulting model of the spacecraft and its control system was simulated on a digital computer.

The same combination of techniques was then extended to the attitude control of a three axis five body model of the rotational dynamics of the same prototype flexible spacecraft. This extension entailed the approximation of the flexible spacecraft by five rigid bodies interconnected by a spring hinge suspension and the development of the model of the rotational dynamics in terms of connection barycenters. The resulting model was linearized and then recast into a state variable form amenable to the application of time domain control methods such as multilevel and LQR approaches or a combination of the two. When each of the vector-matrix

equations comprising this model was expanded into its scalar components a regrouping of these scaler equations according to spatial axis was found to yield a model in which interaxial coupling was light.

Two approaches were followed in applying attitude control to the above model. Under the first approach the light coupling between the axes was eliminated and LQR control was applied to each axis. Under the second approach the interaxial coupling was temporarily suppressed by applying multilevel control techniques in conjunction with an extended form of LQR techniques. The three axis five body model of the rotational dynamics of the flexible spacecraft and its attitude control system was simulated for each of the two approaches described to facilitate comparison.

The hybrid ML-LQR approach was further extended to the attitude control of a three axis ten body model of the rotational dynamics of a prototype space platform comprised of two spacecraft interconnected by a deployable truss. This model was derived utilizing the same techniques as those used in the development of the three axis five body model described above.

As was the case with the five body model the ten body model was linearized, cast into state variable form and expanded in terms of scalar components. The scalar equations of this model were then rearranged in such a way that all equations associated with a given spatial axis were placed in the same group. The hybrid ML-LQR approach was then applied to the attitude control of this model. Simulation of the model with hybrid ML-LQR attitude control is pending at this time.

8.1 CONCLUSIONS

The following conclusions are based upon single axis and three axis modeling, control and simulation of a prototype flexible spacecraft and modeling and control formulation for a three axis representation of a prototype space platform.

a. Multilevel techniques reduce a mathematical model of high dimension (involving large numbers of variables and equations) to a hierarchy of submodels each of which is of smaller dimension except for the overall coordination submodel at the top of the hierarchy which generally is of much simpler form than the original model.

b. Multilevel techniques effect a similar reduction of a control problem of high dimension to a hierarchy of subproblems to be solved.

c. Since application of multilevel techniques to a control problem containing second order differential equations becomes ineffective if an attempt is made to reduce any of the first level subproblems to a dimension less than two, such application leads to a vector-matrix formulation of the subproblems in the bottom level of the hierarchy.

d. Application of multilevel techniques to an optimal control problem decomposes the overall two point boundary value (TPBV) problem to be solved to a two level hierarchy of subproblems with TPBV subproblems on the lower level and a coordination subproblem on the upper level.

e. Each of the TPBV subproblems on the lower level of the hierarchy resulting from the application of multilevel techniques to an optimal control problem contains coordination variables on its right hand side requiring an extension of linear quadratic regulator (LQR) techniques for its solution.

f. The combination of multilevel and extended LQR techniques described above represents a new hybrid approach to the application of optimal attitude control to a mathematical model of rotational dynamics of a spacecraft.

g. Digital computer simulation of a single axis model of the rotational dynamics of a prototype flexible spacecraft with a hybrid ML-LQR attitude control system produced very nearly the same responses as a simulation of the same single axis model with an LQR attitude control system.

h. Development of a linearized three axis five body state variable model of the rotational dynamics of the prototype flexible spacecraft was rendered more efficient by utilization of augmented body techniques.

i. Expansion of the three axis five body model in terms of scalar variables and equations revealed that grouping these equations according to spatial axes yielded a model with a high degree of block diagonal dominance in its coefficient matrices with weak interaxial coupling.

j. Digital computer simulation of the three axis five body model with hybrid ML-LQR attitude control produced responses closely similar to those resulting from computer simulation of the same model with axes decoupled and LQR control applied to each axis.

k. Development of a three axis ten body linearized state variable model of the rotational dynamics of a prototype space platform consisting of two spacecraft interconnected by a deployable truss lead to approximation of the truss by four rigid bodies serially connected by a spring hinge suspension.

l. Application of hybrid ML-LQR techniques to the attitude control of the three axis ten body model of the space platform yielded a subproblem hierarchy of a form similar to that developed for the three axis five body model of the prototype flexible spacecraft.

m. The hybrid ML-LQR approach to attitude control of flexible spacecraft is an original concept that appears quite promising for application to a broad variety of spacecraft rotational dynamics models.

8.2 RECOMMENDATIONS

The following items are recommended for future study concerning control of flexible spacecraft.

a. The three axis ten body model of the rotational dynamics of the prototype space platform with hybrid multilevel-LQR attitude control should be simulated on a digital computer in order to evaluate its responses to a variety of standard perturbations. To this end the NASTRAN data for the MSFC/hybrid truss supplied by NASA should be utilized to generate a dynamically equivalent rigid body spring hinge suspension model of the truss comprised of four serially connected rigid bodies.

b. The relative control authority available with actuators on both spacecraft in the space platform should be compared with that which is available when control actuators are restricted to one of the two spacecraft.

c. Different schemes for decomposing the original attitude control problem into a hierarchy of subproblems should be compared with respect to computational efficiency.

d. Techniques for improving the computational efficiency of solving the modified two point boundary value subproblem resulting from the application of the hybrid ML-LQR approach to the attitude control of rotational models of a variety of spacecraft should be developed.

e. Effects of modeling inaccuracies upon the performance of the controlled system should be evaluated.

f. More systematic methods for determining the weighting matrices utilized in the decomposed performance matrices associated with the hybrid ML-LQR approach to attitude control should be sought.

APPENDIX A

EXTENSION OF LINEAR QUADRATIC REGULATOR TECHNIQUES TO FIRST LEVEL TPBV SUBPROBLEMS*

From Equation (2-30)

$$\dot{\underline{x}}_i = A_{ii}\underline{x}_i - \frac{1}{2}\hat{R}_i^{-1}\underline{\lambda}_i + \underline{a}_i(t);$$

$$i = 1,2,3 \qquad \text{(A1)}$$

$$\dot{\underline{\lambda}}_i = -2Q_j\underline{x}_i - A_{ii}^T\underline{\lambda}_i + \hat{\underline{b}}_i(t)$$

with given $\underline{x}_i(t_o)$ and $\underline{\lambda}_i(t_f)$ (A2)

Assume:

$$\underline{\lambda}_i = K_i(t)\underline{x}_i + \underline{m}_i(t) \qquad \text{(A3)}$$

$$\dot{\underline{\lambda}}_i = \dot{K}_i\underline{x}_i + K_i\dot{\underline{x}}_i + \dot{\underline{m}}_i \qquad \text{(A4)}$$

Substituting equation (A3) in equation (A1):

$$\dot{\underline{x}}_i = (A_{ii} - \frac{1}{2}\hat{R}_i^{-1}K_i)\underline{x}_i + \underline{a}_i - \frac{1}{2}\hat{R}_i^{-1}\underline{m}_i \qquad \text{(A5)}$$

Substituting equation (A4) in equation (A2):

$$\dot{K}_i\underline{x}_i + K_i\dot{\underline{x}}_i = -(A_{ii}^TK_i + 2Q_i)\underline{x}_i + \hat{\underline{b}}_i - \dot{\underline{m}}_i \qquad \text{(A6)}$$

*This is similar to an approach presented in Sage (2-7) pp. 96-97.

Substituting equation (A5) in (A6):

$$(\dot{K}_i + K_i A_{ii} - \frac{1}{2} K_i \hat{R}_i^{-1} K_i + A_{ii}^T K_i + 2Q_i)\underline{x}_i$$

$$+ K_i(\underline{a}_i - \frac{1}{2} \hat{R}_i^{-1} \underline{m}_i) + \hat{\underline{b}}_i - \dot{\underline{m}}_i = \underline{0} \qquad \text{(A7)}$$

For solutions for $K_i(t)$ and $\underline{m}_i(t)$ independent of $\underline{x}_i$:

$$\dot{K}_i + K_i A_{ii} - \frac{1}{2} K_i \hat{R}_i^{-1} K_i + A_{ii}^T K_i + 2Q_i = [0] \qquad \text{(A8)}$$

$$\dot{\underline{m}}_i + \frac{1}{2} K_i \hat{R}_i^{-1} \underline{m}_i - K_i \underline{a}_i - \hat{\underline{b}}_i = \underline{0} \qquad \text{(A9)}$$

Since $\underline{\lambda}_i(t_f) = \underline{0}$, for solutions independent of $\underline{x}_i$,

$$K_i(t_f) = [0] \text{ and } \underline{m}_i(t_f) = \underline{0} \qquad \text{(A10)}$$

Also,

$$\underline{u}_i(t) = -\frac{1}{2} \hat{R}^{-1} B_{ii}^T \underline{\lambda}_i(t)$$

$$= -\frac{1}{2} \hat{R}_i^{-1} B_{ii}^T (K_i \underline{x}_i + \underline{m}_i) \qquad \text{(A11)}$$

APPENDIX B

SUCCESSIVE APPROXIMATIONS OF MSFC/HYBRID DEPLOYABLE TRUSS

A perspective drawing of the undeformed MSFC/Hybrid deployable truss that appeared in Ivey (6-1) is reproduced in Figure B-1. The following specifications were received for the truss. The truss is comprised of ten segments each of which is a 55-inch cube. Each of these segments weighs 16.8 pounds. If the segments are numbered consecutively from the left hand end of the drawing, four 8000 pound rigid bodies are rigidly connected in such a way that they are centered above and below the fifth and tenth cubic segments with their centers of mass 89 inches above and below the truss as shown in Figure B-1. Additional data resulting from a vibrational analysis of the truss were presented in Ivey (6-1).

FIG. B-1: PERSPECTIVE VIEW OF HYBRID DEPLOYABLE TRUSS

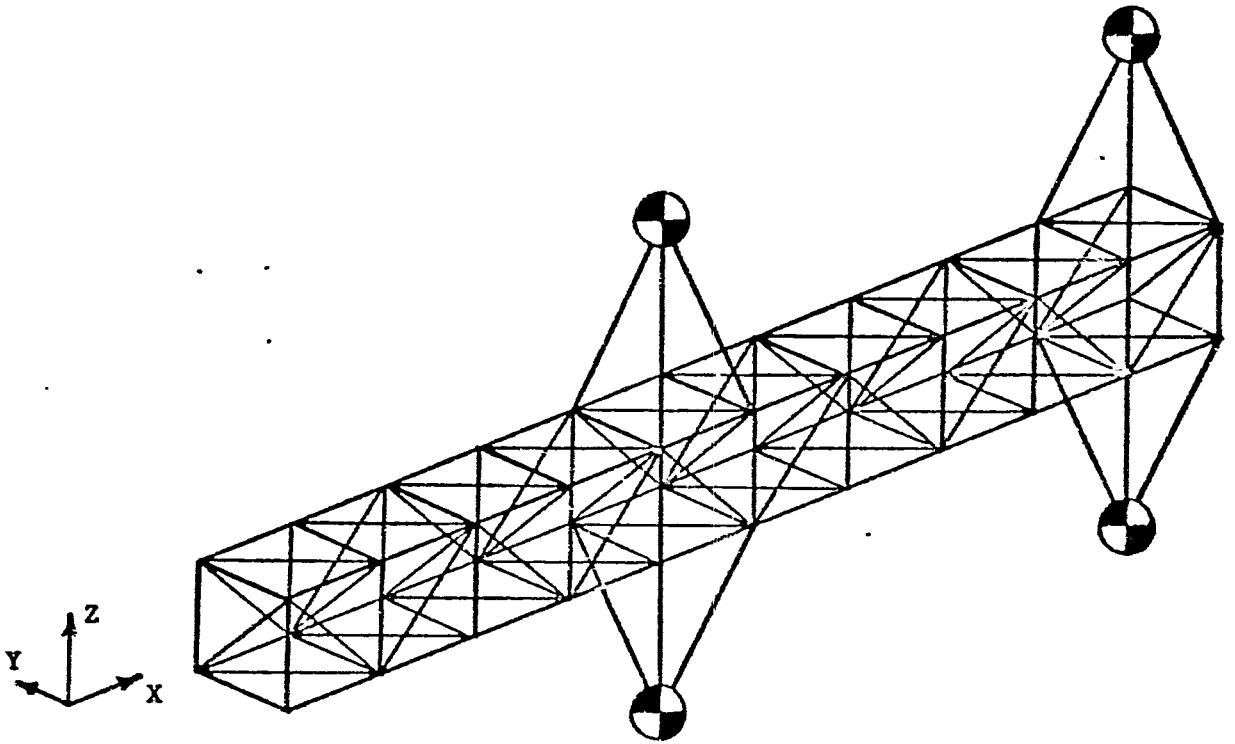

First Approximation of MSFC Truss

1. Each cubic segment of the truss was approximated by a cube of the same dimensions with the total mass of the segment uniformly distributed within the cube.

2. The cubic segments were associated into two pairs of identical modules as shown in Figure B-2.

3. One of the module pairs has external masses associated with it as depicted in Figures B-1, B-2 and B-4.

4. Equivalent principal moments of inertia were obtained for each module pair. (Figures B-3 and B-4).

5. Modules were serially connected by a spring-hinge suspension with spring and damping coefficients associated with each three degree-of-freedom hinge shown in Figure B-2.

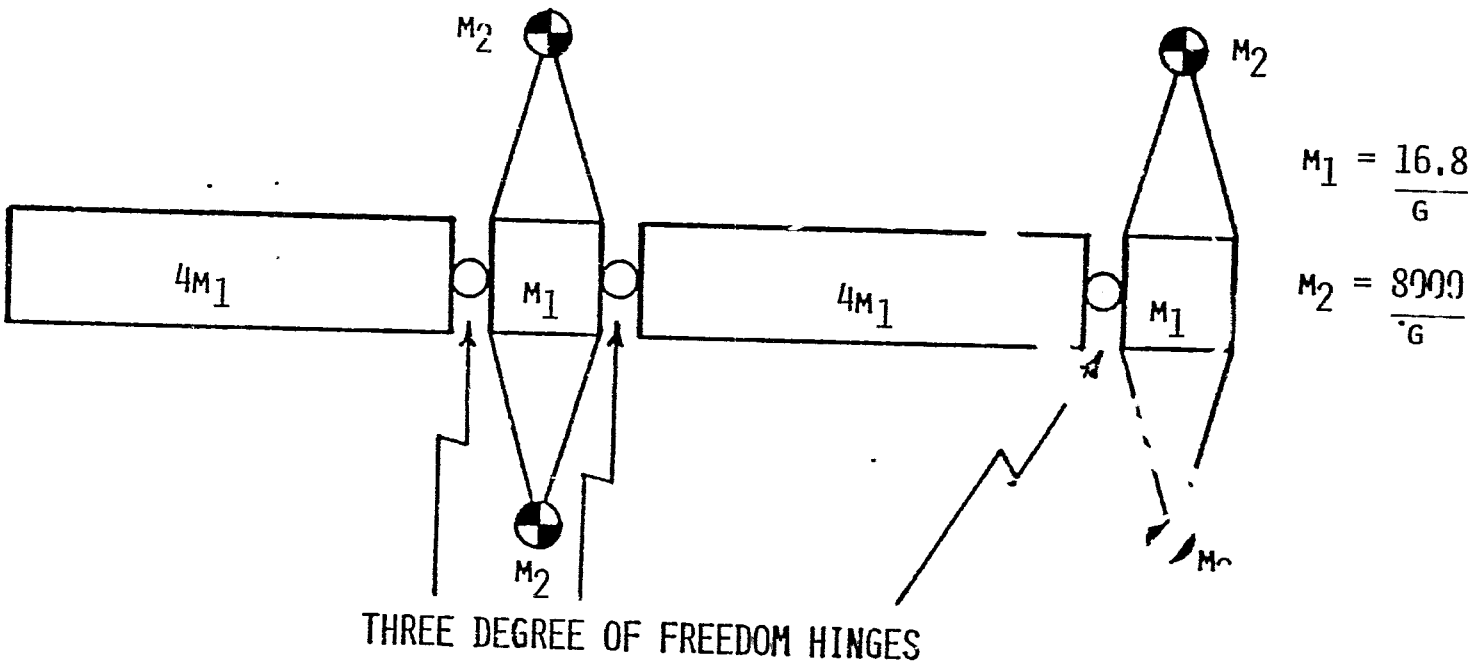

FIG. B-2: SIDE VIEW OF FIRST APPROXIMATION OF MSFC HYBRID DEPLOYABLE TRUSS

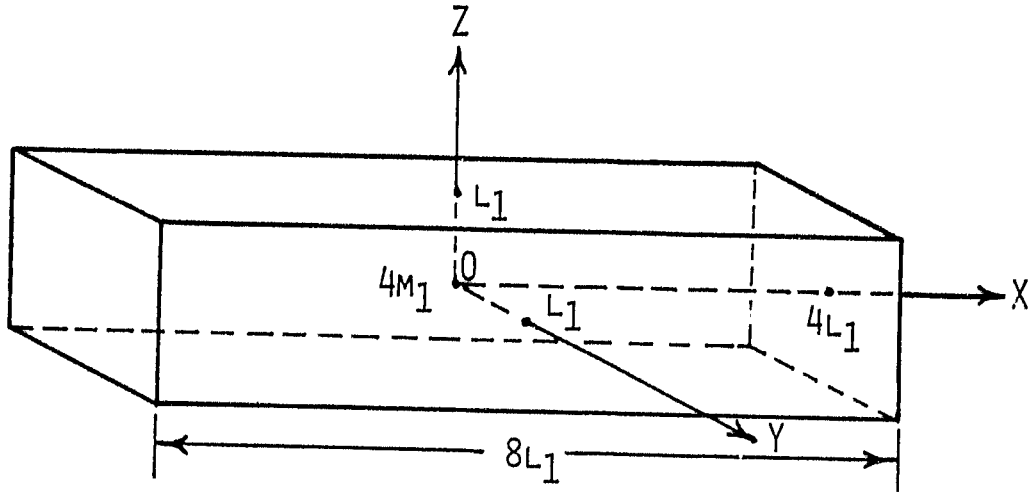

FIG. B-3: TRUSS MODULE 1

TOTAL MASS = $4M_1 = \frac{4(168)}{10G}$ CENTERED AT PT. 0

L_1= 27.5 IN.

THE PRINCIPAL MOMENTS OF INERTIA ARE AS FOLLOWS:

$$I_X = \frac{8}{3} M_1 L_1^2$$

$$I_Y = \frac{68}{3} M_1 L_1^2$$

$$I_Z = \frac{68}{3} M_1 L_1^2$$

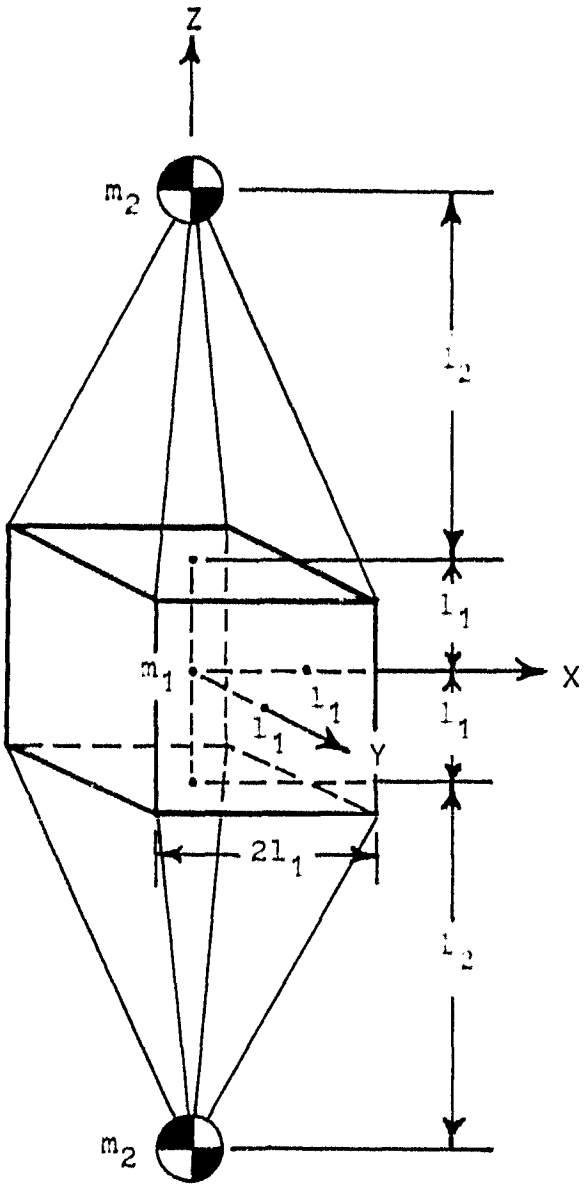

FIG. B-4: TRUSS MODULE 2

$l_1 = 27.5$ inches $\quad l_2 = 89$ inches $\quad m_1 = \frac{16.8}{g} \quad m_2 = \frac{8000}{g}$

Principal Moments of Inertia

$$I_x = m_2(l_1 + l_2)^2 + \frac{2}{3}m_1 l_1^2 = m_2\left[(l_1 + l_2)^2 + \frac{2m_1}{3m_2}l_1^2\right] = I_y$$

$$I_z = \frac{2}{3}m_1 l_1^2$$

Second Approximation of MSFC Truss

1. Truss may be approximated by four serially connected rigid bodies as depicted in Figure B-5.

2. Each rigid body of the second approximation has the same principal moments of inertia as the corresponding truss module in the first approximation of the truss depicted in Figure B-2.

3. The second approximation has the same three degree-of freedom hinges, spring constants and damping coefficients as the first approximation.

FIG. B-5: THREE AXIS FOUR BODY MODEL OF TRUSS

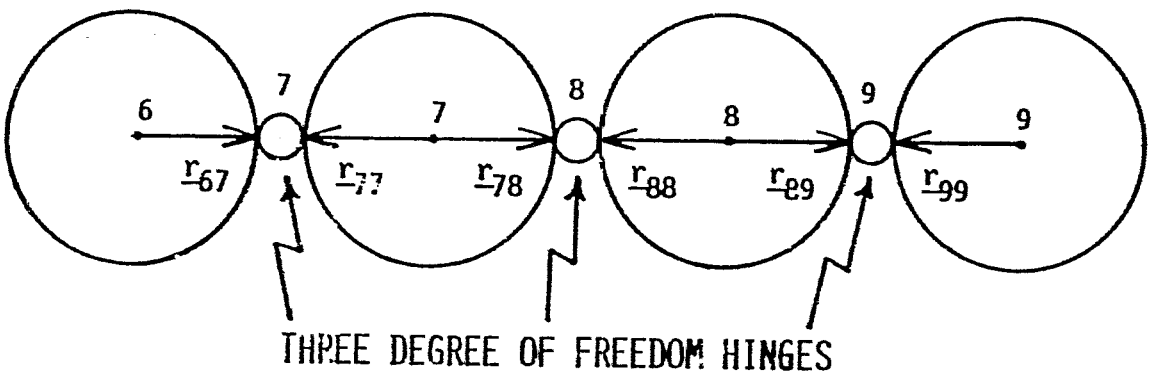

$M_8 = M_6 = 4M_1$

$M_9 = M_7 = 2M_2 + M_1 >> 4M_1$

$R_{88} = R_{66} = R_{67} = R_{89} = 4L_1$

APPENDIX C

DEFINITIONS FOR MATRICES APPEARING IN THE TEN BODY STATE VARIABLE ROTATIONAL DYNAMICS MODEL

$$G = \begin{bmatrix} g_{11} & \cdots & g_{1,30} \\ \vdots & & \vdots \\ g_{30,1} & \cdots & g_{30,30} \end{bmatrix} = A^{-1}$$

$$\hat{G} = \begin{bmatrix} \hat{G}_{11} & \hat{G}_{12} & \hat{G}_{13} \\ \hat{G}_{21} & \hat{G}_{22} & \hat{G}_{33} \\ \hat{G}_{31} & \hat{G}_{32} & \hat{G}_{33} \end{bmatrix}$$

$$\hat{G}_{1k}^T = (\underline{g}_{1k}, \underline{g}_{4k}, \underline{g}_{7k}, \cdots, \underline{g}_{28k})$$

$$\hat{G}_{2k}^T = (\underline{g}_{2k}, \underline{g}_{5k}, \underline{g}_{8k}, \cdots, \underline{g}_{29k})$$

$$\hat{G}_{3k}^T = (\underline{g}_{3k}, \underline{g}_{6k}, \underline{g}_{9k}, \cdots, \underline{g}_{30k})$$

$$\underline{g}_{j1}^T = (g_{j1}, g_{j4}, g_{j7}, \cdots, g_{j28})$$

$$\underline{g}_{j2}^T = (g_{j2}, g_{j5}, g_{j8}, \cdots, g_{j29})$$

$$\underline{g}_{j3}^T = (g_{j3}, g_{j6}, g_{j9}, \cdots, g_{j30})$$

SUSPENSION MATRIX

$$L = \begin{bmatrix} -I & -I & [0] & [0] & -I & [0] & [0] & [0] & [0] \\ I & [0] & -I & [0] & [0] & [0] & [0] & [0] & [0] \\ [0] & I & [0] & -I & [0] & [0] & [0] & [0] & [0] \\ [0] & [0] & I & [0] & [0] & [0] & [0] & [0] & [0] \\ [0] & [0] & [0] & I & [0] & [0] & [0] & [0] & [0] \\ [0] & [0] & [0] & [0] & I & -I & [0] & [0] & [0] \\ [0] & [0] & [0] & [0] & [0] & I & -I & [0] & [0] \\ [0] & [0] & [0] & [0] & [0] & [0] & I & -I & [0] \\ [0] & [0] & [0] & [0] & [0] & [0] & [0] & I & -I \\ [0] & [0] & [0] & [0] & [0] & [0] & [0] & [0] & I \end{bmatrix}$$

$$I = \begin{bmatrix} 1 & 0 & 0 \\ 0 & 1 & 0 \\ 0 & 0 & 1 \end{bmatrix} \qquad [0] = \begin{bmatrix} 0 & 0 & 0 \\ 0 & 0 & 0 \\ 0 & 0 & 0 \end{bmatrix}$$

SPRING CONSTANT MATRIX

$$K_S = \begin{bmatrix} [0] & -K_{s12} & [0] & [0] & [0] & [0] & [0] & [0] & [0] & [0] \\ [0] & [0] & -K_{s13} & [0] & [0] & [0] & [0] & [0] & [0] & [0] \\ [0] & [0] & [0] & -K_{s24} & [0] & [0] & [0] & [0] & [0] & [0] \\ [0] & [0] & [0] & [0] & -K_{s35} & [0] & [0] & [0] & [0] & [0] \\ [0] & [0] & [0] & [0] & [0] & -K_{s16} & [0] & [0] & [0] & [0] \\ [0] & [0] & [0] & [0] & [0] & [0] & -K_{s67} & [0] & [0] & [0] \\ [0] & [0] & [0] & [0] & [0] & [0] & [0] & -K_{s78} & [0] & [0] \\ [0] & [0] & [0] & [0] & [0] & [0] & [0] & [0] & -K_{s89} & [0] \\ [0] & [0] & [0] & [0] & [0] & [0] & [0] & [0] & [0] & -K_{s9,10} \end{bmatrix}$$

DAMPING COEFFICIENT MATRIX

$$C_s = \begin{bmatrix} C_{s12} & -C_{s12} & [0] & [0] & [0] & [0] & [0] & [0] & [0] & [0] \\ C_{s13} & [0] & -C_{s13} & [0] & [0] & [0] & [0] & [0] & [0] & [0] \\ [0] & C_{s24} & [0] & -C_{s24} & [0] & [0] & [0] & [0] & [0] & [0] \\ [0] & [0] & C_{s35} & [0] & -C_{s35} & [0] & [0] & [0] & [0] & [0] \\ C_{s16} & [0] & [0] & [0] & [0] & -C_{s16} & [0] & [0] & [0] & [0] \\ [0] & [0] & [0] & [0] & [0] & C_{s67} & -C_{s67} & [0] & [0] & [0] \\ [0] & [0] & [0] & [0] & [0] & [0] & C_{s78} & -C_{s78} & [0] & [0] \\ [0] & [0] & [0] & [0] & [0] & [0] & [0] & C_{s89} & -C_{s89} & [0] \\ [0] & [0] & [0] & [0] & [0] & [0] & [0] & [0] & C_{s9,10} & -C_{s9,10} \end{bmatrix}$$

TRANSFORMATION MATRIX

$$K = \begin{bmatrix} I & [0] & [0] & [0] & [0] & [0] & [0] & [0] & [0] & [0] \\ -I & I & [0] & [0] & [0] & [0] & [0] & [0] & [0] & [0] \\ -I & [0] & I & [0] & [0] & [0] & [0] & [0] & [0] & [0] \\ [0] & -I & [0] & I & [0] & [0] & [0] & [0] & [0] & [0] \\ [0] & [0] & -I & [0] & I & [0] & [0] & [0] & [0] & [0] \\ -I & [0] & [0] & [0] & [0] & I & [0] & [0] & [0] & [0] \\ [0] & [0] & [0] & [0] & [0] & -I & I & [0] & [0] & [0] \\ [0] & [0] & [0] & [0] & [0] & [0] & -I & I & [0] & [0] \\ [0] & [0] & [0] & [0] & [0] & [0] & [0] & -I & I & [0] \\ [0] & [0] & [0] & [0] & [0] & [0] & [0] & [0] & -I & I \end{bmatrix}$$